QUANTITATIVE INVESTIGATION OF INLET VORTEX FLOW FIELD

by

Hyoun-Woo Shin and Cheryl Shippee

GT&PDL Report No. 179 March 1984

GAS TURBINE & PLASMA DYNAMICS LABORATORY
MASSACHUSETTS INSTITUTE OF TECHNOLOGY
CAMBRIDGE, MASSACHUSETTS

QUANTITATIVE INVESTIGATION OF INLET VORTEX FLOW FIELD

by

Hyoun-Woo Shin and Cheryl Shippee

GT&PDL Report No. 179 March 1984

This research was supported by the Air Force Office of Scientific Research under Contract no. F49620-82-K-0002, Dr. J.D. Wilson, Program Manager.

ABSTRACT

A quantitative investigation of the flow field of an inlet in cross-wind has been carried out for various operating conditions, including flow regimes representative of aircraft engine inlets at take-off. The measurements were made to show the influence of two non-dimensional parameters, height of the inlet above the ground to the inlet diameter ratio (H/D), and velocity ratio (U_i/U_e), on the vortex strength (i.e., circulation) and the position of the vortex inside the inlet. In general, as H/D is decreased and/or U_i/U_e is increased, the vortex strengthens. In addition, at an operating condition where a strong inlet vortex was present, the circulation of both the inlet and trailing vortices was determined. These were found to be essentially equal in magnitude but opposite in sign, verifying a previous hypothesis concerning the vortical structure of the flow.

Qualitative flow visualization has been done to examine two aspects of the inlet/trailing vortex flow field. One is the nature of the transition between regimes in which an inlet vortex is present and those in which no inlet vortex exists. The other deals with the extent of the separated region on the inlet body. The results of this study were used to support a conceptual model of the formation of an inlet/trailing vortex system for an inlet in a cross-wind.

ACKNOWLEDGEMENTS

The authors would like to take this opportunity to thank their advisor, Professor E.M. Greitzer, for his invaluable assistance during the course of this research. Special thanks are also due to Dr. C.S. Tan and Professor W.K. Cheng for their interest and involvement in the work presented in this paper.

The authors want to recognize Mr. D.L. Motycka for his active involvement and suggestions during this experiment. The authors also would like to express an appreciation to Dr. E.E. Covert (Director of GT&PDL), Dr. J.L. Kerrebrock (Head of Aeronautics and Astronautics Dept.) and Dr. F.E. Marble (of Caltech) for their insight, comments, and recommendations on the course of the program.

Of great assistance to the authors was Mr. F.H. Durgin and Mr. Peter Lorber, with their knowledge of the wind tunnel.

This research was supported by the Air Force Office of Scientific Research under Contract No. F49620-82-K-0002, Dr. J.D. Wilson, Program Manager.

TABLE OF CONTENTS

LIST OF FIGURES

FIGURES PAGE

FIGURES PAGE

FIGURES PAGE

FIGURES PAGE

LIST OF TABLES

LIST OF SYMBOLS

C	contour
C_p	pressure coefficient
D	inlet inside diameter
D_o	inlet outside diameter
F	pressure coefficient
H	height of inlet centerline above ground plane
$H_{dynamic}$	dynamic pressure coefficient
P_{atm}	atmospheric pressure
P_i	pressure on inlet surface
P_s	static pressure
P_t	total pressure
r	radial distance from center of inlet
U	local velocity magnitude
U_c	inlet circumferential velocity magnitude
U_e	free stream axial velocity magnitude
U_i	inlet axial velocity magnitude
$\dot{V}$	volumetric flow rate
Γ	circulation
ρ	density

Subscripts

duct	blower ducting quantity
pitch	pitch plane quantity
pitot	free stream quantity
ref	reference quantity
total	total (stagnation) condition
yaw	yaw plane quantity

CHAPTER I

INTRODUCTION

A gas turbine engine operating near a ground surface is often observed to create a strong vortex between the ground and itself. This "inlet vortex" (or ground vortex) is of concern because of the effects it has on the engine. These include blade erosion (due to dirt ingestion) [1], compressor surge [2], and foreign object damage.

Investigations of inlet-vortex formation have identified two basic mechanisms of inlet vortex formation [3]. The first of these, which has been qualitatively known for some time, is the amplification of the ambient vertical vorticity as it is drawn into the inlet. The second mechanism, previously not recognized, does <u>not</u>, however, depend on ambient (i.e., far upstream) vorticity, but rather results from the variation in circulation along the length of the inlet. An inlet vortex can thus form in a flow that is irrotational upstream of the inlet. In this situation, the circulation variation will lead to the formation of an inlet/trailing vortex system as described in detail in [3]. A schematic of the vortex lines associated with this system is shown in Fig. 1-1, [3].

The quantities which govern the above phenomenon are the inlet volumetric flow rate $\dot{\forall}$, the characteristics freestream velocity U_e, the heights of the inlet centre line above the ground H, and the inlet outer diameter D_o. These quantities may be grouped into two nondimensional parameters $\dot{\forall}/U_e D_o^2$ and H/D_o. Note that for a fixed value of $\dot{\forall}$, the inlet inside diameter D does not influence the phenomenon significantly. For inlets with thin wall ($D_o \simeq D$), or inlets with fixed D_o, the two parameters U_i/U_e, where U_i is an averaged inlet velocity, and H/D may

be used instead. We have used the latter two parameters throughout this report so that the results may be compared to the previous measurements. For a given inlet shape and yaw angle, equivalence of U_i/U_e as well as H/D implies kinematic similarity. For high values of velocity ratio, or low values of H/D, an inlet/trailing vortex system is formed, as illustrated in Fig. 1-2(a). When the H/D is fixed and the velocity ratio is lowered, or H/D is increased when the velocity ratio is fixed, there is no longer a (ground to) inlet vortex, but rather two counter-rotating vortices trailing from the rear of the inlet are observed as shown in Fig. 1-2(b). A map of the inlet vortex formation conditions is shown in Fig. 1-3.

The previous investigations [3] were qualitative in nature. The next logical step in understanding the phenomena is quantitative measurements of pertinent aspects of the three dimensional flow. As reported in [4], a facility for making these measurements was designed, built and calibrated, and preliminary measurements were carried out, with focus on the "second mechanism" (which is less well understood). Static pressure measurements around the inlet were made during this study and, from these, one could infer flow fields which were consistent with the conceptual picture based on the water tunnel observations in [3].

With these two recent studies as a foundation, this report presents detailed measurements of the three dimensional flow associated with the inlet vortex. The purpose of these measurements is to quantify: 1) the relation between the circulations of the inlet and trailing vortices, and 2) the strength and location (inside the inlet) of the inlet vortex for several representative conditions.

For the first objective, at the conditions of U_i/U_e = 45, H/D = 1.5, detailed velocity and pressure measurements were made. The velocity was measured inside the inlet and at a plane parallel to the inlet axis behind the cylinder. Static pressure measurements were made on the inlet outside surface.

In addition to the above measurements, a parametric study was done to find the global properties of the vortex system. The velocity distributions inside the inlet not only allowed the circulation around the inlet vortex to be determined, but also allowed quantitative determination of the regions of high tangential velocities. Flow visualization was used to determine the vortex core location.

Additional qualitative information about the inlet vortex was obtained from flow visualization studies. A water tunnel flow visualization study was carried out to examine several features about the formation of the inlet vortex. Flow visualization was done in the wind tunnel to illustrate features of the flow in and on the inlet. From the combination of qualititative and quantitative studies a conceptual model of an inlet in a cross-wind has been developed.

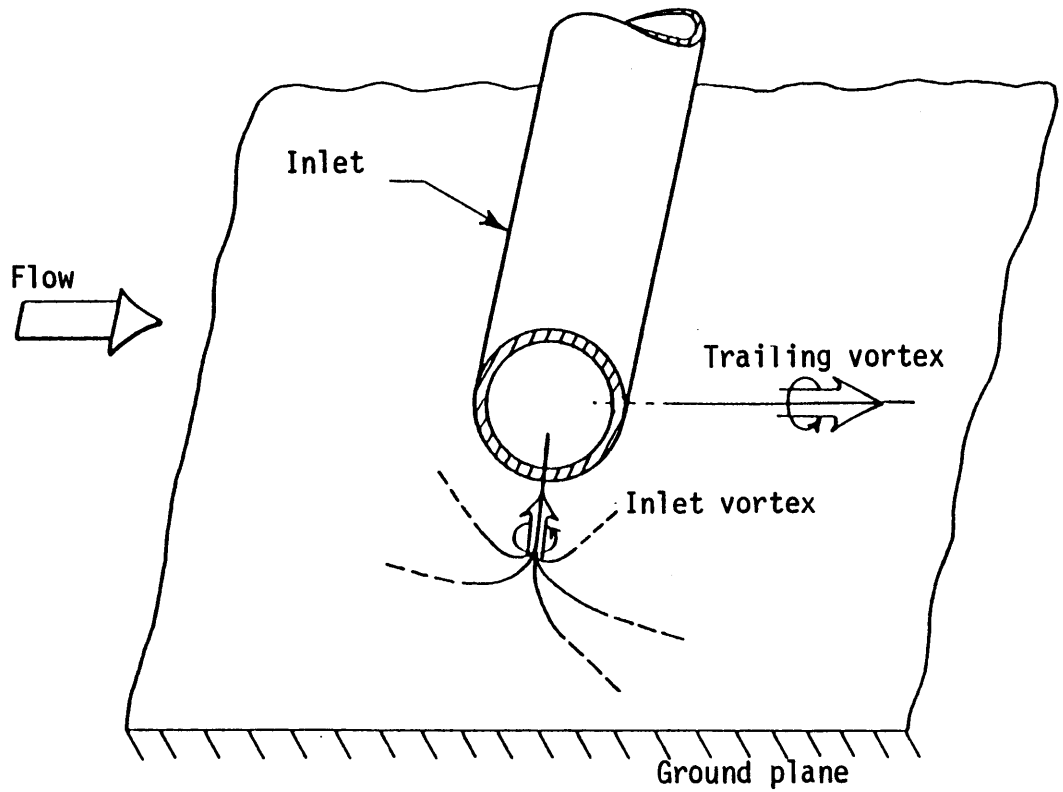

Figure 1-1 Schematic vortex lines for an inlet at 90° of yaw in an irrotational upstream flow [3]

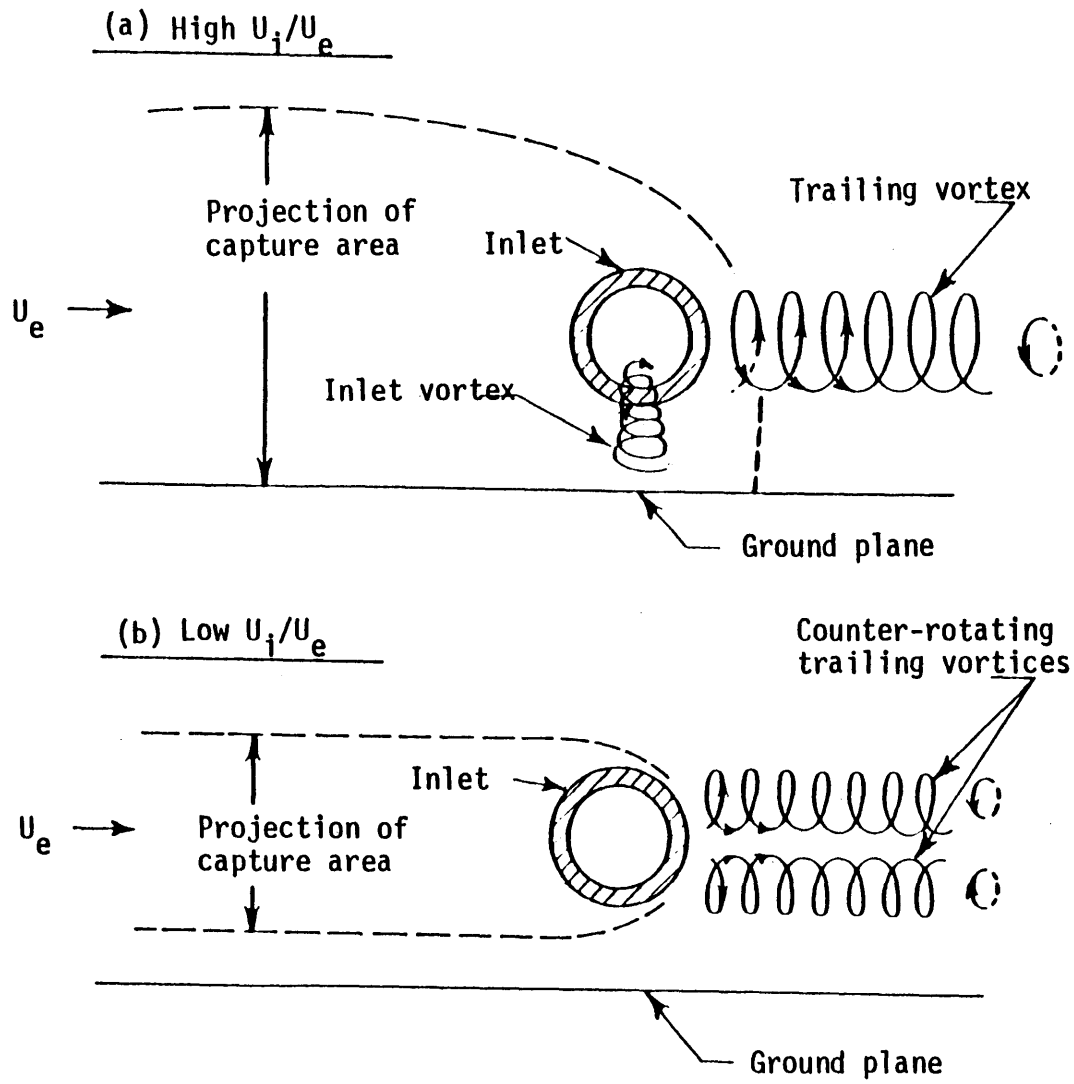

Figure 1-2 Flow regimes at low and high values of U_i/U_e. Inlet at 90° of yaw in an irrotational upstream flow [3]

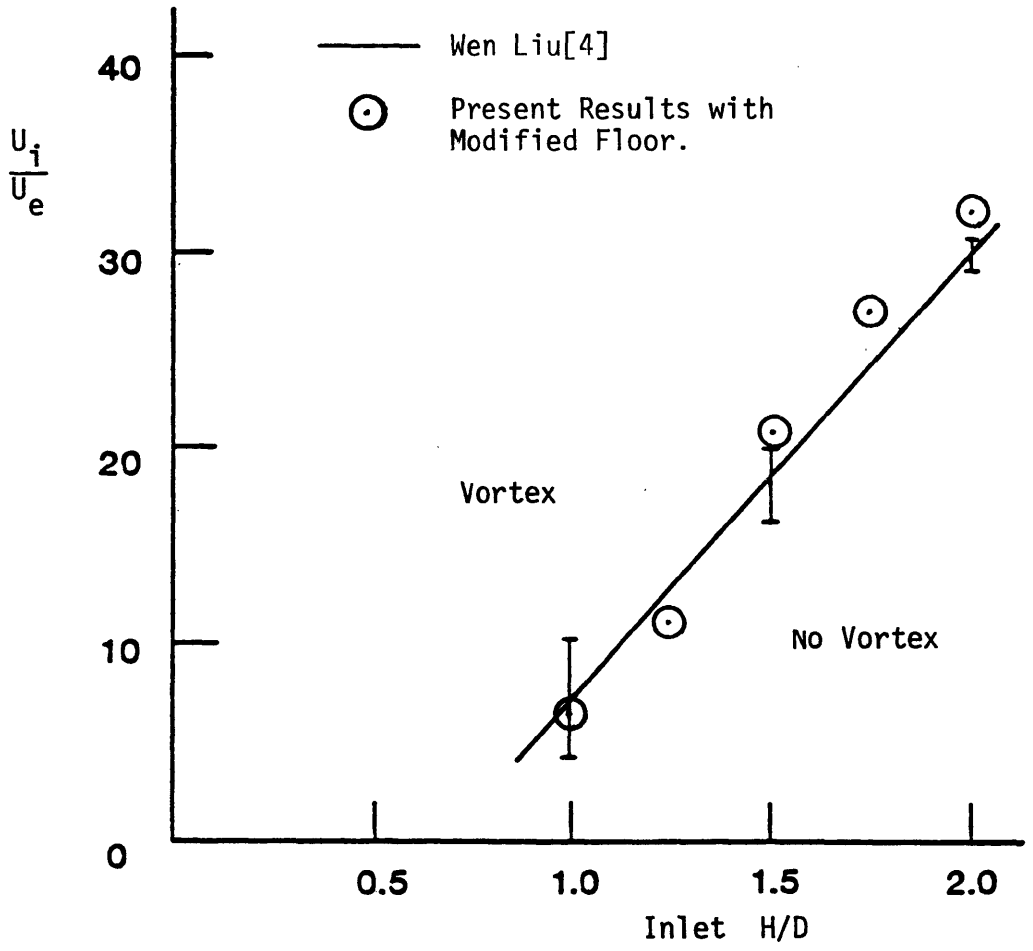

Figure 1-3 Boundary of inlet vortex formation for an inlet at 90° of yaw in an irrotational upstream flow

CHAPTER II

EXPERIMENTAL FACILITY

A detailed description of the construction and calibration of the test facility is presented in [5]. A brief description is included here since some design changes have been made during the course of the investigation.

2-1 WIND TUNNEL

All of the measurements during this investigation were conducted in the Wright Brothers Wind Tunnel of the Department of Aeronautics and Astronautics at MIT. A schematic of the tunnel is shown in Fig. 2-1 and further information can be found in Markham [6]. The tunnel is closed circuit with an elliptical test section 3.05 m wide, 2.3 m in height and 4.6 m long. During the investigation, a 2.44 m wide ground plane was used, which was mounted 0.46 m above the bottom. The ground plane has a drooped leading edge to suppress separation.

The tunnel velocity is controlled by either a variable pitch propeller, which can induce velocities up to 80 m/sec, or, for low speed wind (0-3 m/sec), an auxiliary fan (a large attic fan). The auxiliary fan is driven by a D.C. motor controlled by a silicon control rectifier speed controller. The propeller, fan, and data acquisition equipment controls are located in a control room adjacent to the test section.

2-2 BLOWER AND DUCTING

To induce the inlet flow a blower and the necessary ducting were installed. The method adopted to determine the flow rate in the inlet was to measure the pressure drop across a 50% porosity perforated plate, for which the loss coefficient was known.

2-3 INLET MODELS

The inlet model is a circular cylinder with no centerbody. The inside diameter is 0.15 m and the outside diameter of 0.2 m, as shown in Fig. 2-2. The lip was designed to be non-separating over the conditions of interest based on the criteria given by Boles and Stockman [7] (which yield a lip geometry of elliptical segments). Details are given in [5].

Two models were machined for the experiment, one of plexiglass and the other of aluminum. The former was used for flow visualization only and had two static taps for determining the inlet velocity. The aluminum model was used for the pressure measurements. It was originally constructed with an array of 40 static taps on its surface as shown in Fig. 2-3. During this investigation it was modified to also contain additional pressure probes, located as shown in Fig. 2-4.

The inlet support stand was designed to allow the inlet to turn about its axis and allow the inlet's height above the ground to be varied. The stand is shown in Fig. 2-5, with the range of height variations from H/D = 5/6 to H/D = 15/6 indicated.

2-4 COORDINATE SYSTEM

It is necessary to define a coordinate system to be adopted throughout this report. A right hand coordinate system has been established, as shown in Fig. 2-6. Mean flow is generated by the wind tunnel propeller or fan. The X-coordinate is normal to mean flow and in the ground plane, the Y-coordinate is normal to both the ground and the mean flow and the Z-coordinate is in the flow direction. The X-Z plane is thus the ground plane. The X-axis is also defined so that zero is at the inlet lip (which coincides with the center of the ground plane) and

the positive X direction is towards the right (looking upstream). Ninety degrees of yaw is when the inlet faces in the negative X-direction.

It is also necessary to define locations on the inlet. A cylindrical coordinate system has been established, as shown in Fig. 2-7. The x-coordinate is the axial direction, zero being at the lip, the positive x-direction is into the inlet. The R-coordinate is the radial distance from the center. The θ-coordinate refers to (degree) angle position around the inlet, 0 deg, is defined as directly upstream when the inlet is at 90 deg of yaw and the θ angles increase in the clockwise direction when looking in the positive x-direction. Thus 90 deg is the top of the cylinder and 270 deg is the bottom.

2-5 FLOOR AND INLET MODIFICATIONS

It was important to try to achieve dynamic and kinematic similarity between the inlet model and a jet engine. The first of these implies that one has turbulent separation over the inlet. This occurs because the Reynolds number for an engine operating on an airfield is a factor of ten larger than the inlet model in the wind tunnel. In addition, preliminary testing of the model at a tunnel velocity of 6 m/sec showed that the flow was in the transition regime and was hence sensitive to very small surface nonuniformities.

To achieve closer correspondence to aircraft engine conditions, it was also desired to increase the velocity ratio U_i/U_e from previous tests. In order to do this without decreasing U_e it was necessary to position the inlet so that the connecting ducting (inlet/diffuser) had no bends, thereby allowing a higher flow rate to be achieved. The

position of the inlet inside the wind tunnel was also influenced by another key point of the quantitative measurements, which was to measure only the circulation associated with the flow over the inlet. Thus the growth of the boundary layer on the tunnel floor had to be minimized.

With these three features in mind, turbulent separation, increased inlet velocity, and a thin tunnel boundary layer, several modifications were made from the configuration described in [5]. The inlet was positioned such that the flexible hose connecting the fixed ducting and the inlet stand would be both straightened and significantly reduced in length, increasing the inlet velocity to 135 m/sec. The length of the ground plane was also decreased. The modified floor and model positions inside the wind tunnel are shown in Fig. 2-8.

The problem of inducing turbulence in the boundary layer on the inlet was also re-examined. (Previously a 2.3 mm diameter rod had been used as a "trip" wire.) Several methods were tried. First, a 50% porous screen was inserted upstream to create increased freestream turbulence. The screens available, however, produced a velocity shear and hence were unacceptable.

Three types of "tripping" strips were examined, a metal strip with a serrated edge, a metal strip with wood wedges, and two different sized rods. The performance of each trip was judged by plotting the change in Cp ($= P_i/(1/2\ \rho U_e^2)$), at a tap located at 87 deg, as the tunnel velocity was increased. The results are shown in Fig. 2-9. Since the inlet velocity was zero and the pressure tap was two diameters from the lip (thus reducing end effects), the flow was similar to that about a circular cylinder.

Experimental data of flow about a circular cylinder reported by Schlichting [8] is shown in Fig. 2-10. Comparing Figs. 2-9 and 2-10 it can be seen that 1.5 mm tripping wire (with the auxiliary fan) was the most effective tripping device.

In summary, maintaining separation and velocity ratio similiarity led to facility modifications. The first was to make the ground plane shorter and to install the inlet stand along the axis of the blower ducting. The second was decreasing the trip wire diameter and using the auxiliary fan.

In the new configuaration, a study was made of the boundary layer and the mean flow shear at the inlet position. The purpose of this study was to verify that the boundary layer was thin and to assess the amount of ambient sharp shear in the velocity profile. Detailed measurements of the boundary layer and the mean flow were therefore not necessary. It can be seen in Fig. 2-11 that the boundary layer thickness is considerably less than the height of the bottom of the inlet (12.7 cm). Figure 2-12 shows that the mean flow at the inlet height is reasonably uniform, with only a slight total pressure variation across the wind tunnel test section.

2-6 FLOW MEASURING INSTRUMENTS

Several types of flow measuring probes were used during this experiment. These include three-hole pitot tubes, Kiel probes, prism and hemispherical five-hole pitot tubes and a hot wire anemometer. A description of their calibration is included in Appendix A.

The three-hole probes and kiel probes were used inside the inlet near the wall to determine flow angle and total pressure respectively.

This enabled the velocity magnitude and yaw angle to be determined.

Five-hole probes were used to determine the velocity magnitude and two flow angles. The prism five-hole probe was used to make a (nearly) diametric traverse across the inside of the inlet.

A hemispherical five-hole probe was used in the trailing vortex region. The probe was used to measure the velocity magnitude and direction at points on a grid 2.5 diameters from the inlet model. Motorized X (horizontal) and Y (vertical) traversers were used to position the probe at the desired points. Figure 2-13 shows the probe set-up in the wind tunnel. A description of the equipment is included in Appendix B. The vertical traverse is mounted on the horizontal traverse which is held by Unistrut beams installed along the sides of the wind tunnel. The vertical traversing unit also had a motorized rotator which could rotate the probe in the X-Z plane (yaw plane). Rotating the probe became necessary when the yaw of the oncoming flow was out of the ± 30 deg. range of the calibration for the probe.

All of the stepping motors for the traversing and rotating units were operated manually from the wind tunnel control room. The range of the vertical traverse was 0.2 m but by manually raising the units the required range of 0.56 m could be obtained.

The hot wire anemometer was used to measure the wind tunnel floor boundary layer.

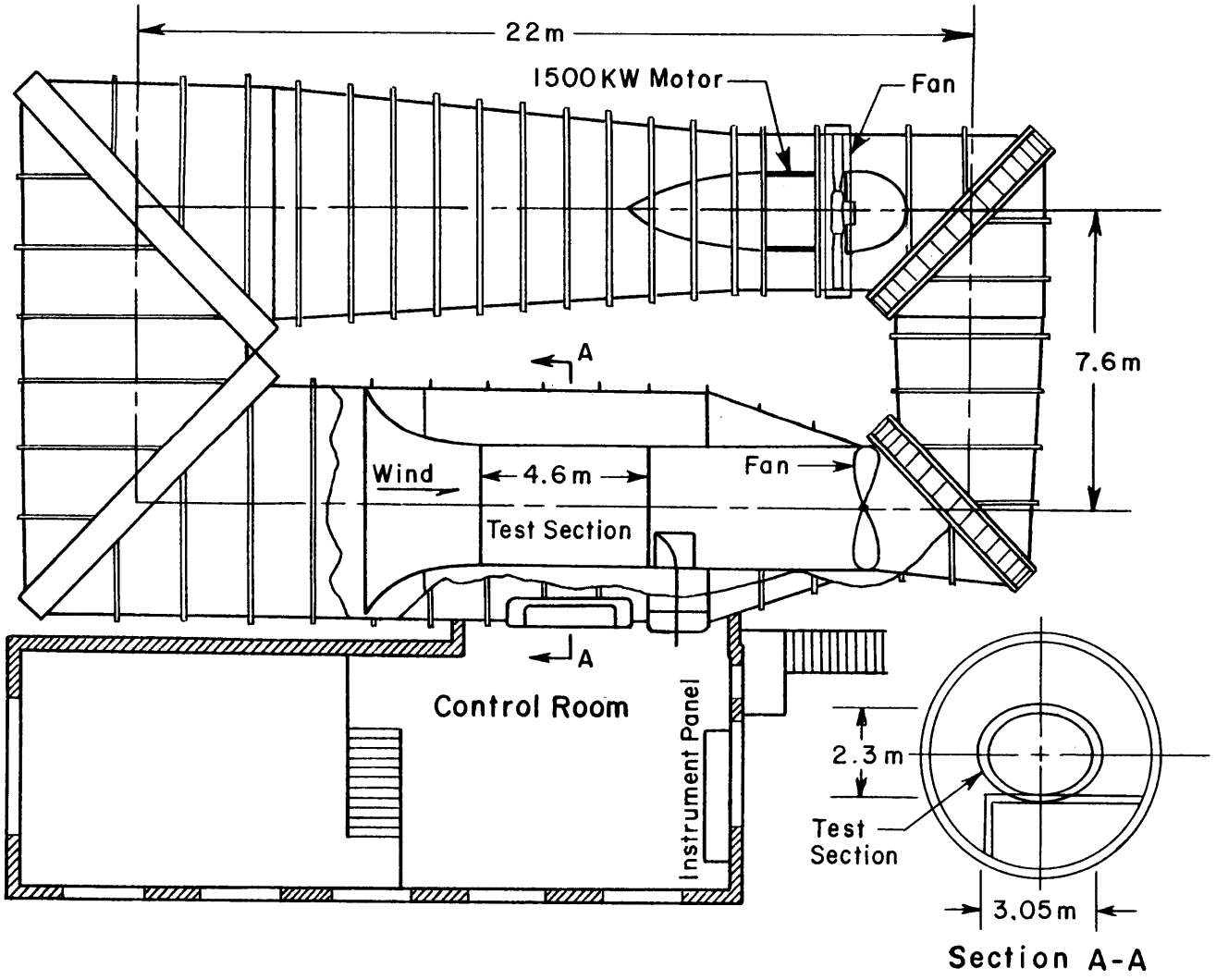

Figure 2-1 Schematic diagram of Wright Brothers Wind Tunnel

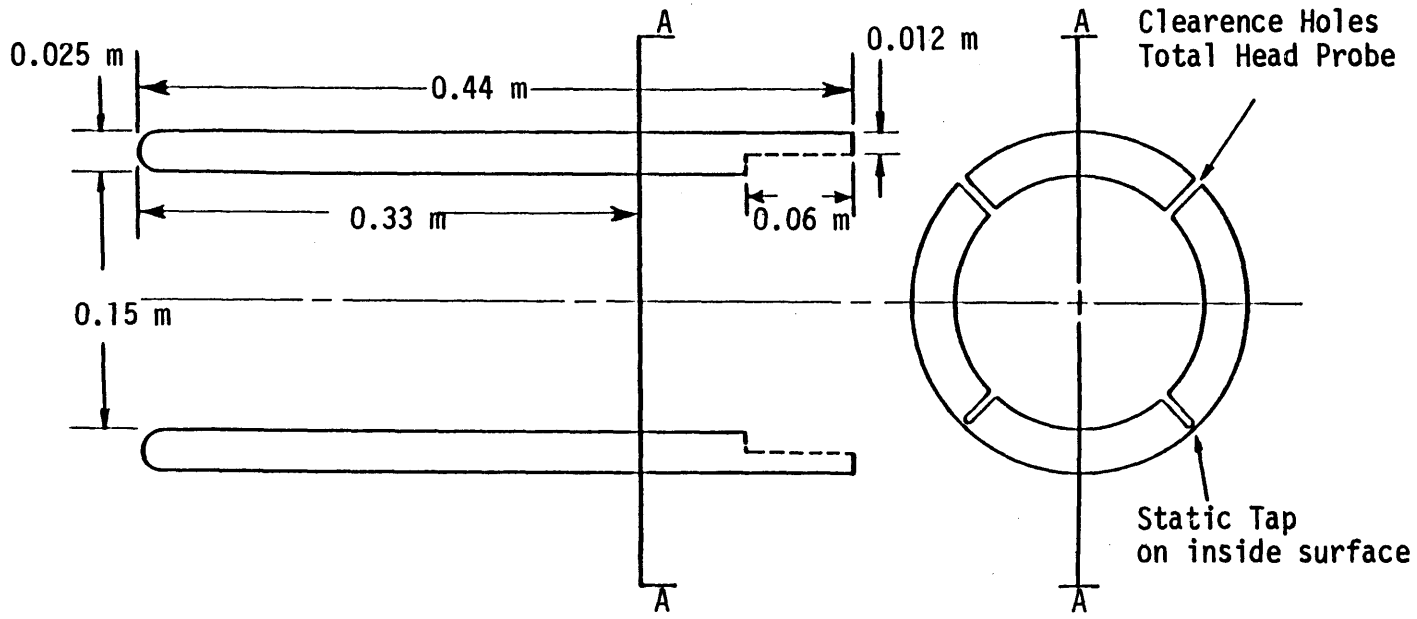

Figure 2-2 Inlet model (plexiglass) [5]

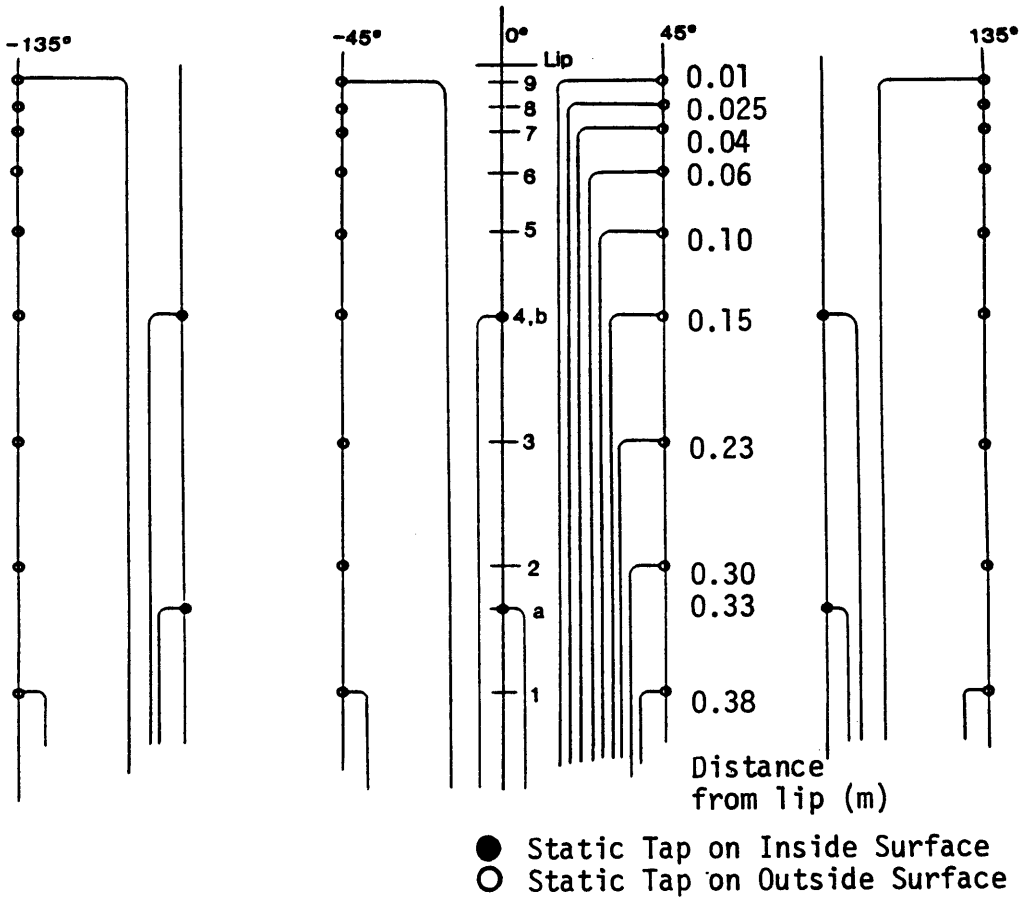

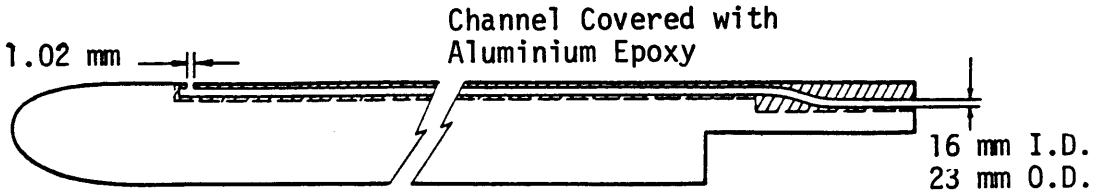

Figure 2-3 Location and construction of static pressure taps on aluminum inlet model [5]

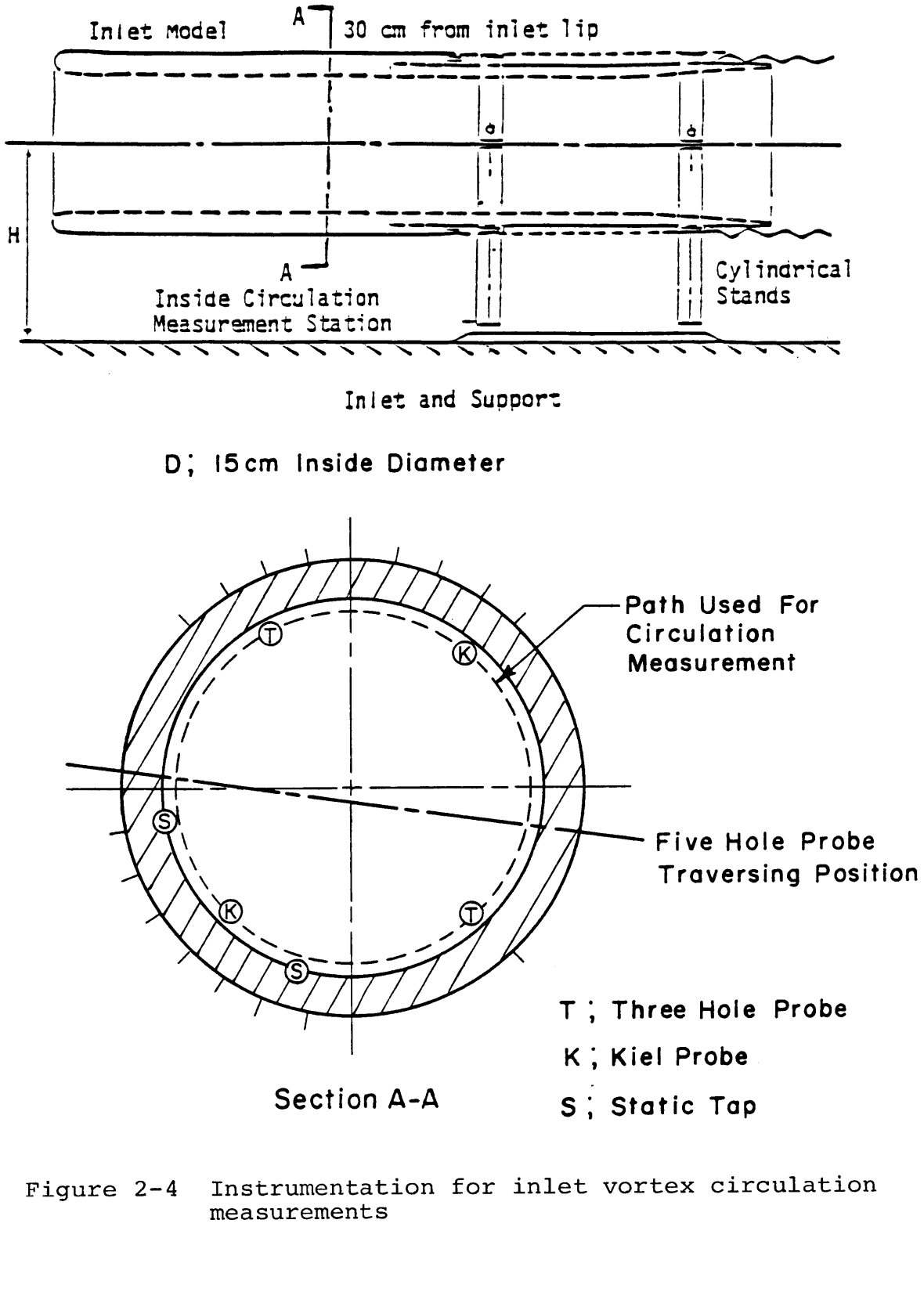

Figure 2-4 Instrumentation for inlet vortex circulation measurements

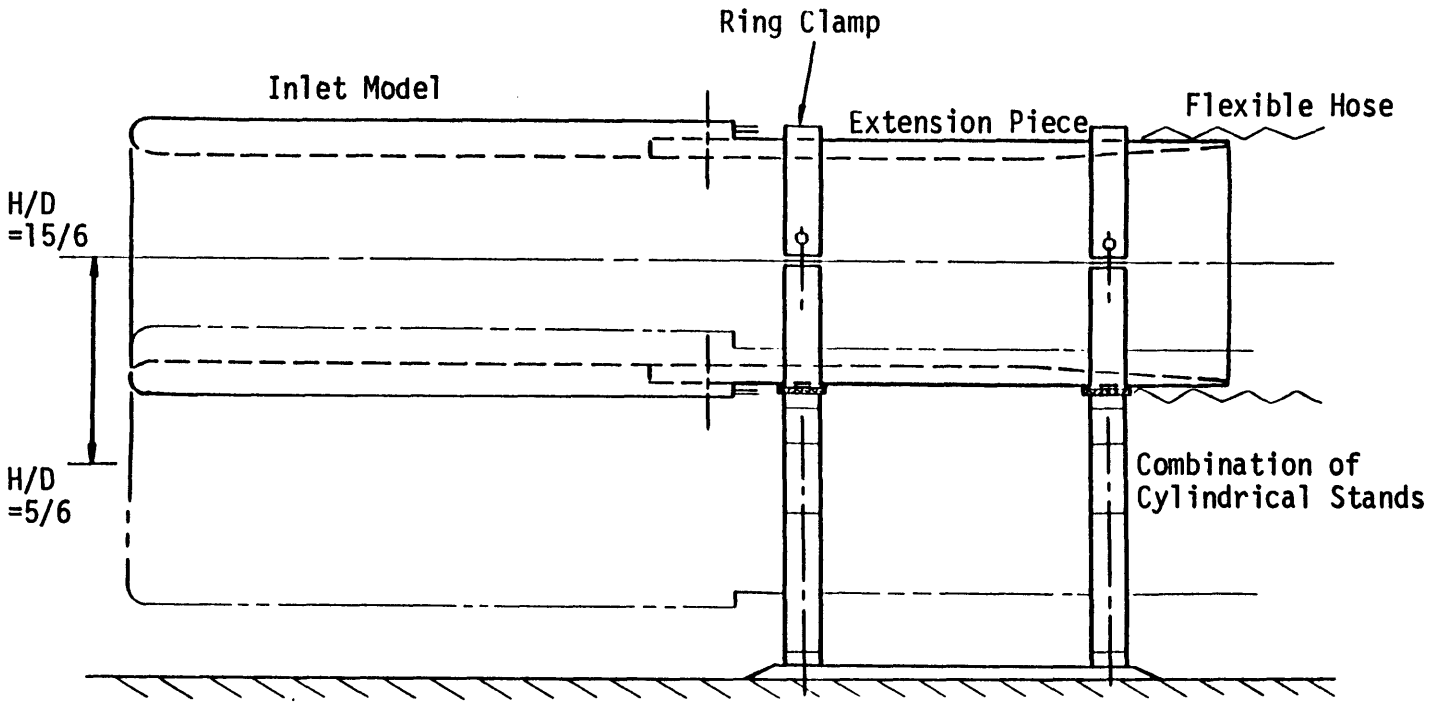

Figure 2-5 Inlet and support

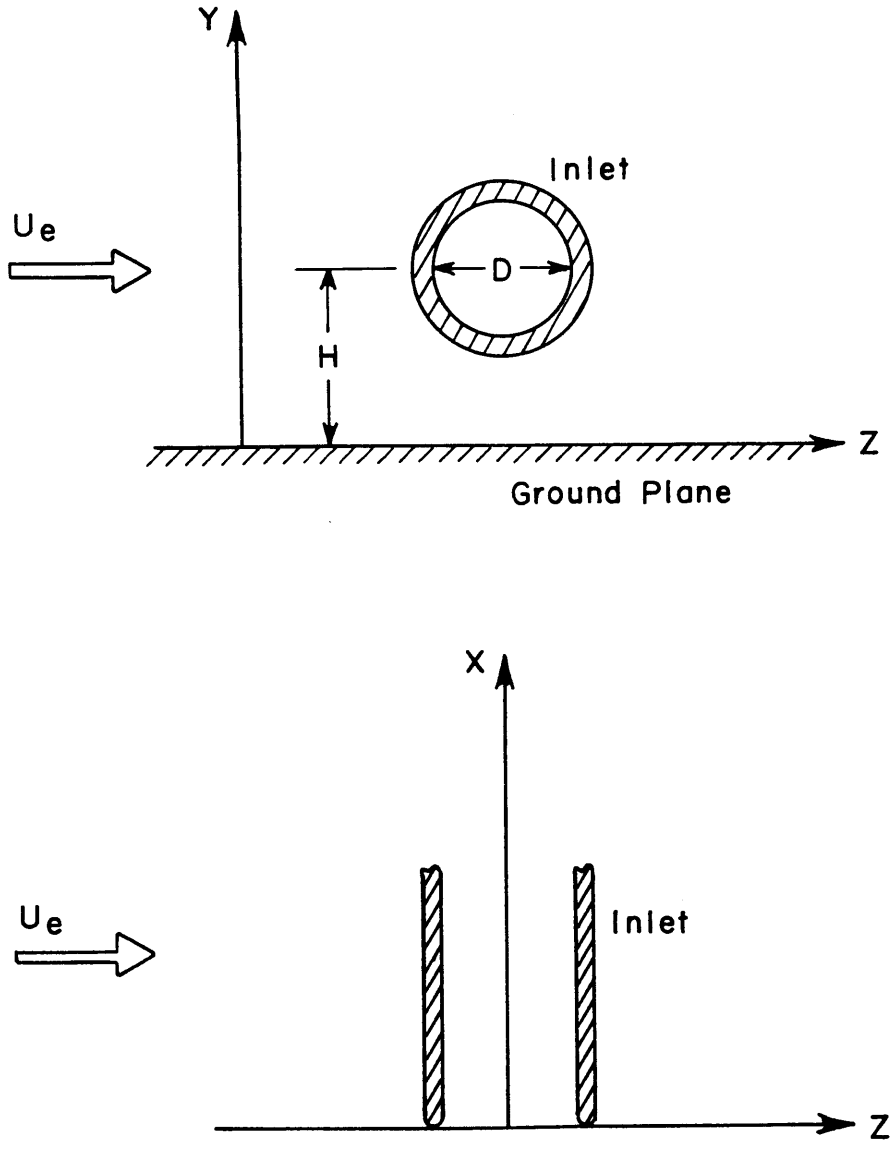

Figure 2-6 Flow coordinate system

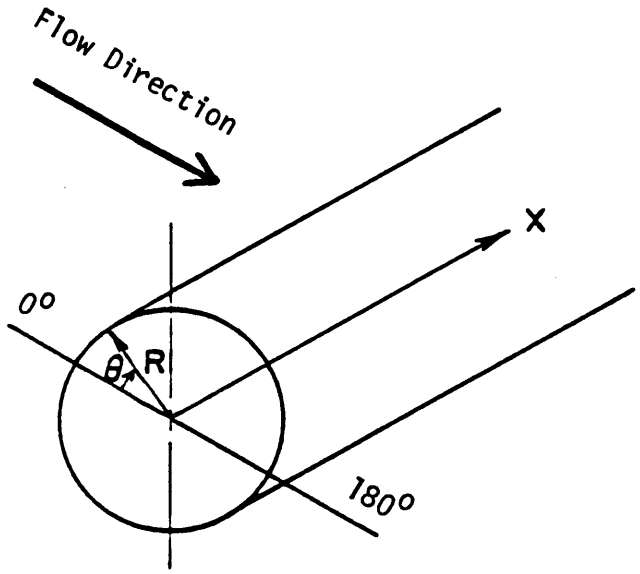

Figure 2-7 Inlet cylindrical coordinate system

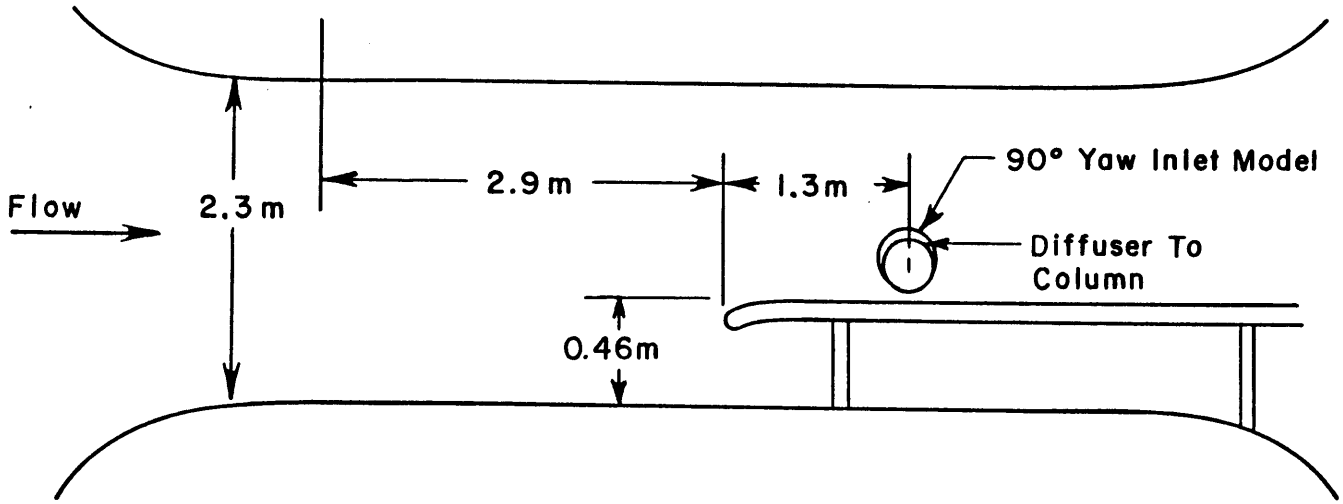

Figure 2-8 Schematic diagram of wind tunnel test section

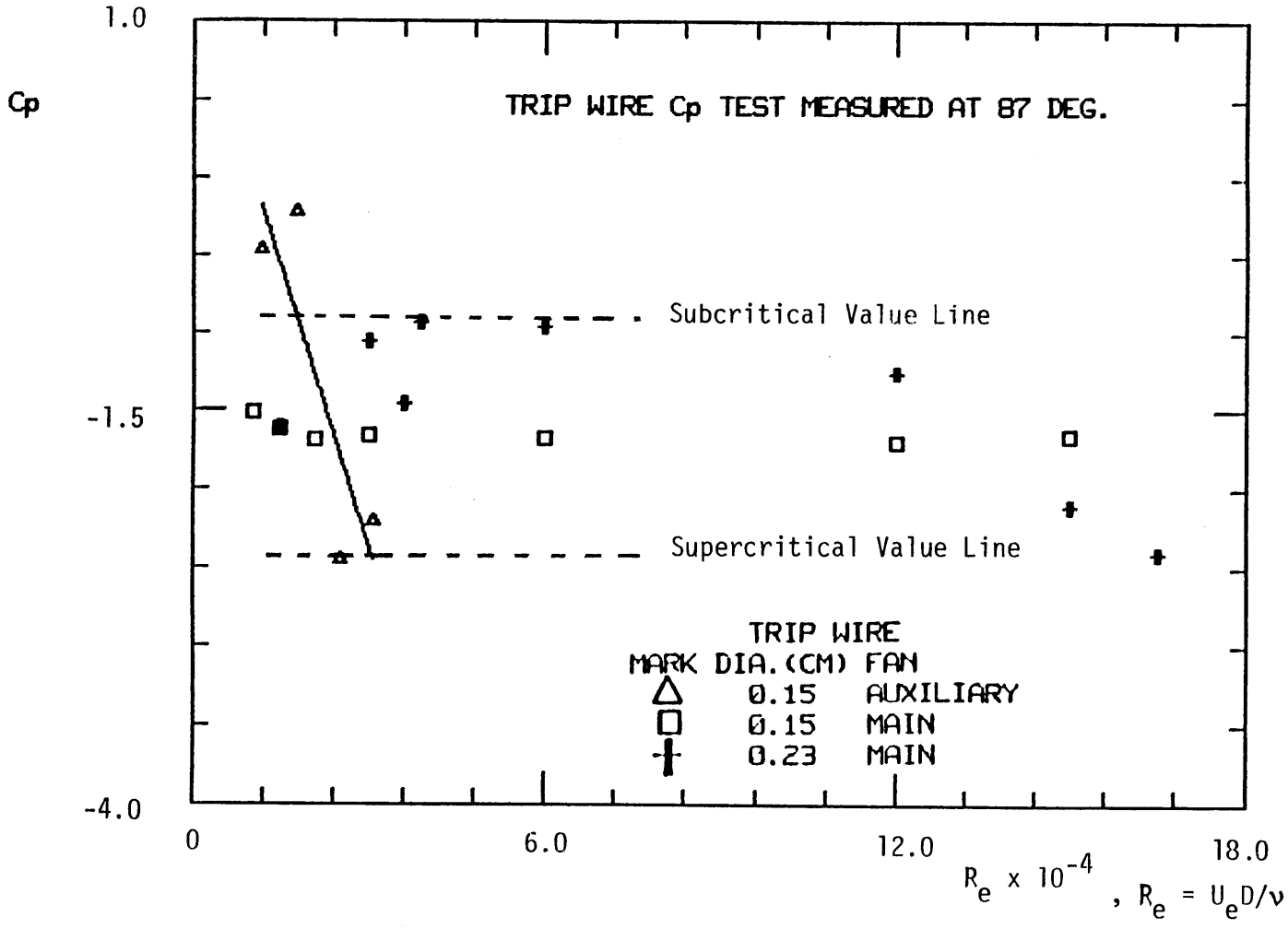

Figure 2-9 Pressure distribution at 87° position on inlet for increasing Reynolds number for three "tripping" wires

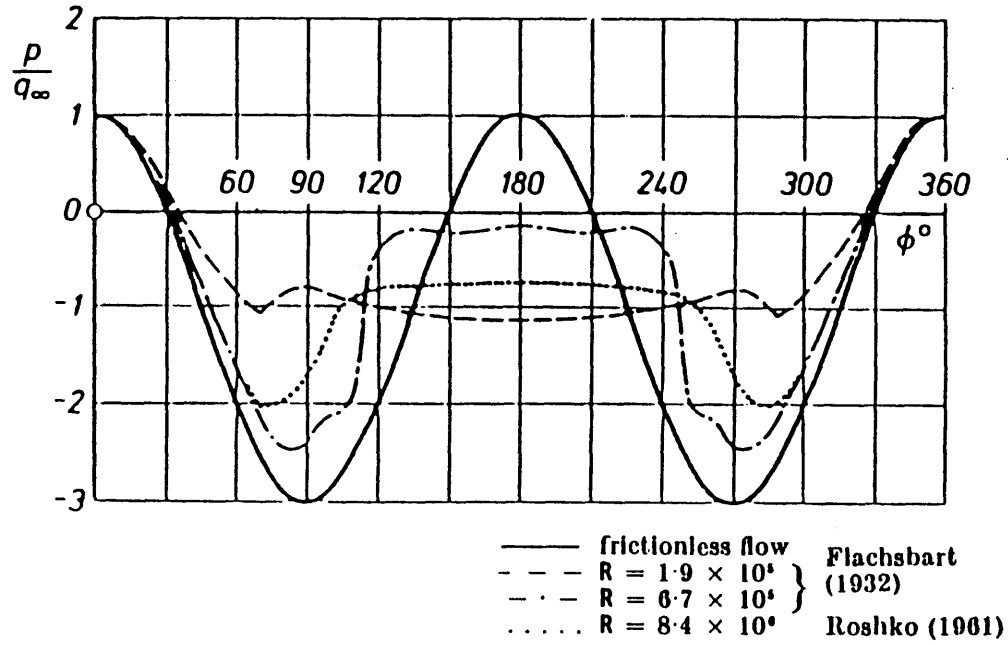

Figure 2-10 Pressure distribution on a cylinder in subcritical and supercritical range of Reynolds number. $q^{\infty} = 1/2\ \rho\ U_e$ is stagnation pressure of oncoming flow [8]

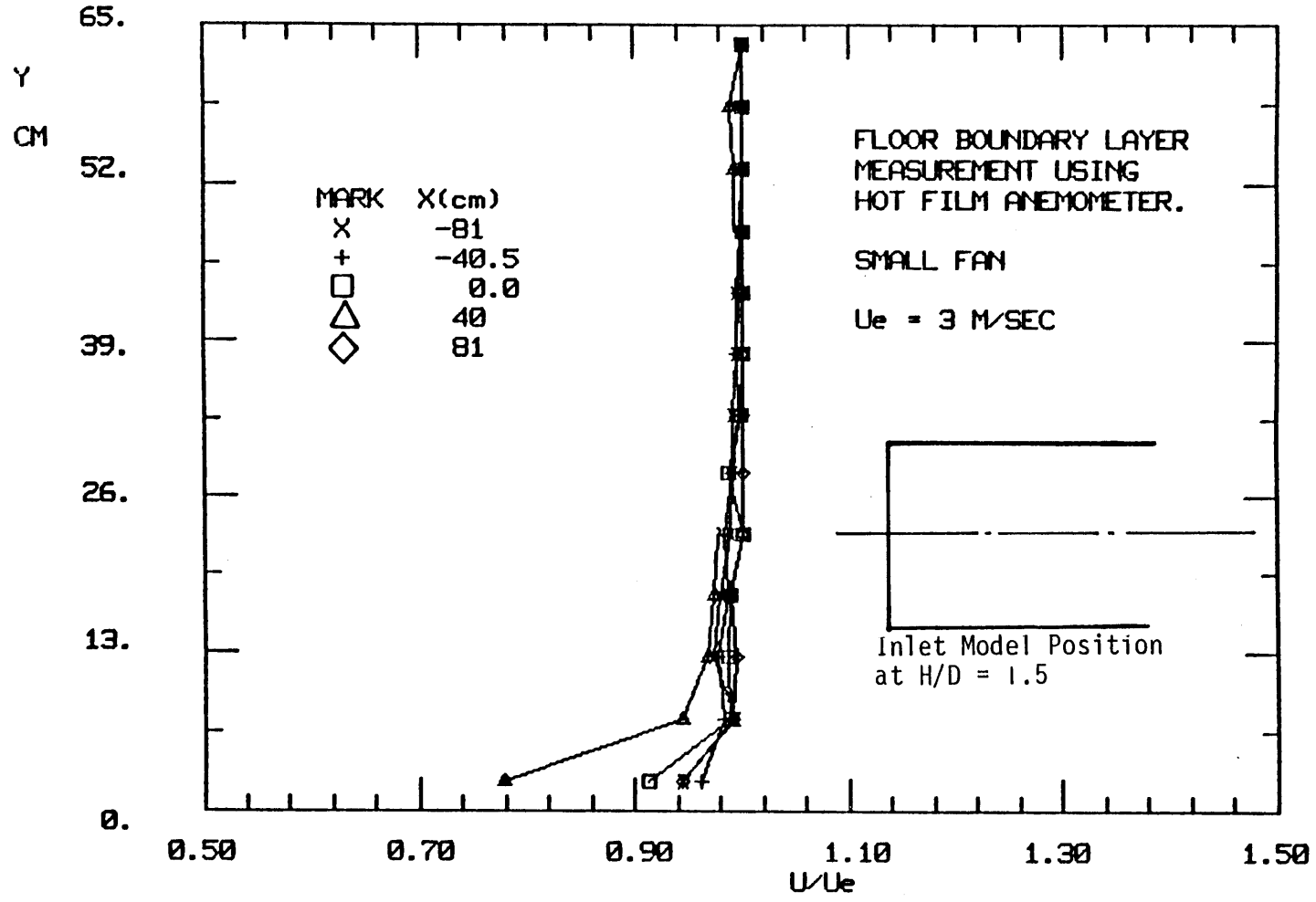

Figure 2-11 Total pressure distribution in wind tunnel boundary layer at 90 cm downstream from floor leading edge

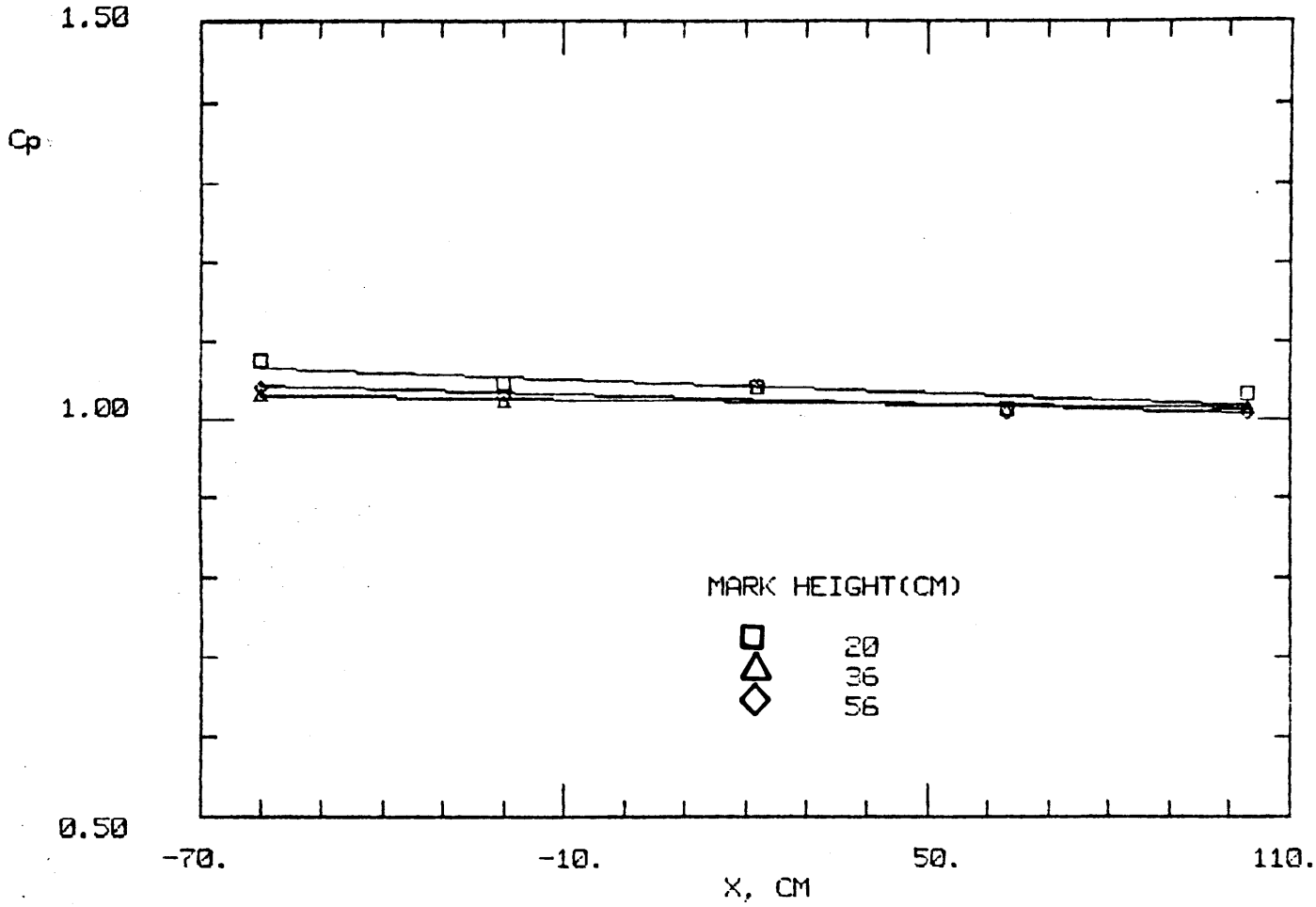

Figure 2-12 Total pressure distribution across wind tunnel at 90 cm downstream from floor leading edge

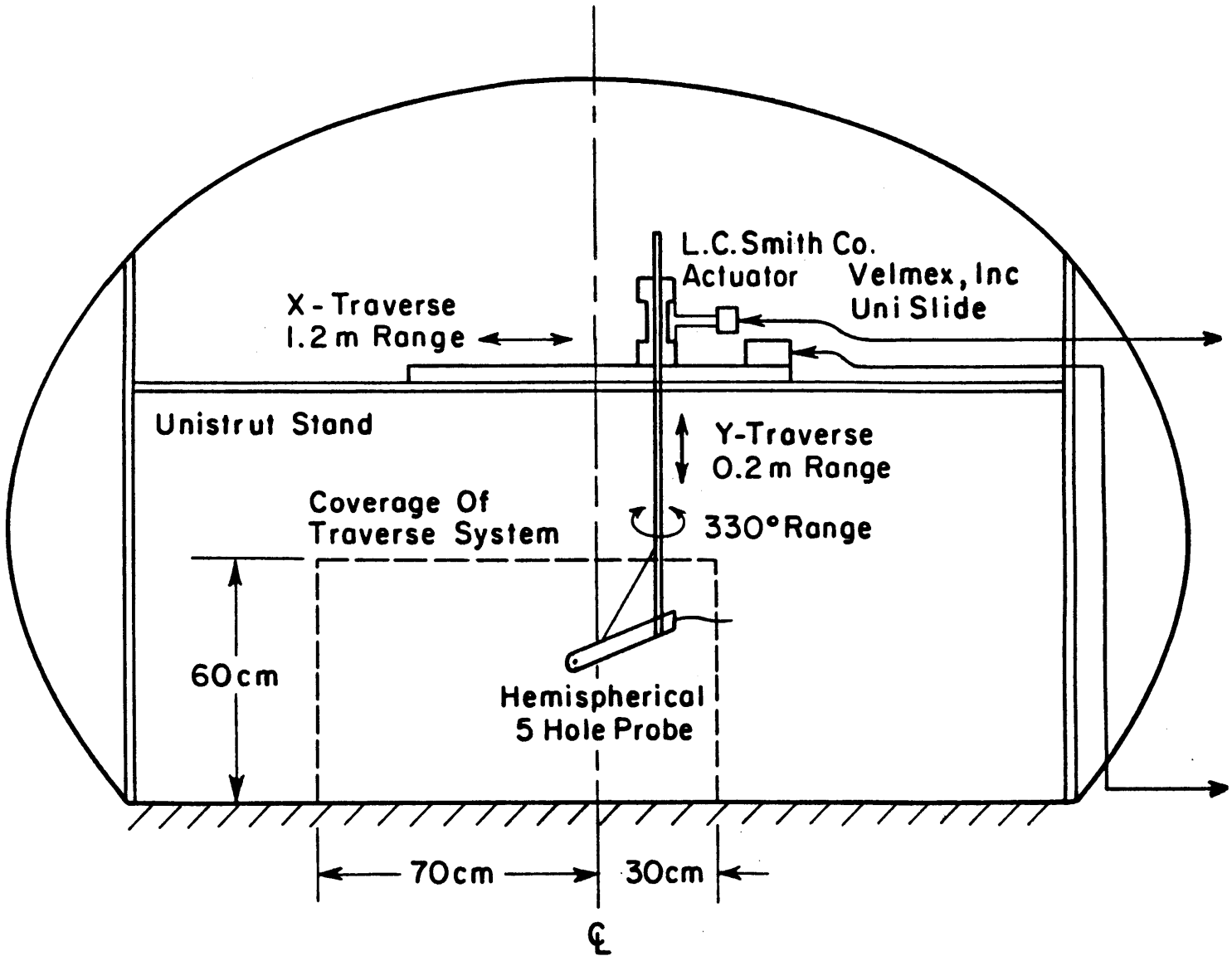

Figure 2-13 Trailing vortex traverse measurement system

CHAPTER III

COMPARISON OF INLET AND TRAILING VORTEX STRENGTHS

As stated the features of the vortex system associated with an inlet in a cross flow have previously only been studied qualitatively. The purpose of this investigation was to obtain quantitative data on the vortex system characteristics. The central questions concern the strength and location of the vortices. The vortex strength may be obtained by determining the velocity around a closed path enclosing the vortex, and then (numerically) doing a line integral to give the circulation. The location of the vortices may be determined from the measured velocity field (i.e., large peripheral velocity implies proximity to the vortex core) and from flow visualization.

The existence of two vortices, an inlet and a trailing one, had been recognized previously and it was hypothesized that the two vortices necessarily had circulations that were essentially equal and opposite. In order to compare the circulation, velocity measurements were taken along two contours, one around each vortex. The circulation around the inlet vortex was measured inside the inlet at a location two diameters from the lip. Such measurements were possible because, if viscous effects were small, the circlation around the inlet vortex would be constant and the circulation of the vortex inside the inlet would be the same as that of the ground vortex. The circulation of the trailing vortex was measured about 3 diameters downstream of the inlet. The locations for the measurements were selected so that (as much as could be achieved) they enclosed all the vorticity (of the particular vortex of interest) without including

vorticity from other sources. In particular, a major concern was to avoid including boundary layer vorticity. All of the vortex velocity measurements were done using multi-hole pressure probes.

The test condition for the study was chosen primarily to have the vortices located so that there were measurement paths that avoided boundary layer vorticity, as well as to have a strong vortex so the effects to be measured would be large. It was desired to position the inlet vortex far from inlet inside surface and position the trailing vortex high above the ground plane in order to avoid boundary layer vorticity. Extensive smoke visualization showed that (for constant velocity ratio) as H/D was increased from 1.0 to 1.75 both the inlet and trailing vortices moved slightly away from the boundary surfaces. Therefore, H/D = 1.5 and U_i/U_e = 45 was chosen for the testing conditions.

3-1 INLET VORTEX MEASUREMENT

The inlet vortex circulation was calculated by integrating the velocity vectors around a closed path inside the inlet. It was found from measurement that there were two vortices inside the inlet. The first one, located at the lower half of the inlet at about the 6.5 o'clock position, is the inlet vortex. The second one, located at the upper half of the inlet at approximately the 2 o'clock position, is connected to the trailing vortex. To obtain the circulation of the inlet vortex, therefore, a half moon shape contour is chosen with the straight segment nearly diametrically across and the circumferential segment at a radial location of 0.6 cm from the inlet wall.

The axial location of the contour was chosen to be two diameters, 30 cm, from the inlet lip to avoid potential flow effects on the velocity field (i.e. to avoid measuring large opposite-signed contributions to the line integral that would tend to cancel each other). The potential flow effects are due to the flow turning at the lip and the associated pressure variation.

Positioning the pressure measuring probes at 0.6 cm from the inlet wall was a compromise to achieve two conflicting conditions. One was to have the probes close to the wall so that flow could be considered two dimensional, having axial and circumferential components only. (A two dimensional flow was preferred because the flow angle could then be accurately determined with a three-hole probe.) The second condition was to make the velocity measurements outside of the boundary layer so that vorticity from the boundary layer would not be included in the contour.

Using a flat plate turbulent boundary layer calculation, the boundary layer thickness 30 cm from the lip is estimated to be 0.6 cm. This value could be considered a conservative estimate of the boundary layer thickness. Using a potential flow calculation of a vortex inside a cylinder, the radial velocities lead to pitch angles less than 5 deg at this radial location. Thus, at the location 0.6 cm from the wall, the probes would see a nearly two-dimensional flow.

The velocity along the path was determined by the combined use of a three-hole probe, a Kiel probe and a wall static tap on the inlet inner surface. The three-hole pressure probe was used to determine the flow angle. The difference between the total pressure, determined from the Kiel

probe, and the measured static pressure yields the dynamic pressure which can be used to determine the absolute velocity. (In point of fact, the velocities found using this procedure and using only the three-hole probes agreed very well.)

The magnitude and direction of the velocity was determined at 45/8 deg increments around the inlet by using two sets each of three-hole, Kiel, and static probes and rotating the inlet in 45/4 deg increments. The increments were machined onto the inlet using an indexer, which is accurate to 0.1 deg. The location of the probes inside the inlet is shown in Fig. 2-4. The probes were positioned such that as the inlet was rotated through 360 deg one of each probe type would measure at each of the 64 locations. Measuring in this fashion assumes that the vortex is stationary because the flow angle, total pressure and static pressure measurements for one location are done at different times. An averaging period of 8 seconds was used for the probe measurements (four cycles of 2 second averaging) at each tap. With an 8 second averaging it took about 1-1/2 hours to take the data for the 64 locations.

Flow visualization has shown that the inlet vortex is located near the bottom of the inlet, around the 6:00 position (as seen looking at the inlet as the face of a clock). A cross-diameter traverse was thus done to enclose the lower half of the inlet. The velocity along this diametrical traverse was determined with a prism five-hole probe. The probe was inserted into the inlet as shown in Fig. 2-4. Since the contribution from this traverse could be estimated to be small the probe was manually incremented across the inlet in 1.27 cm steps (as opposed

to the 0.75 cm increments around inlet circumference).

The circumferential velocity around the inside of the inlet 0.6 cm from the wall is shown in Fig. 3-1. The figure is a view looking into the inlet, with the freestream velocity coming from the left to the right. The ground is not shown. This data represents the average at each point of three runs, and is the combination of the two sets of three-hole, Kiel, and static probes. Two separate figures for the individual sets of probes are shown in Fig. 3-2. The most striking result of the circumferential velocity measurement is the existence of a second area of large tangential velocity, indicating a second vortical region at the 2:00 position.

The region at the bottom of the inlet, at roughly 6:30, is associated with the inlet vortex which has a clockwise sense of rotation. This vortex is readily observed in visualization experiments. The second region, at 2:00, has a counter-clockwise sense of rotation. It has not been observed in the previous flow visualization studies, although our hypotheses about the structure of the vortex system around an inlet have implied its presence.

A graph of the tangential velocity non-dimensionalized with the inlet velocity (U_i) versus circumferential angle is shown in Fig. 3-3. The solid line is a Fourier curve fit through the average of the data at each point. The curve fit uses the first 20 terms of a Fourier expansion that describes a curve passing through the data points. From this, the circumferential locations corresponding to maximum tangential velocity (at 0.6 cm from the wall) can be approximately determined. The

location of the maximum tangential velocity induced by the inlet vortex is at 287 deg (± 6 deg) and for the weak vortex, at 147 deg (± 6 deg). The location of the maximum tangential velocity is the location where the vortex core is closest to the wall. The core location, which is a function of axial distance from the lip, can be described by a radial distance from the wall and a circumferential angle. Therefore, the maximum tangential velocity is useful for estimating one coordinate of the core location.

Three runs were done to investigate the repeatability as well as the accuracy of the measurements, and the results, presented in a non-dimensionalized tangential velocity vs circumferential angle graph, are shown in Fig. 3-4. Numerical integration of the velocity (along a path from 191 deg to 5 deg) showed an 11% difference between runs.

A first check on the plausibility of the measured tangential velocities was made by comparing them with tangential velocities determined from a theoretical calculation. The calculation, described in Appendix C, is based on two-dimensional rotational inviscid flow in a cylinder. It was found that by choosing appropriate values of the parameters needed for the calculation, the tangential velocities calculated fit the experimental data very well, indicating that the data was consistent with what was theoretically expected.

The assumptions, which had led to positioning the probes at 0.6 cm from the wall 30 cm from the lip, were checked for validity. These assumptions were that with the probes so placed they would be away from the influence of potential flow effects and out of the boundary layer;

this corresponds to a station where the static and total pressures are constant. This condition was studied by looking at the pressure distribution around the inside of the inlet for each run. Figure 3-5 shows a typical pressure distribution, with total pressure from the Kiel probes and static pressure from the static taps. It can be seen that the static pressure is nearly constant around the inlet indicating that the potential flow effects have decayed.

The value of the total pressure indicates whether the measurements had been taken in the boundary layer. From Fig. 3-5 it can be seen that there are two total pressure defect regions indicating that the probe possibly is inside the boundary layer in the two regions.

One total pressure defect, in the neighborhood of the inlet vortex, begins at 280 deg, reaches a maximum at 310 deg and ends at 360 deg. By comparing this with the fact that the maximum tangential velocity, where the (clockwise) vortex is closest to the wall, was at 287 deg, it appears that there is an upwash of boundary layer fluid due to the vortex. In other words, the flow induced by the vortex makes the boundary layer accumulate on one side of the vortex as indicated by the maximum defect at 310 deg. A similiar pattern is seen for the (counter-clockwise) second vortex. The pressure defect begins at 165 deg, reaches a maximum at 100 deg and ends at 85 deg, compared with the maximum tangential velocity which is at 147 deg.

This analysis of the pressure defects, boundary layer up-washing, explains the two defect regions. It also implies that there may not be one position near the wall where total pressure around the inlet would

be constant. Due to the measurement scheme it was not feasible to take data during one run at various distances from the wall. The 0.6 cm location, however, was considered adequate for the present set of experiments.

With the measuring probes inside the boundary layer, errors will be incurred in determination of the circulation due to the addition of boundary layer vorticity to the contour as well as from the decrease in velocity magnitude. To compensate for this, a simple velocity correction was examined. The correction amounted to using the average velocity magnitude in the region of constant total pressure (between 165 deg and 280 deg). This correction was small (amounting to a 3% increase of the uncorrected circulation), which in fact was smaller than the estimated experimental error. Thus, the effect of the total pressure defect was not significant here.

The specific closed contour that was used to measure the inlet vortex followed the inlet wall (0.6 cm away) from 191 deg to 5 deg and then (almost) diametrically across the inlet. The cross traverse was done with a prism five-hole probe. There was a discrepancy in the velocity measured by the five-hole probe and that calculated from the inlet mass flow of 8%, however this resulted in only a 1% difference in the circulation integration. Hence this error also is not considered significant, being an order of magnitude smaller than the estimated overall uncertainty (see below).

The velocity components in the direction of the contours are shown in Fig. 3-6. The circulation of the inlet vortex was calculated by

integrating the velocity, using the trapezoidal rule. The circulation for this case (H/D = 1.5, U_i/U_e = 45) was determined to be

$$\Gamma = 3.0 \text{ m}^2/\text{sec}.$$

The average of the integrations along the cross traverse was 0.4 m^2/sec and along the inside wall was 2.6 m^2/sec. The small velocity corrections mentioned above have been made in the pressure defect areas.

In order to ensure that the circulation did not depend significantly on axial position, the same circumferential velocity measurements were also made at 20 cm from the lip. Since the contours at 20 cm and 30 cm each enclosed the inlet vortex, and there is not any mechanism between the two locations that could cause appreciable decrease in circulation, it is expected that the two circulations measured should be equal.

The circumferential velocities (averaged from three runs) at 20 cm from the lip, are shown in Fig. 3-7. This appears much the same as Fig. 3-1 (measured at 30 cm). Figure 3-8 shows the non-dimensionalized tangential velocity versus circumferential angle for the the three runs at 20 cm. There is a slightly larger (15.8%) difference between runs in the velocity integration along 191 deg to 5 deg than there had been at 30 cm. (Recall that at 30 cm there was an 11% difference between runs in this integration.)

Figure 3-9 compares the average tangential velocity versus circumferential angle for both axial locations. The angle of the maximum tangential velocity associated with the inlet vortex is 275 deg at 20 cm and 287 deg at 30 cm, indicating a 12 deg (clockwise) shift

from 20 to 30 cm. For the weak counter-clockwise vortex, the angle of maximum tangential velocity shifts 5 deg counter-clockwise between 20 cm (152 deg) and 30 cm (147 deg). This shifting of the vortices can be explained as the interaction of the vortex and the wall. A simple estimation of the induced velocity due to the image vortex (using the radial position measurement described in Ch. 5) implies that the inlet vortex should drift 7 deg in 10 cm. This is reasonably consistent with the observed value.

The pressure distribution for the 20 cm location was also examined. The static pressure was nearly constant, indicating that by 20 cm the potential flow effects have essentially been eliminated. There were again two total pressure defect regions, similar to those at 30 cm location but to a lesser extent. The same correction procedure as that used at 30 cm was employed to correct for the velocities in the pressure defect regions.

The five-hole probe was traversed across the inlet and the velocities along the paths were integrated. The circulation at an axial location 20 cm from the lip was calculated to be

$$\Gamma = 3.1 \ m^2/sec.$$

The average of the circumferential paths was 2.7 m^2/sec (corrected velocities were used), and the average of the diametric traverses was 0.4 m^2/sec. Comparing this with the circulation reported for the 30 cm axial location (3.0 m^2/sec), there is 3% difference in circulation between locations, which is substantially less than the difference between individual runs. This result verifies that to the accuracy of

the measurement the contours enclose the same vortical fluid.

3-2 MEASUREMENT ERROR

The total error was estimated as follows. Appendix D describes the error associated with the data acquisition system in the Wright Brothers Wind Tunnel and estimates it at 1%. The wind tunnel mean flow velocity, measured by pitot tube through a baratron pressure meter, is determined to within 2% error which includes the unsteadiness of the tunnel flow (driven by the auxiliary fan) and the reading error from the digital DC voltmeter. The inlet velocity is calculated by obtaining 1) the static pressure in the inlet 2) the static pressure at a station upstream of the grid in the ducting, 3) the pressure drop across the grid, 4) atmospheric pressure and 5) the wind tunnel air temperature. By considering the effect of the unsteadiness of the inlet velocity (driven by the compressor) and the reading error on these measurements and the combination error from the calculation, the error involved in the velocity measurement is estimated to be 7%. Therefore the error in the circulation of the inlet vortex is evaluated to be 10% by summing the above-mentioned errors.

With these factors in mind, the circulation of the inlet vortex is

$\Gamma = 3.0 \pm 0.3 \ m^2/sec$

(at $H/D = 1.5$ and $U_i/U_e = 45$) where $U_e = 3$ m/sec.

3-3 TRAILING VORTEX MEASUREMENT

The trailing vortex circulation was calculated from a velocity map taken at a X-Y plane three diameters downstream of the inlet. Smoke visualization was used to determine at which plane to take the measurements. It was important to choose a plane far enough downstream

so that all of the trailing vorticity could be enclosed but not so far downstream that the vortex diffusion and interaction with the ground would be of concern.

At stations less than 2.5 diameters from the axis of the inlet a clearly defined trailing vortex could not be seen using smoke visualization. At a station more then four diameters downstream smoke visualization revealed that the vortex had widened to reach the ground. Interaction with the ground was undesirable for two reasons. One was that vorticity from the ground boundary layer would necessarily be included in the contour and the other reason was that boundary layer fluid would tend to accumulate along the edge of the contour, making it difficult to choose an appropriate integrating contour. From the visualization, a plane 3.3 diameters (50 cm) downstream of the inlet was chosen to make the measurements, a plane where the vortex was "rolled up" but not affected by the ground.

One item to note is that the contour was not done entirely in one X-Y plane. This is due to the fact that when the probe was rotated in the traversing mechanism (described in Ch. 2) the distance from the inlet to the probe head is changed thereby changing the X-Y plane where the measurement is made. This effect of changing planes is, however, included in the circulation calculation. At a few points along the contour the pitch of the oncoming flow was greater than 30 deg. which would be out of the range of the calibration for the five-hole probe if the probe were used with its axis horizontal. At those points it was necessary to use a motorized vertical stand in order to allow the pitch

angle to be (manually) adjusted so that probe could be used in its calibration range. The stand could also be easily positioned so that one X-Y plane was maintained even as the pitch angle was changed.

Since the trailing vortex is in the wake of the inlet where the flow was unsteady, it was necessary to choose an appropriate time averaging period. Frequency analysis of the wake showed a low frequency peak at 0.16 Hz. (It was this 6 second fluctuation that precluded the use of a nulling device to determine the flow angles and speed because the probe could not zero in this unsteady flow.) A repeatability study was made to determine a proper time averaging period. It was found that while 6 seconds appeared too short, the difference in standard deviations between 12 second, 18 second, and 20 second averaging was not enough to warrant using the longer times. Based on this, 12 second time averaging was used during data acquisition with the five-hole probe in the trailing vortex.

A velocity vector map was obtained using the five-hole hemispherical probe in the traversing mechanisms and using a 12 second time average on the pressure measurements. The velocity vector at each point was determined by using calibration curves (presented in Appendix A) and the averaged pressure measurements. Figure 3-10 shows the X and Y components of the velocity as seen looking upstream at the inlet, and the trace of the inlet is also shown. The region in the middle of the figure was not measured because wake effects are dominant in that region. However, the circulation calculation depends on the integral of the velocity along a contour enclosing the vortex and therefore the

velocities in this region are not necessary for determining the circulation. The majority of the points on the map were taken 3.3 diameters (50 cm) downstream of the inlet, but as previously mentioned those points where the probe had to be rotated, primarily along X=-25,-20,-15 cm between Y=23 and 53 cm, the probe was as close as 37 cm to the lip. The vertical stand was used in the region of X=51,56,61 cm between Y=23,38 cm.

The C_p ($C_p = Pt_{pitot} - P_t$ / $1/2\ \rho U_e^2$) distribution for the velocity grid is shown in Fig. 3-11. The total pressure was determined by the five-hole at the same position that the velocity was determined. The map shows the regions of high and low total pressure for the trailing vortex as seen looking upstream at the inlet. The map also indicates two different contours that were used for integrating the velocity to determine the circulation. The contours were chosen such that the total pressure was close to that of freestream ($C_p < 0.2$). At low C_p, it could be assumed that the fluid originated in the freestream (which had a slight non-uniformity inherent to the wind tunnel) and did not contain any vorticity from the boundary layer. From the velocity vector map (Fig. 3-10), it can be seen that both of these contours included nearly all the vorticity associated with the trailing vortex.

The circulation was calculated by integrating the velocity vectors around the closed contours using the trapeziodal rule. The circulation for trailing vortex was determined to be

$\Gamma = 3.0 \pm 0.3\ m^2$ / sec

(at H/D = 1.5 and U_i/U_e = 45, where U_e = 3 m/sec). The 10% error results from previously discussed measurement error. (The difference in circulation between the two contours was less than 1%.)

3-4 DISCUSSION

The hypothesis that the circulations of the inlet and trailing vortices should be nearly equal and of opposite sign was first presented in [3], and is illustrated in Fig. 3-12 (taken from [3]). The situation is as follows: the circulation round contour C_1 (Γ_1), which is far from the lip, is small. This requires that the net circulation round the inlet at any station along the inlet be small. Thus the circulation round C_2 (Γ_2), which encloses the inlet vortex, must be balanced by a circulation of opposite sign and comparable magnitude round the necessary trailing vortex.

The results presented in this paper verify this hypothesis. From static pressure measurements on the inlet, presented in Ch. IV, the circulation round the inlet at a station two diameters from the lip was determined to be small (0.03 m^2/sec). The velocity vector maps of the inlet and trailing vortices indicate that they have the senses of rotation illustrated in Fig. 3-12, that is the two are opposite in sign. The circulations calculated show that, within the limits of error of the experiment, the trailing vortex (Γ = 3.0 m^2/sec) is essentially equal in magnitude to the inlet vortex (Γ = 3.0 m^2/sec).

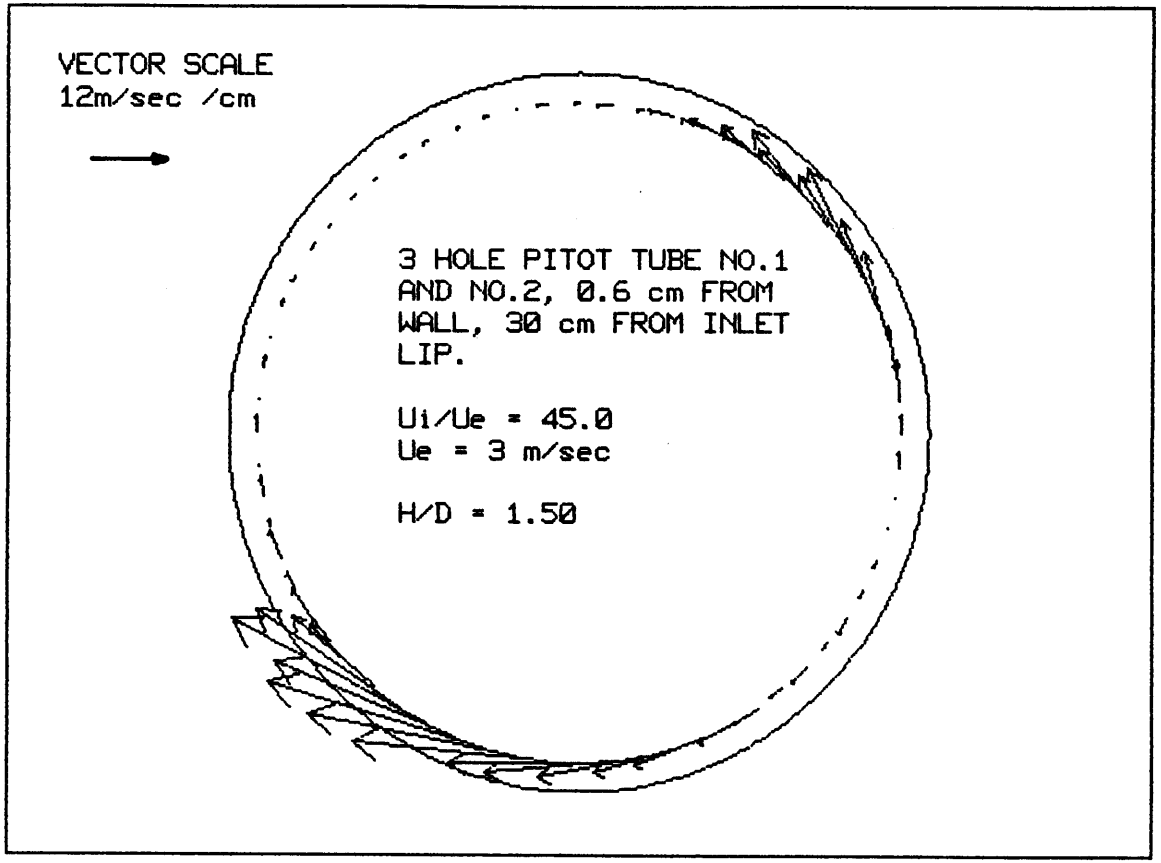

Figure 3-1 Tangential velocity distribution around inside inlet at positions 0.6 cm from wall at a station 30 cm from inlet lip, H/D = 1.5, U_i/U_e = 45

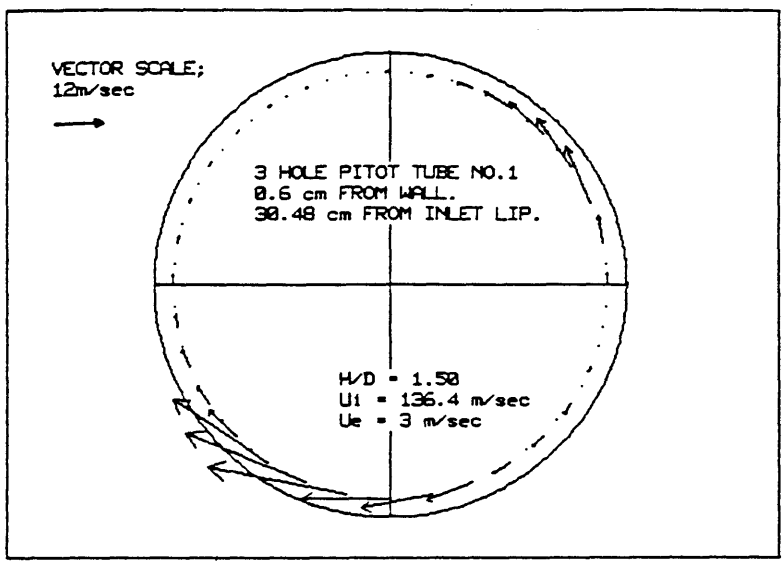

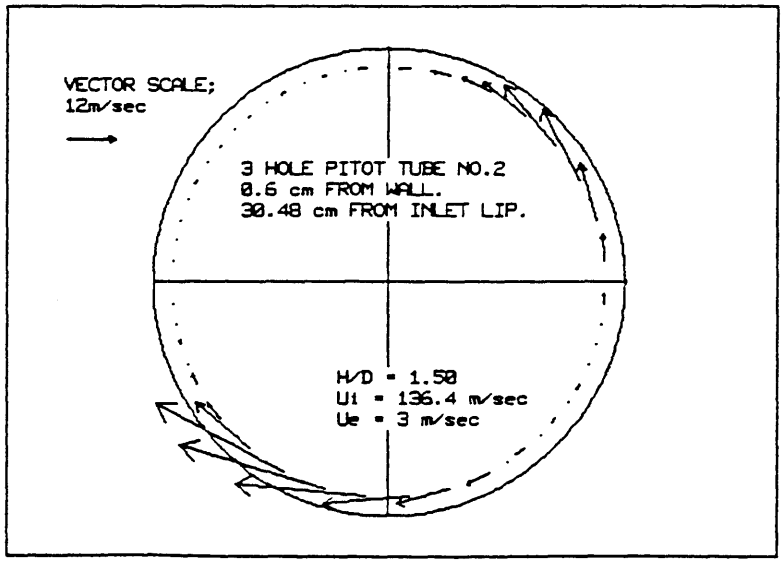

Figure 3-2 Tangential velocity distribution around inside inlet as determined by each set of probes, H/D = 1.5, U_i/U_e = 45

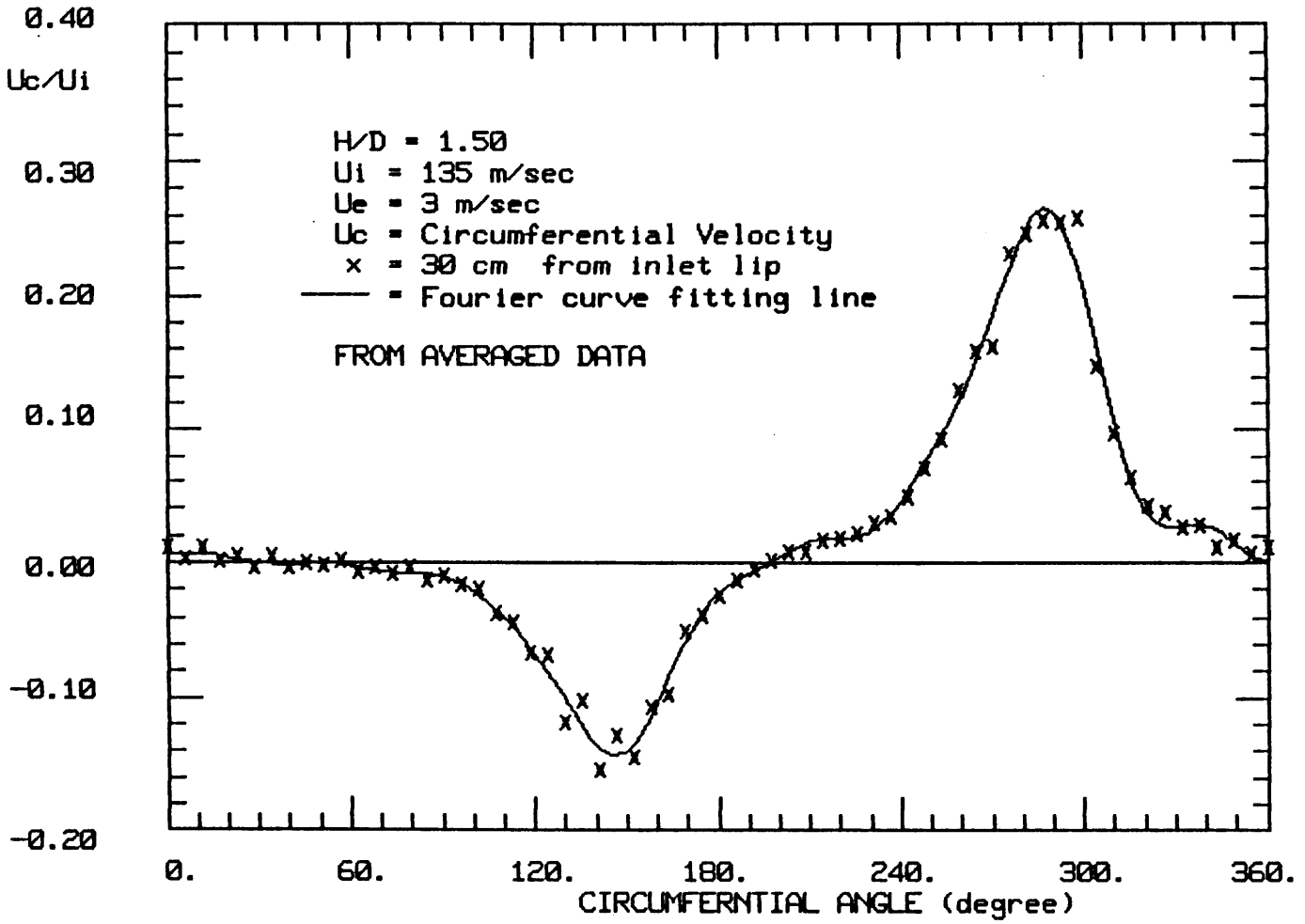

Figure 3-3 Tangential velocity distribution inside inlet, x = 30 cm, H/D = 1.5, U_i/U_e = 45

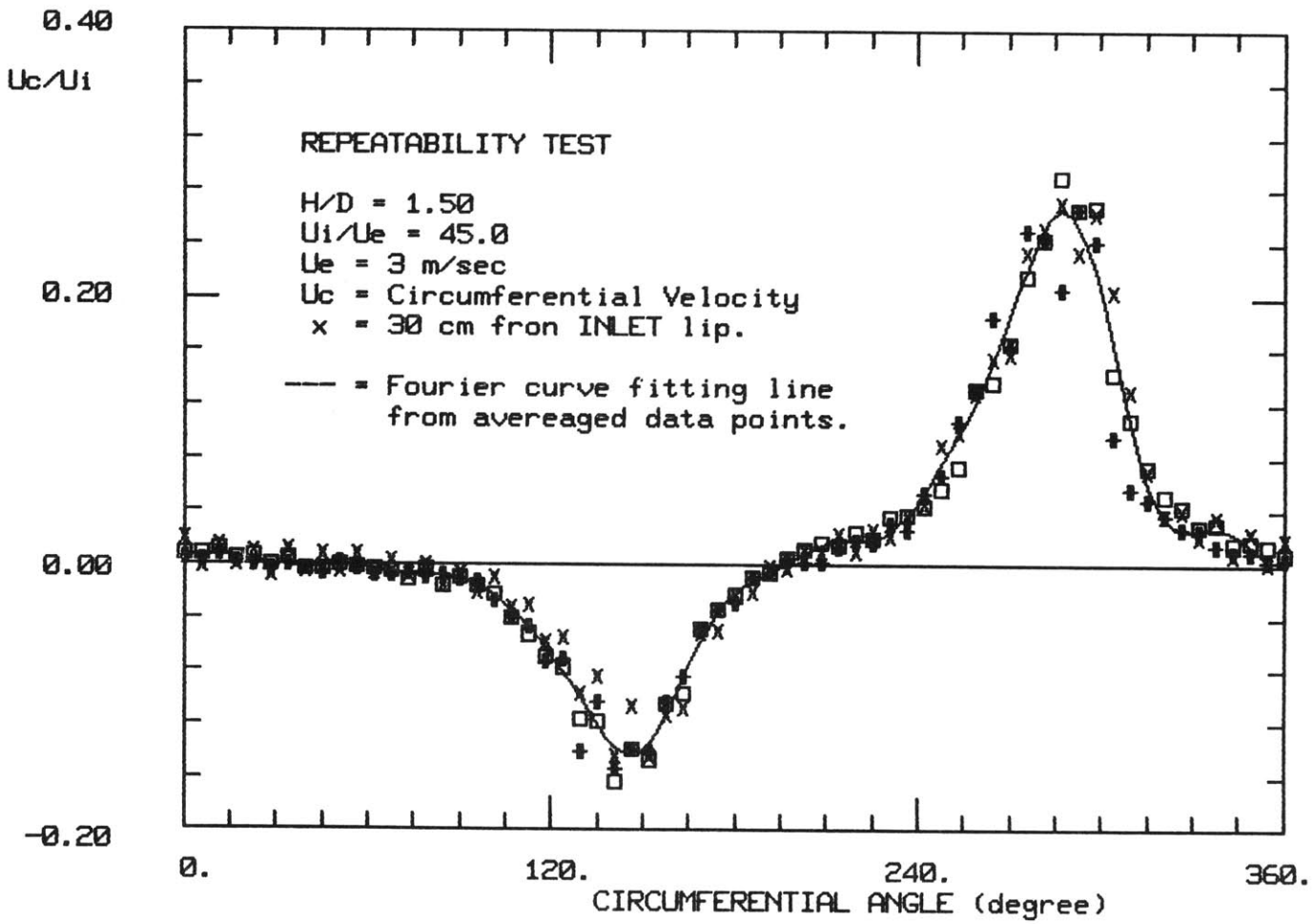

Figure 3-4 Repeatability of tangential velocity distribution inside inlet, x = 30 cm, H/D = 1.5, U_i/U_e = 45

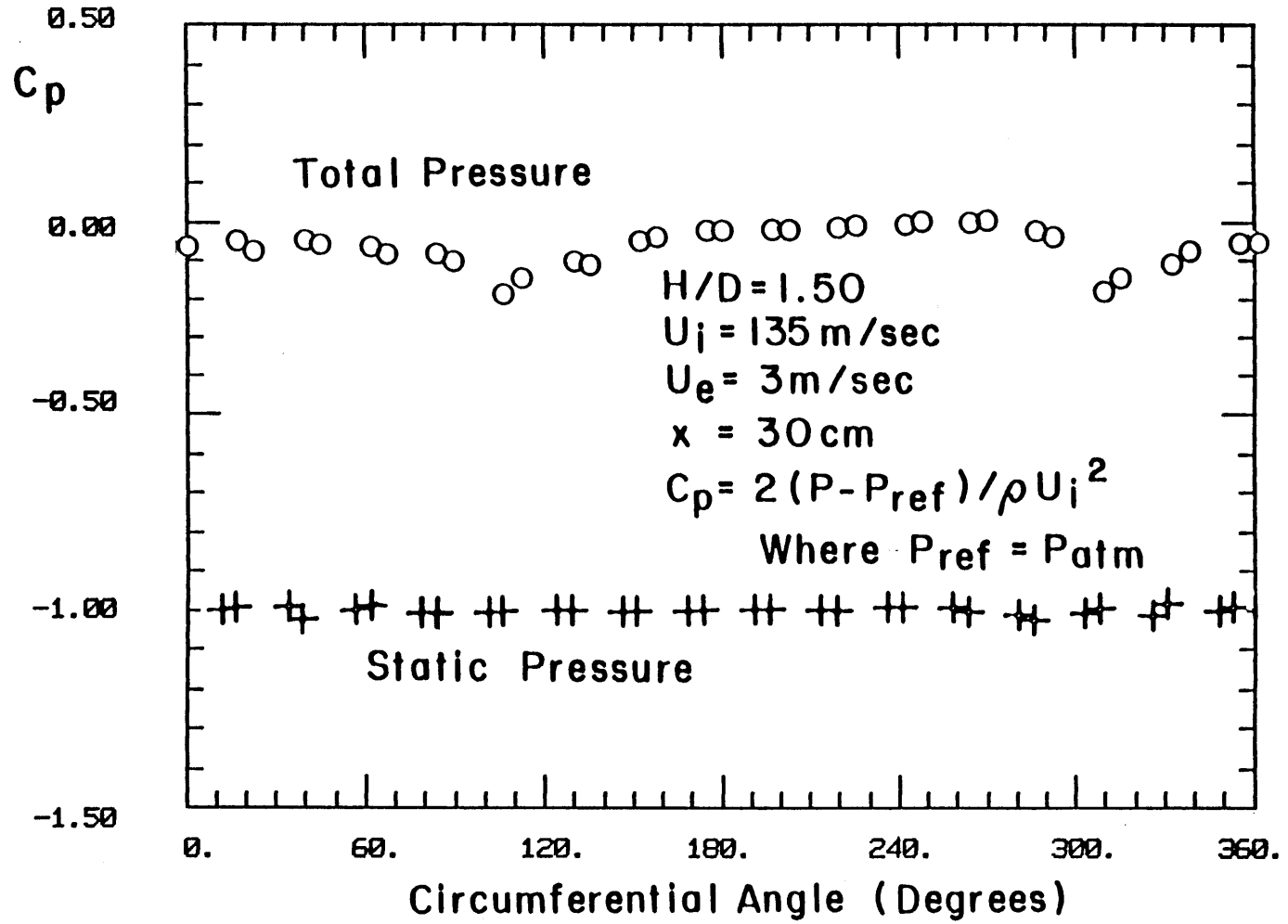

Figure 3-5 Total and static pressure distribution at 0.6 cm from wall and 30 cm from inlet lip

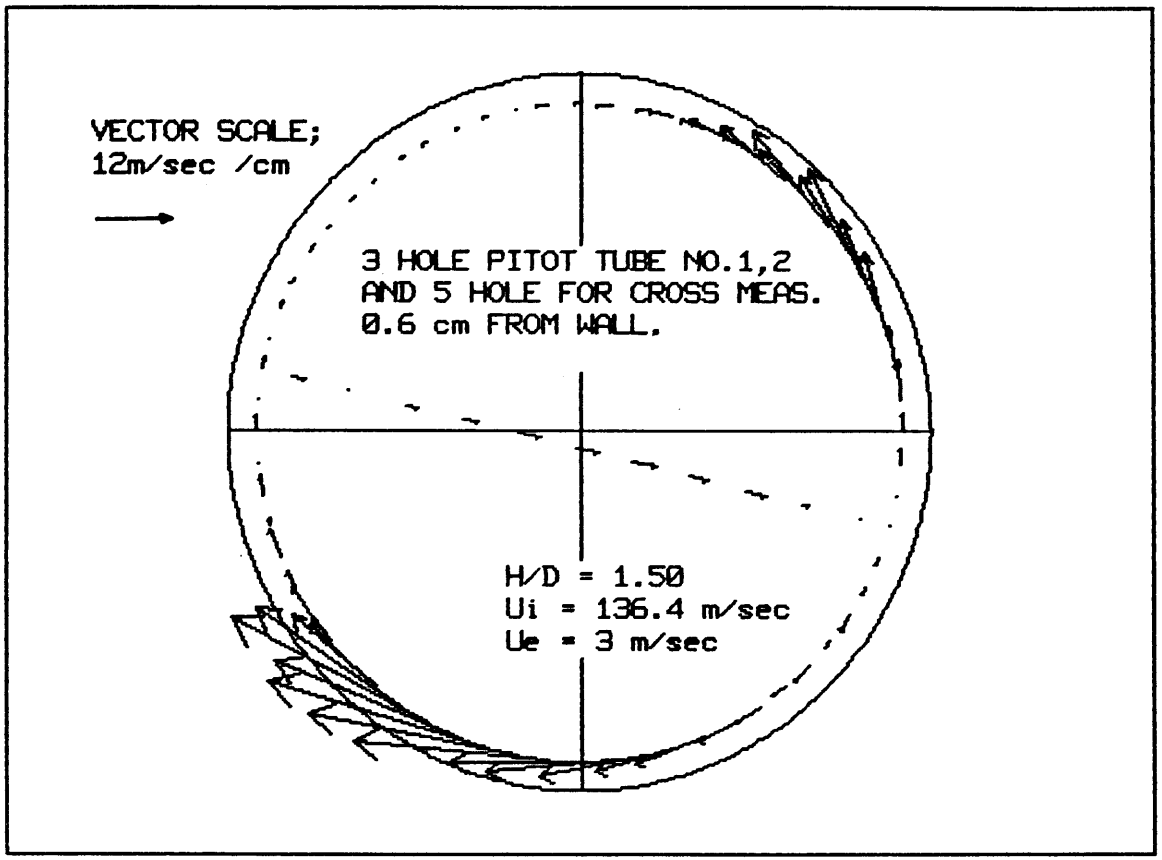

Figure 3-6 Tangential and traverse velocity distribution for circulation calculation 30 cm from inlet lip

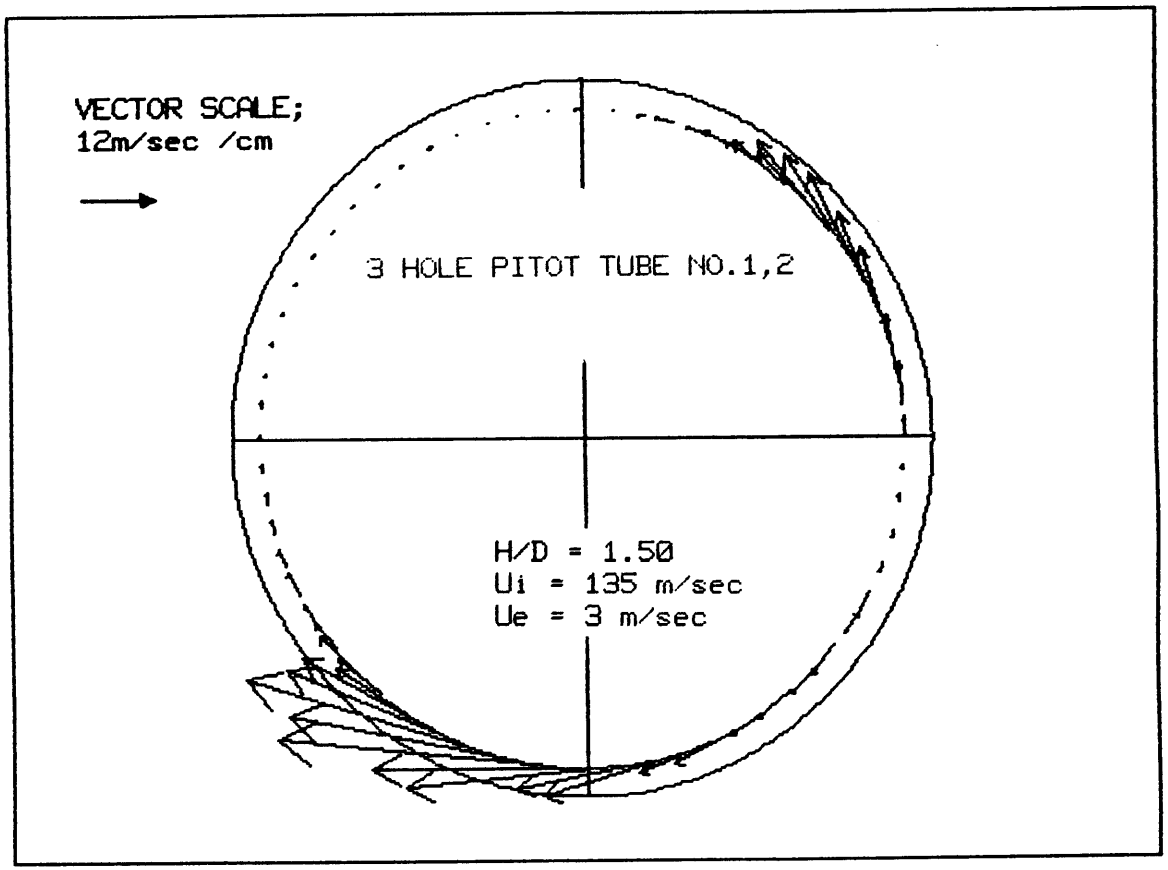

Figure 3-7 Tangential velocity distribution around inside of inlet at position 0.6 cm from wall at a station 20 cm from inlet lip, H/D = 1.5, U_i/U_e = 45

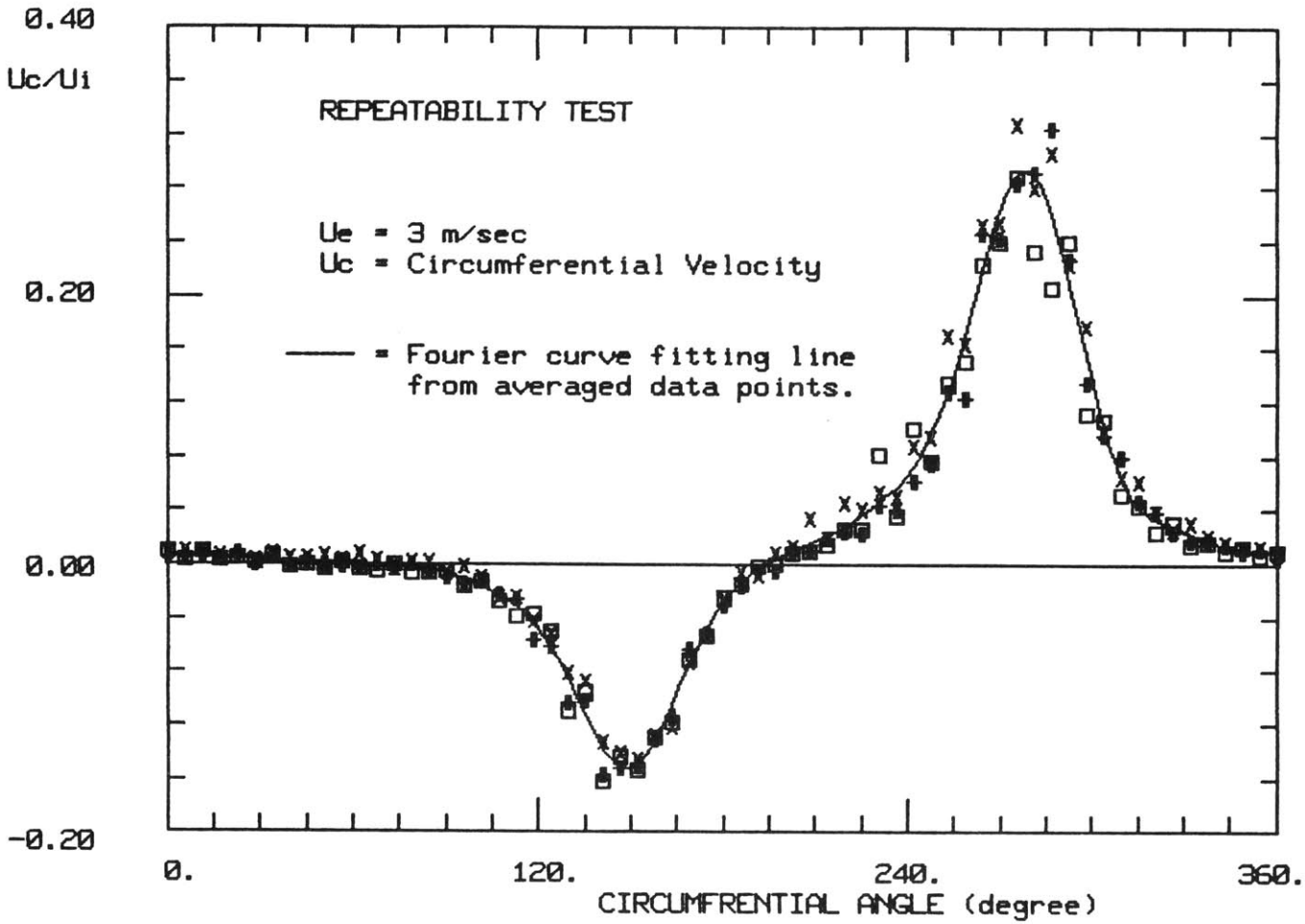

Figure 3-8 Repeatability of tangential velocity distribution inside inlet, x = 20 cm, H/D = 1.5, U_i/U_e = 45

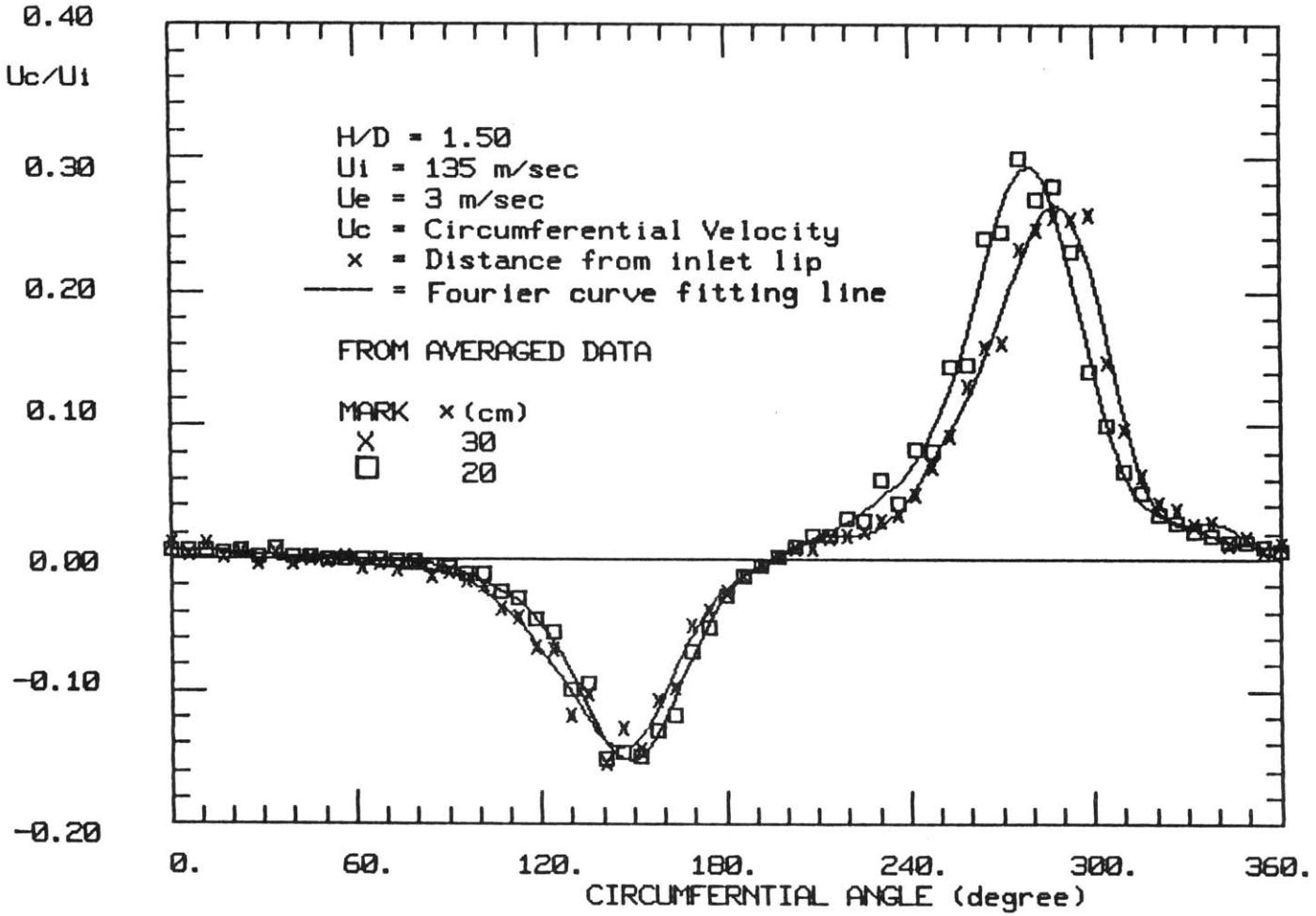

Figure 3-9 Comparison of tangential velocity distribution for x = 20 and 30 cm

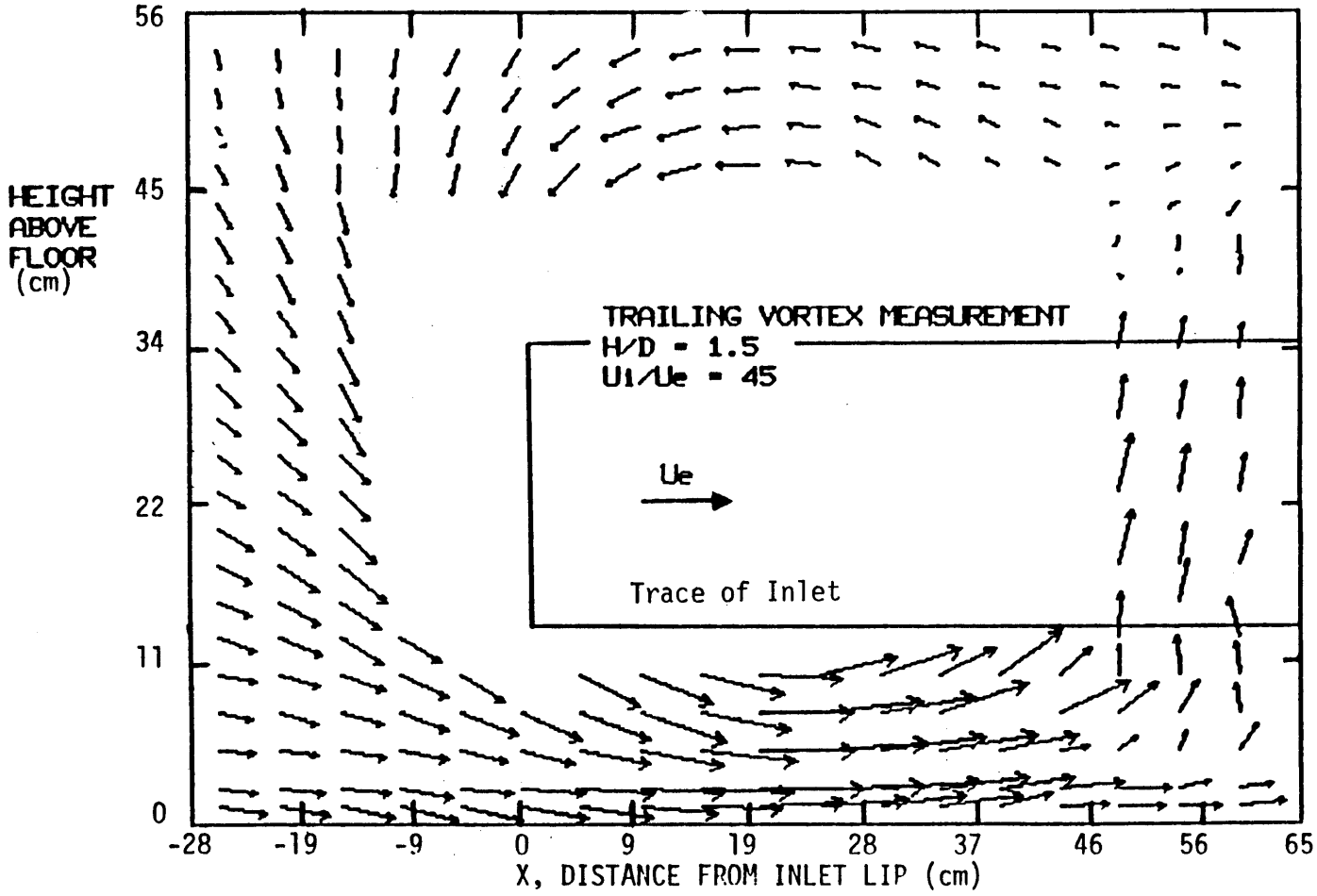

Figure 3-10 Trailing vortex velocity distribution in X-Y plane, Z ~ 50 cm

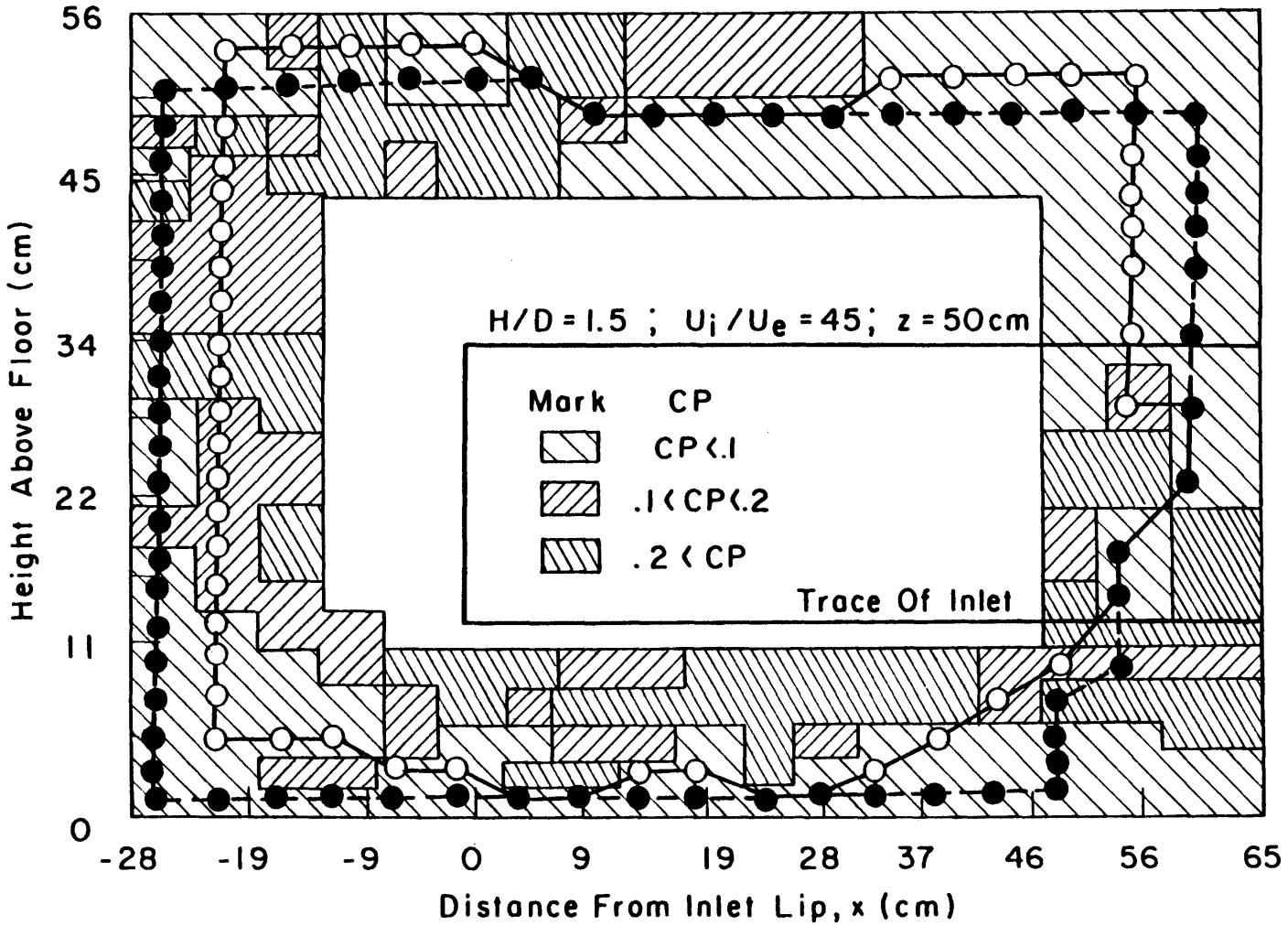

Figure 3-11 Trailing vortex pressure distribution and integrating contours, Z ~ 50 cm

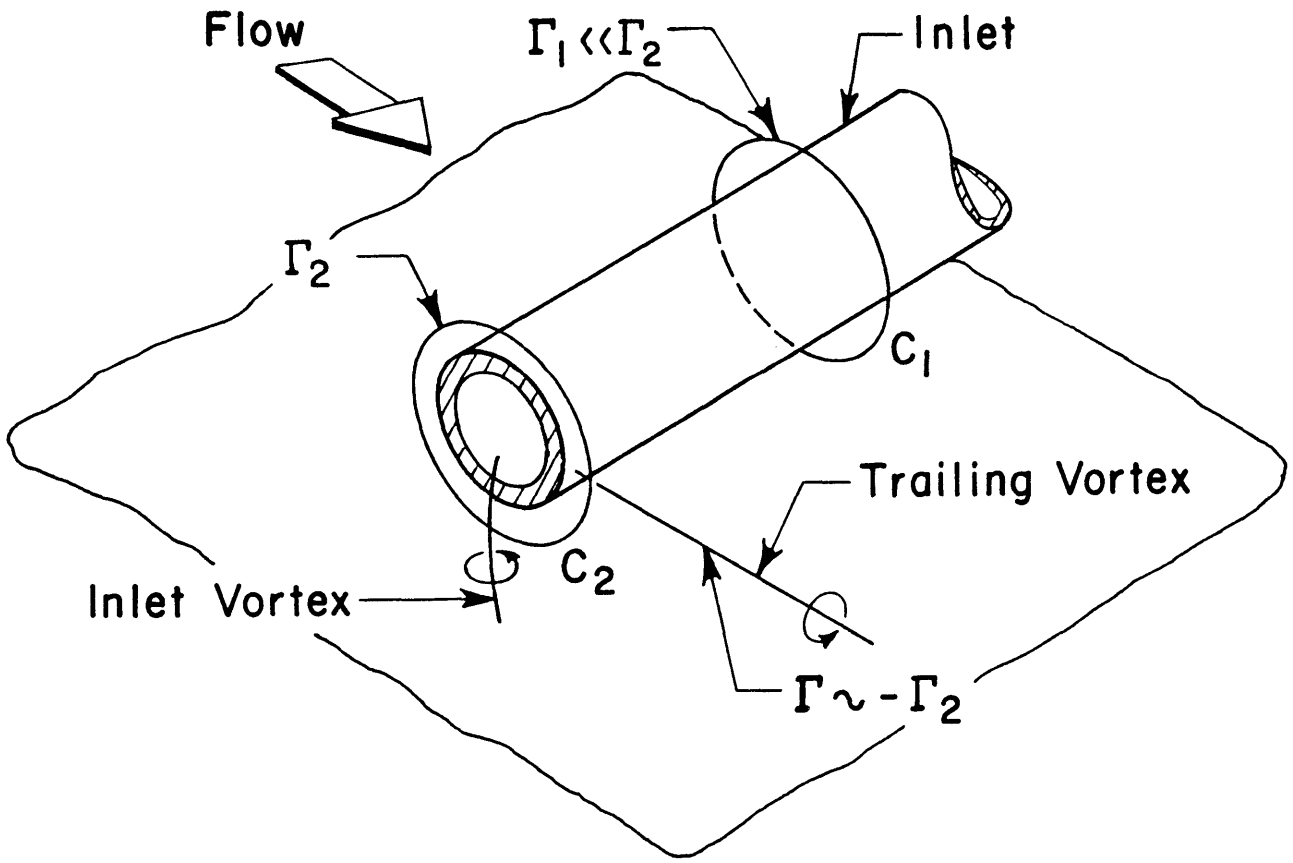

Figure 3-12 Variation of circulation along the length of an inlet at 90° yaw in an irrotational upstream flow [3]

CHAPTER IV

C_p DISTRIBUTION ON INLET

Static pressure measurements have been carried out on the inlet surface for an inlet in crosswind (i.e., 90 degrees of yaw). The results are presented as plots of C_p (defined $C_p = [P_i - (P_s)_{pitot}]/ (P_t - P_s)_{pitot}$). The subscript "pitot" refers to the measurement of the pitot-static probes mounted at the freestream region of the tunnel. The condition was at H/D = 1.5, U_i/U_e = 45, which is a case with a strong inlet vortex present. The measurements can be regarded as an extension of those carried out in [4] to a higher velocity ratio.

4-1 METHOD

The aluminum inlet, which was constructed with arrays of static taps flush-mounted on the surface, was used for this test. The pressure taps were arranged in four rows, as shown in Fig. 2-3, therefore 8 indexings resulted in 32 circumferential points for each of the 9 axial locations. Since the velocities near the lip had been previously shown to be much higher than those on the rest of the body [4], two different pressure transducers were used; one of 0.5 psi range for the 3 axial locations closest to the lip and the other had a 0.1 psi range for the rest of the locations. Each tap was sampled for 30 seconds, at a rate of 65 Hz in order to average out the 6 second cycle in the wake that had been observed.

4-2 RESULTS

The circumferential C_p distribution at each axial section is shown in Figs. 4-1(a-h). These are plots of C_p versus angle, where zero degree is directly upstream (as defined in Ch. 2), and angle varies in a clockwise

manner looking into the inlet. In these figures, the solid line represents a smooth curve fit through the data. Note each graph is plotted on a different scale. Figure 4-2 is a composite plot of the C_p distributions on a single scale, and Fig. 4-3 is a perspective composite plot.

At stations 2.5, 2.0, and 1.5 diameters away from the lip the C_p distributions indicate a form similar to a 2 dimensional turbulent flow over a cylinder, with a wake region behind the cylinder. As the lip is approached the flow becomes strongly three-dimensional. The C_p plots show that the mean pressure from 300 deg. (through 0 deg.) to 160 deg. is significantly decreased for stations closer to the lip. This lowering in the pressure indicates higher velocities and is due to the increased influence of the inlet flow through nearer to the lip.

The C_p plots also show a peak at the 215 degree location indicating a region of low velocity. Details of this type of static pressure distribution are given by Liu, et al. and have been explained as the interaction between the trailing vortex and the overall flow into the inlet with a more local contribution from the inlet vortex, as shown in Fig. 4-4 (taken from [4]). The model of the interaction of the trailing vortex and inlet flow appears to qualitatively explain the pressure distributions on the surface; high velocities (low pressure) as the lip is approached except in the region where the trailing vortex induces velocities to cancel the inlet flow (creating low velocity and high pressure).

Figure 4-5 is the C_p distribution for 8 evenly spaced circumferential locations, plotted C_p versus non-dimensionalized axial location. This method of presenting C_p data was suggested by Motycka [9] as a means of

noting the velocity, and thereby circulation, variation around the inlet for different axial locations. It can be seen for stations greater than one diameter away from the lip there is no change in the velocity pattern, implying no change in circulation. As the lip is approached from one diameter the velocity pattern makes a sharp change indicating a variation in circulation. This variation in circulation has been shown to be the mechanism of inlet/trailing vortex formation.

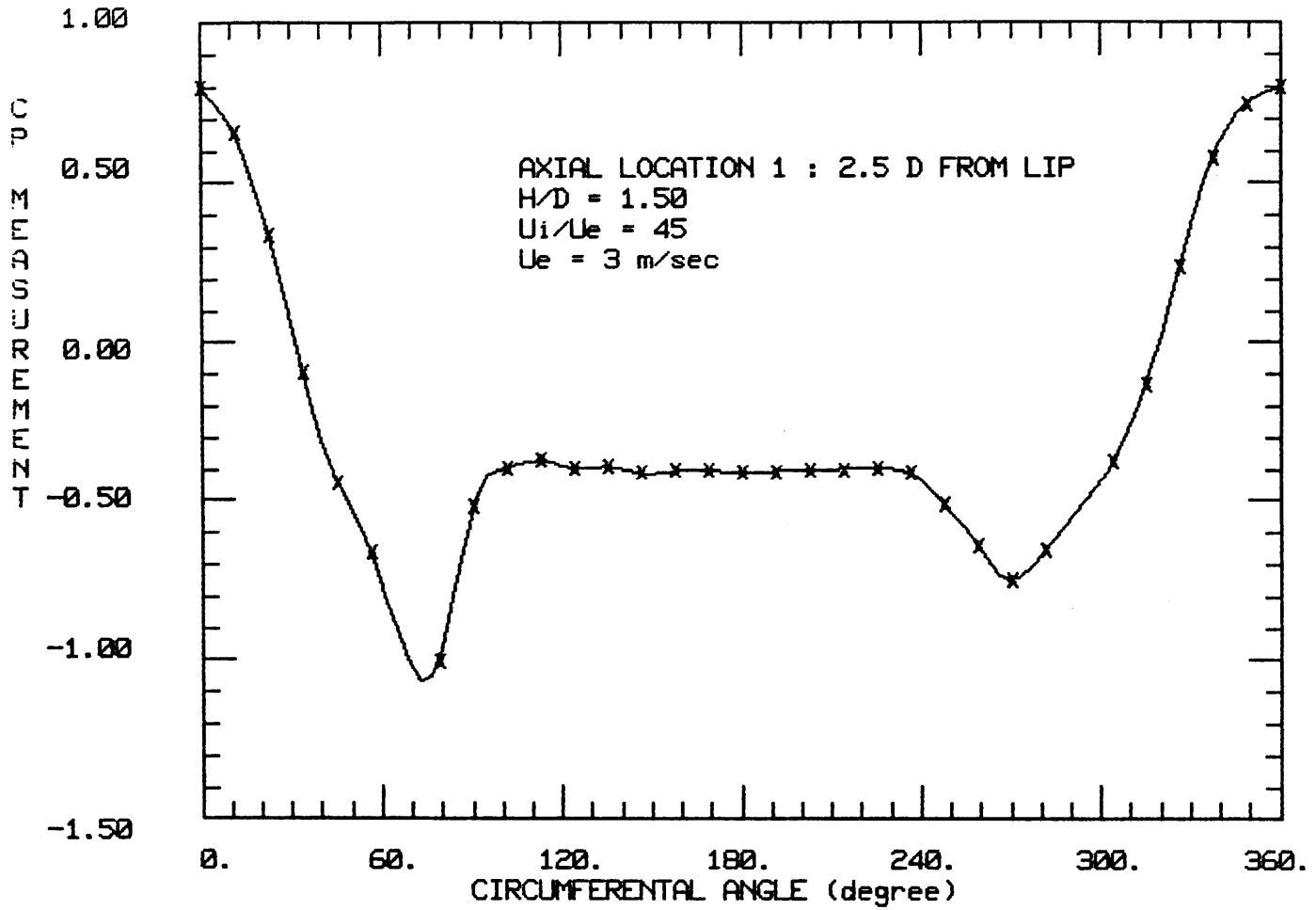

Figure 4-1(a) Circumferential Cp distribution on inlet at H/D = 1.5, U_i/U_e = 45 (inlet vortex present)

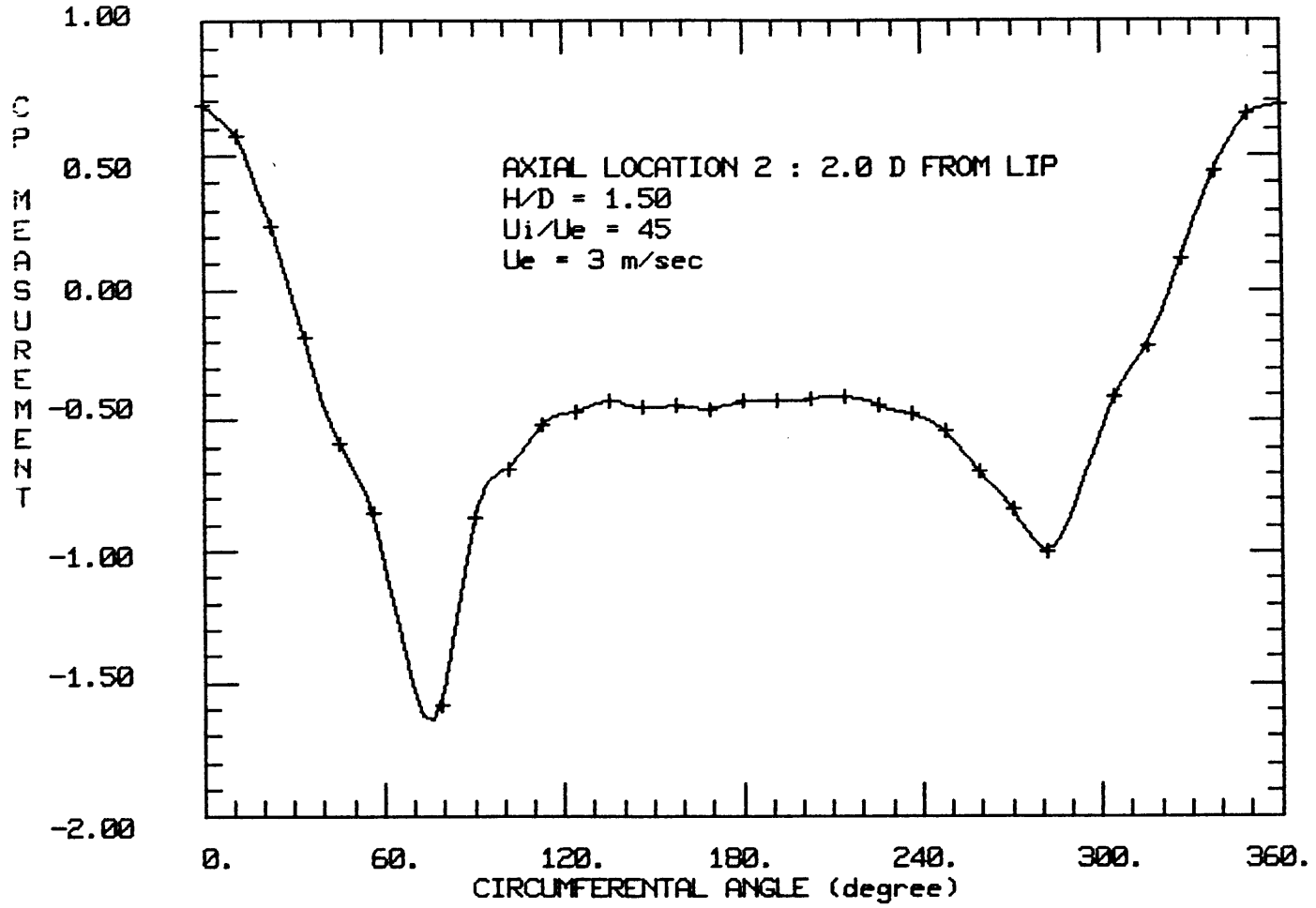

Figure 4-1(b) Circumferential Cp distribution on inlet at H/D = 1.5, U_i/U_e = 45 (inlet vortex present)

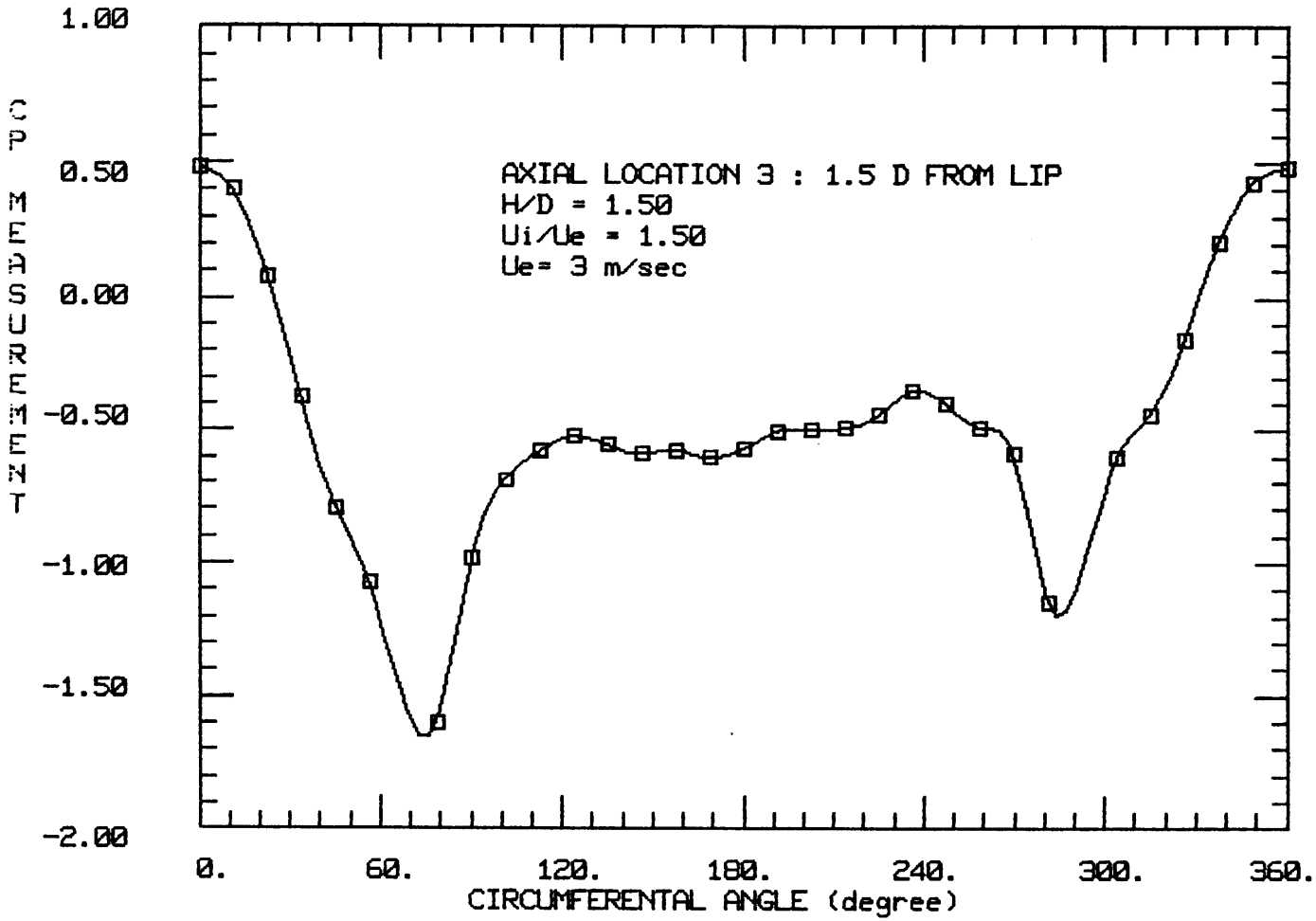

Figure 4-1(c) Circumferential Cp distribution on inlet at H/D = 1.5, U_i/U_e = 45 (inlet vortex present)

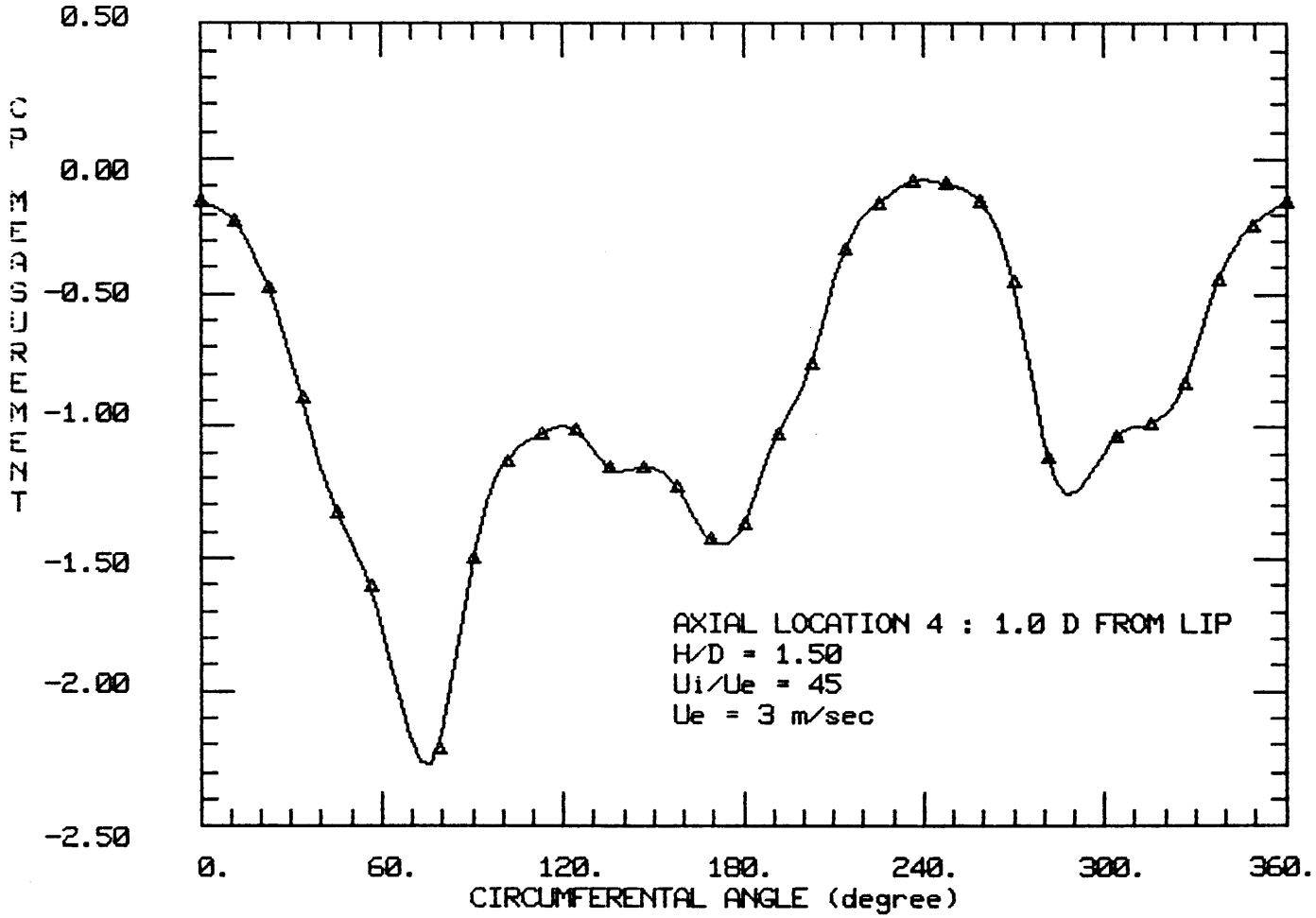

Figure 4-1(d) Circumferential Cp distribution on inlet at H/D = 1.5, U_i/U_e = 45 (inlet vortex present)

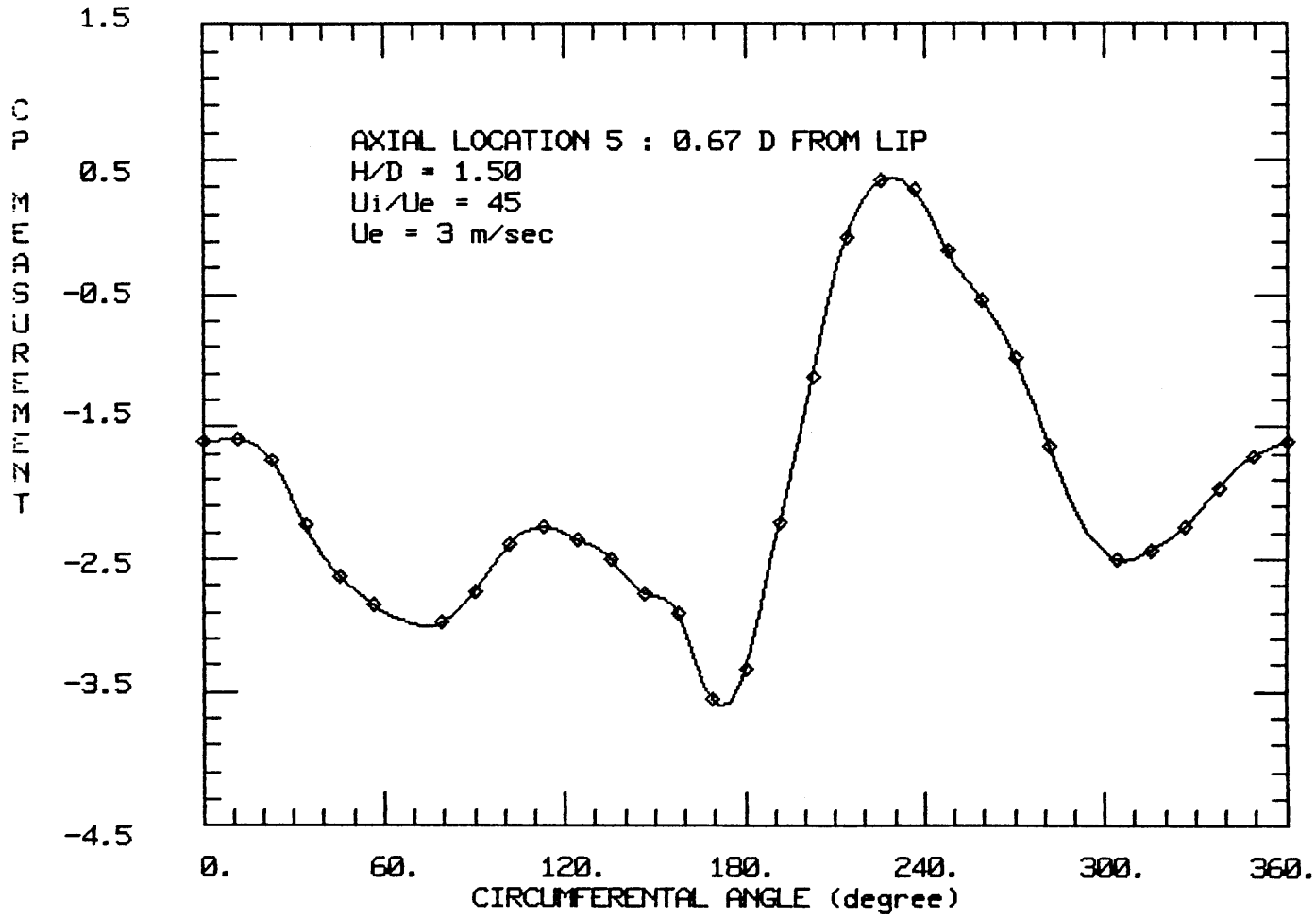

Figure 4-1(e) Circumferential Cp distribution on inlet at H/D = 1.5, U_i/U_e = 45 (inlet vortex present)

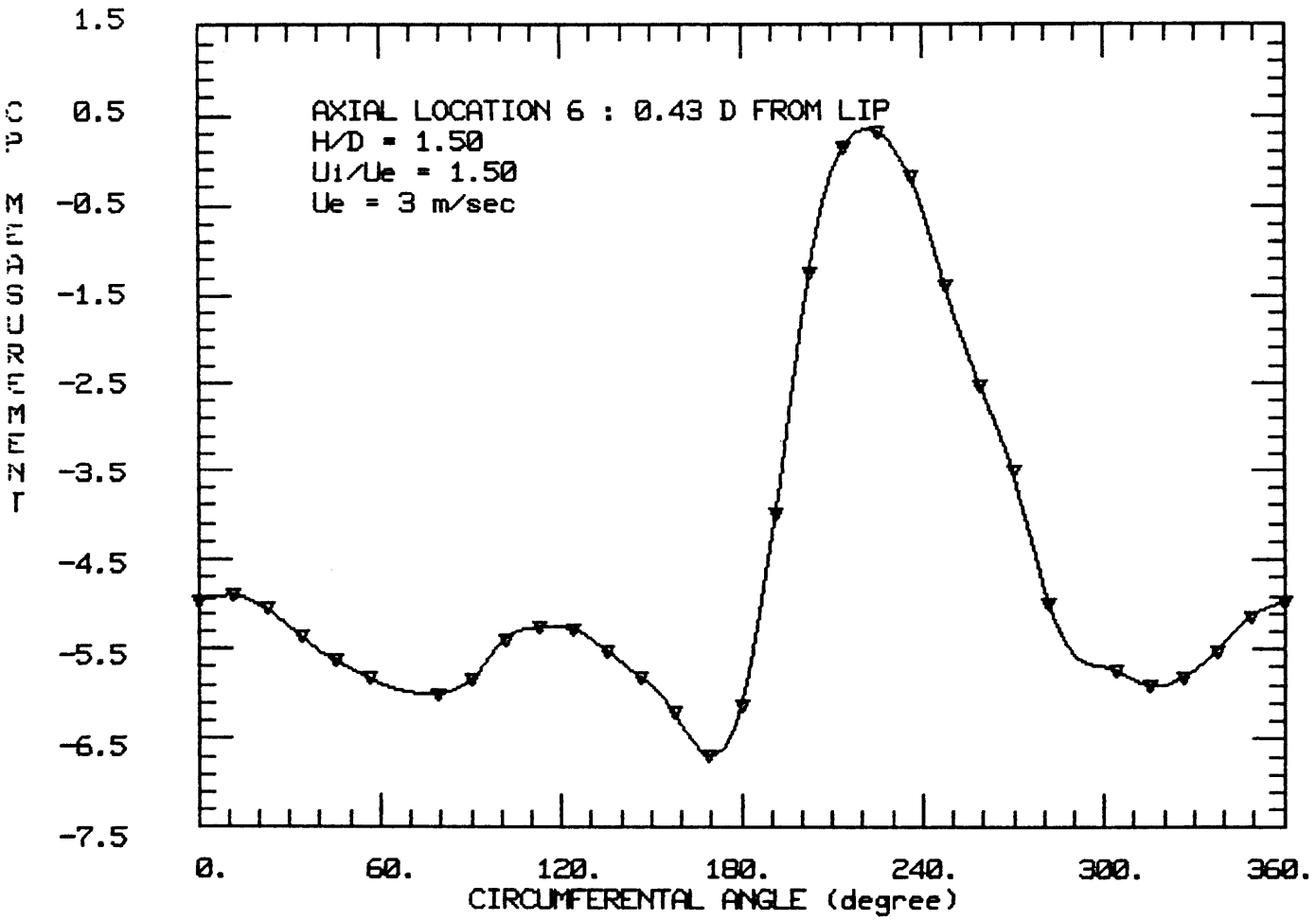

Figure 4-1(f) Circumferential Cp distribution on inlet at H/D = 1.5, U_i/U_e = 45 (inlet vortex present)

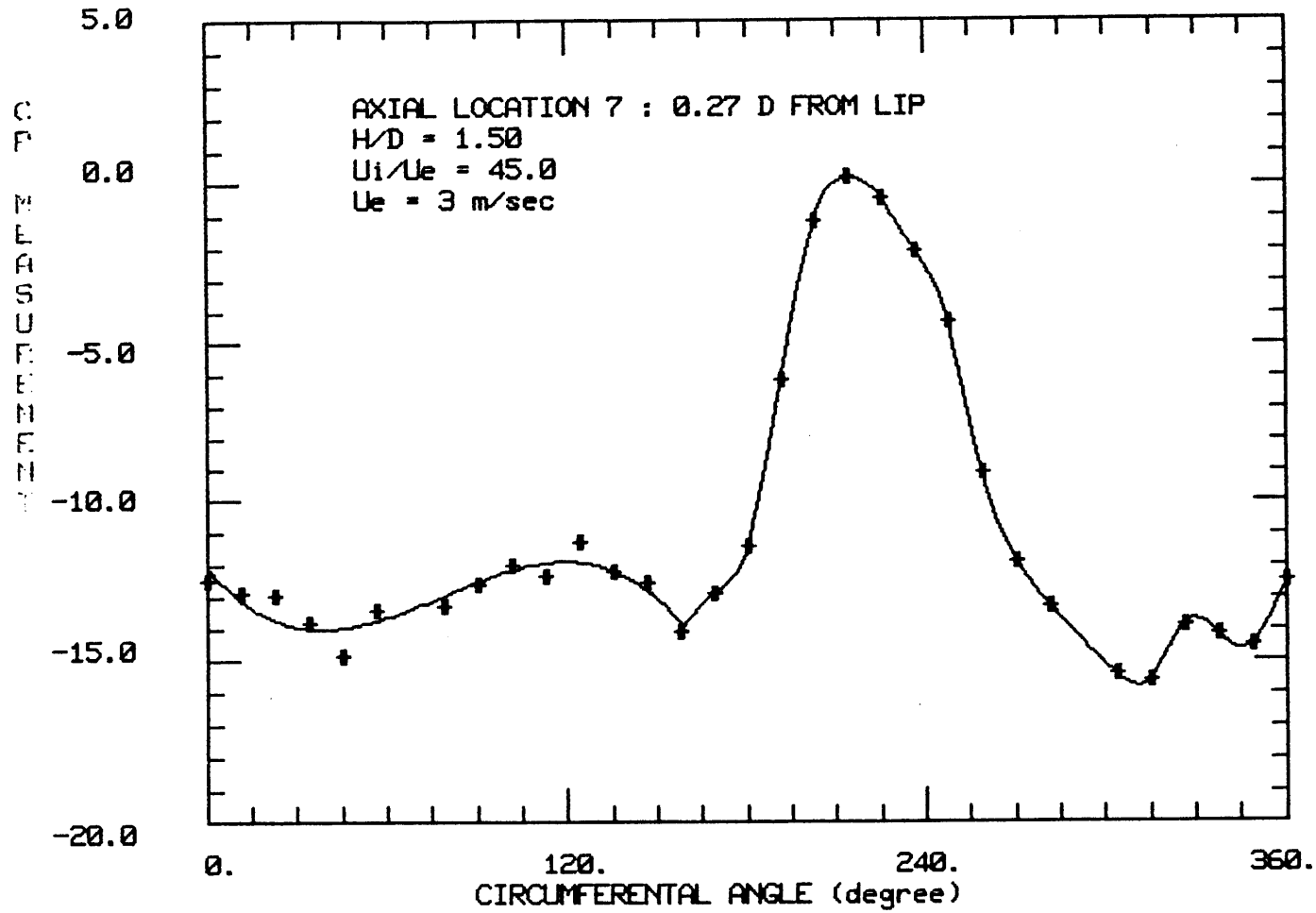

Figure 4-1(g) Circumferential Cp distribution on inlet at H/D = 1.5, U_i/U_e = 45 (inlet vortex present)

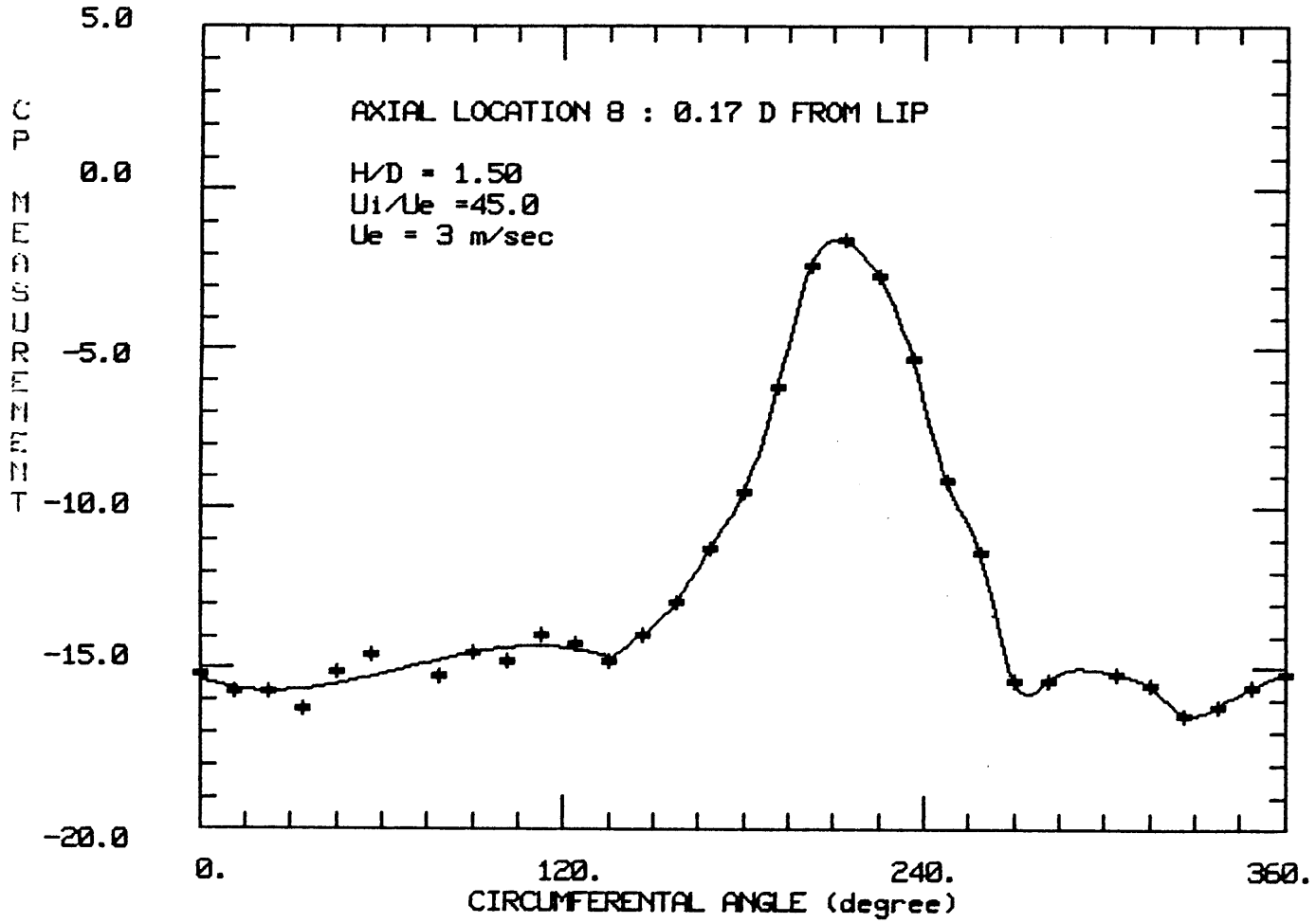

Figure 4-1(h) Circumferential Cp distribution on inlet at H/D = 1.5, U_i/U_e = 45 (inlet vortex present)

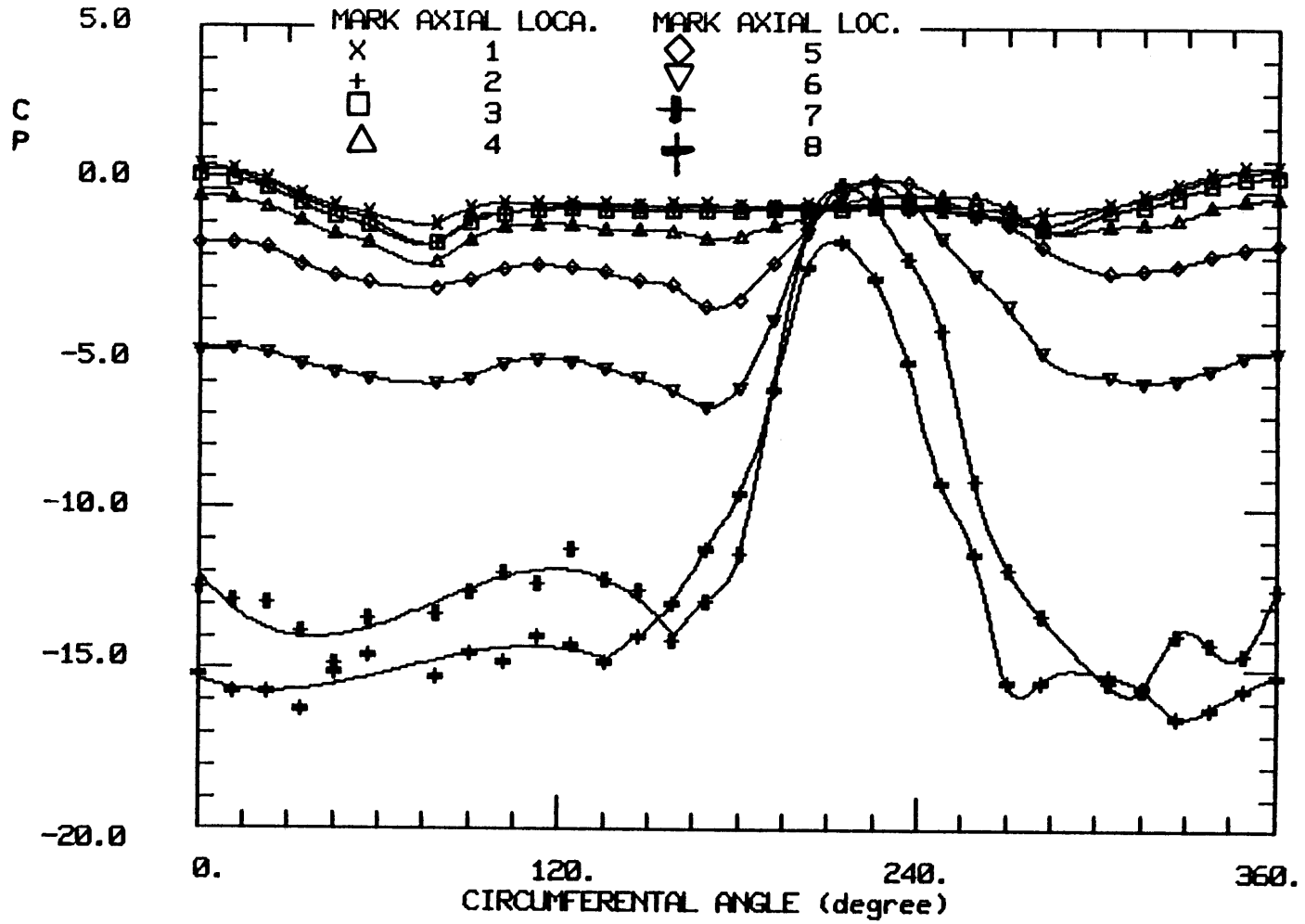

Figure 4-2 Axial comparison of circumferential Cp distribution on inlet at H/D = 1.5, U_i/U_e = 45

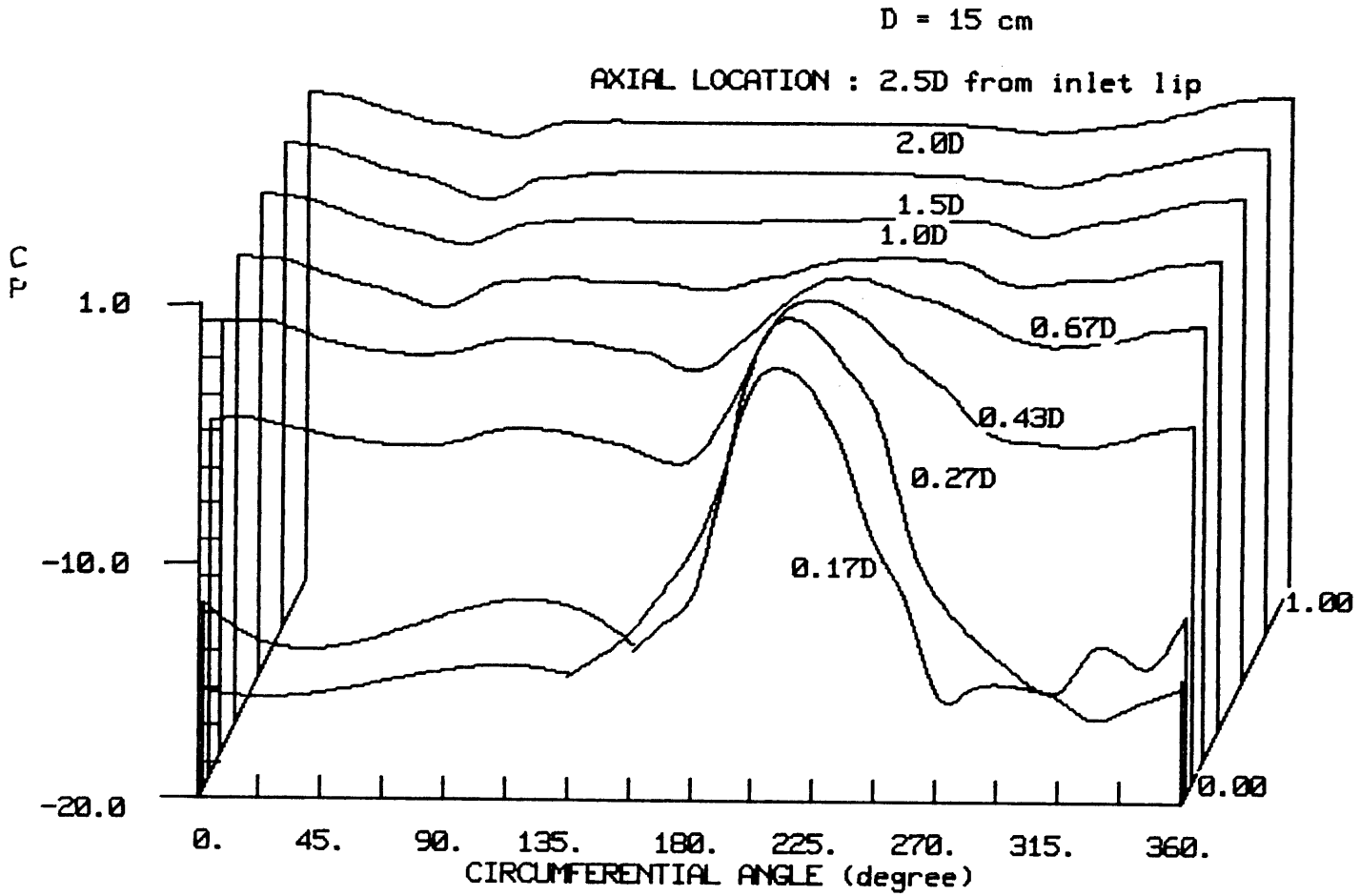

Figure 4-3 Perspective axial comparison of circumferential Cp distribution on inlet at H/D = 1.5, U_i/U_e = 45

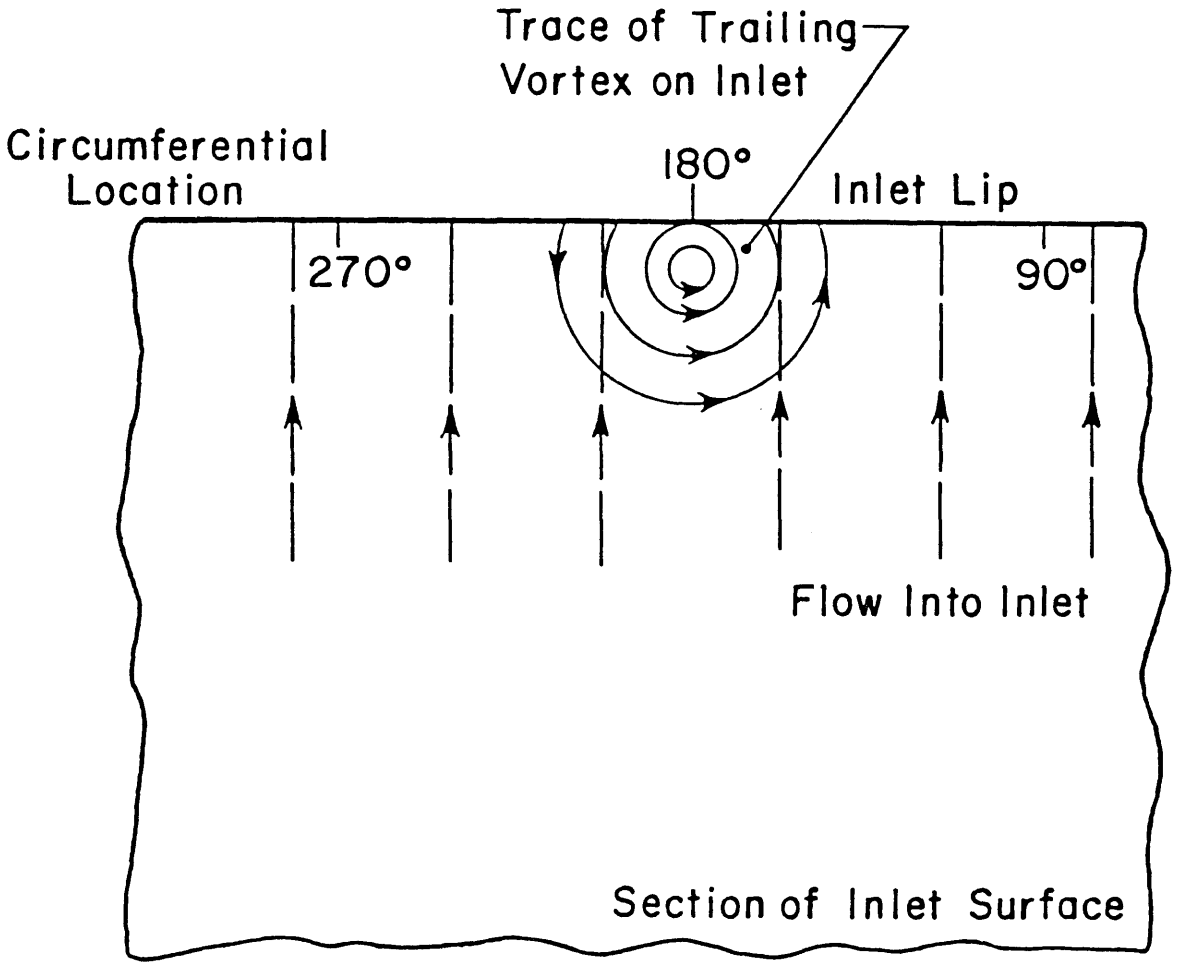

Figure 4-4 Conceptual model for interaction (on inlet surface) of trailing vortex and flow into inlet at high U_i/U_e [4]

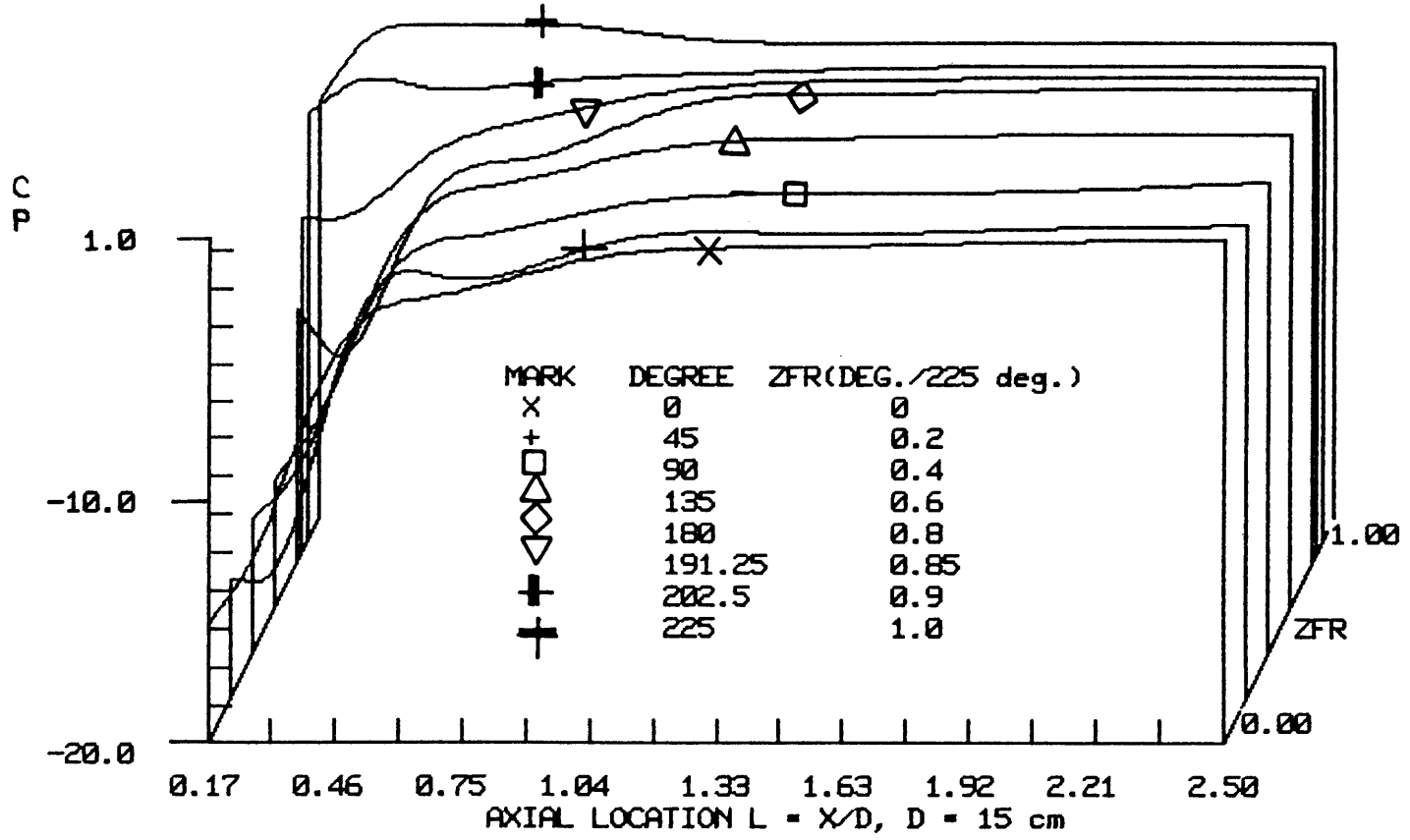

Figure 4-5 Perspective circumferential comparison of axial Cp distribution on inlet at H/D = 1.5, U_i/U_e = 45

CHAPTER V

PARAMETRIC STUDY OF INLET VORTEX STRENGTH AND LOCATION

A limited parametric study was done of the inlet vortex strength and the location of the two vortices inside the inlet. Different values of U_i/U_e and H/D were used. The flow regimes ranged from strong vortex to no inlet vortex. The specific cases considered are shown in Table 5-1, U_i/U_e = 45, H/D = 1.0, 1.25, 1.50, 1.75, 1.91 and 2.0 and H/D = 1.0, U_i/U_e = 17 and 4.

5-1 CIRCULATION MEASUREMENT (VORTEX STRENGTH)

Velocity measurements inside the inlet were taken at a station 30 cm from the lip in the same manner as that described in Chapter III. three-hole, Kiel and static probes were used on the contour along the inside wall and a five-hole probe was used for the diametrical traverse. From these measurements, the vortex circulation and the circumferental location of the maximum tangential velocity can be determined.

Figures 5-1(a-f) and 5-2(a-c) show the tangential velocities inside the inlet for each of the conditions. From these figures a general pattern of the changes in the location and in the strength of the inlet vortex can be seen. Figures 5-1(a-f) indicate the influence of increasing H/D while the velocity ratio is held constant, specifically increasing H/D from 1.0 to 2.0 at U_i/U_e = 45. At H/D = 1.0 the velocity vectors inside the inlet show a strong vortex near 6:30 and a weak vortex region at 2:30. As H/D is increased to 1.75 the inlet vortex tangential vectors decrease in magnitude, until at H/D = 1.91 and 2.0 the two vortex regions appear nearly equal and opposite in sense,

and are located at 2:00 and 5:00.

Figures 5-2(a-c) show a similiar trend as the velocity ratio is reduced at constant H/D (H/D = 1.0). The inlet vortex weakens and then changes to two vortices of equal strength but of opposite sign, when the capture ratio is reduced from U_i/U_e = 45 in (a) to 17 in (b) and 4 in (c). When the overall vortex system is considered, these two weak vortices must be the extension into the inlet of the two counterrotating trailing vortices, illustrated in Fig. 1-2(b), that had been seen during flow visualization at H/D = 1.0 and U_i/U_e = 4.

Graphs of tangential velocity versus circumferential angle also indicate the pattern described, and, additionally, readily show the quantitative differences between the cases. Figure 5-3 shows five cases at U_i/U_e = 45 plotted together, H/D = 1.0, 1.25, 1.5, 1.75, and 2.0. This figure illustrates that the inlet vortex clearly decreases in strength (as indicated by the decrease in area under the velocity line between 191 and 5 degs) as the inlet height increases.

Clarification of the sudden decrease of vortex tangential velocities at U_i/U_e = 45 is shown in Fig. 5-4, where four cases have been graphed together, H/D = 1.5, 1.75, 1.91, and 2.0. Figure 5-4 indicates the abrupt decrease of tangential velocities that occur between H/D = 1.75 and 1.91 (for this velocity ratio) due to vortex core moving away from the wall as we can see later.

Figure 5-5 illustrates the influence of reducing the velocity ratio, from U_i/U_e = 45 to 4 at H/D = 1.0. While the pattern is qualitatively similiar to that of increasing H/D, there are quantitative

differences. Decreasing the velocity ratio not only reduced the vortex strength as increasing the height to diameter ratio had done, but also shifted the angle of the maximum tangential velocity. Another difference is that reducing the velocity ratio greatly reduced and shifted the weak second vortex, where increasing H/D only reduced and shifted it slightly.

The inlet vortex circulation has been calculated for each condition and is presented in Table 5-2. The table shows that as the height from the ground is increased (or the capture ratio is decreased) the circulation decreases. This is also shown graphically in Fig. 5-6a and b. In Fig. 5-6a the circulation has been non-dimensionalized by U_eD and in Fig. 5-6b it has been non-dimensionalized by U_eH. Although previous investigators have viewed the former as most appropriate [4], it is not clear that this is so. Thus, both non-dimensionalizations are presented for completeness. (Note that the two are equivalent in that H/D is known.) Using U_eD, it can be seen that there is a change in slope indicating sudden jump in position of inlet vortex core toward center of inlet. Non-dimensionalizing by U_eH tends to collapse the data for one velocity ratio to a straight line.

5-2 VORTEX LOCATION

To find the location of the inlet vortex inside the inlet, smoke was introduced to the vortex outside of the inlet. Also a single plane was illuminated inside the plexiglass model by a plane of laser light. When the test section was darkened, lighted regions would be where the laser plane was blocked. Inside the inlet, these blockages occurred in

concentrated smoke regions, that is, in the vortex core where the smoke was concentrated. The photographs were taken with a Polaroid 195 Land Camera with 3000 ASA film. The photographs were taken at a plane 2 diameters from the lip, which was the measurement station. A representative photograph of the inlet vortex is shown in Fig. 5-7.

The result of this photographic study was the determination of the average ratio of radial distance from the center to inside diameter (r/D) and circumferential (θ) angle of the inlet vortex for each of the examined conditions. These are presented in a tabular form in Table 5-3, where the angle maximum tangential velocity (determined from the velocity measurements) is also listed for comparison. The vortex location determined from the photographs agreed with the angle of the maximum tangential velocity within 10 deg.

The vortex locations, as indicated by the photographs, are shown graphically in Fig. 5-8. An obvious feature is the sudden jump in position of the vortex between H/D = 2.0 and the other values of H/D (1.5, 1.25, and 1.0) for U_i/U_e = 45. This is consistent with the results of the quantitative measurements.

5-3 CONCLUSION

Velocity measurements and photographs have quantified the strength and location of the inlet vortex when a strong inlet vortex is present and when there are two counter-rotating trailing vortices. The measurements and photographs have shown that inlet vortex weakens and shifts as the inlet height is increased (or U_i/U_e is decreased). The results have also

indicated an inlet vortex core sudden jump in position toward center of inlet between H/D = 1.75 and 1.91 for U_i/U_e = 45.

TABLE 5-1

CONDITIONS OF PARAMETRIC STUDY

U_i/U_e	H/D	Regime
45	1.0	Vortex
45	1.25	Vortex
45	1.50	Vortex
45	1.75	Vortex
45	1.91	Vortex
45	2.0	Vortex
17	1.0	Vortex
4	1.0	No Vortex

TABLE 5-2

INLET VORTEX CIRCULATION

U_i/U_e	H/D	Circulation (m^2/s)
45	1.0	3.4
45	1.25	3.1
45	1.50	3.0
45	1.75	2.8
45	1.91	1.9
45	2.0	1.5
17	1.0	1.8
4	1.0	0.4

TABLE 5-3

POSITION OF INLET VORTEX

U_i/U_e	H/D	r/D	θ(deg)	Maximum Tangential Velocity Angle (deg)
45	1.0	0.42	289	298
45	1.25	0.38	289	298
45	1.5	0.37	285	288
45	2.0	0.28	250	248
17	1.0	0.40	300	298
4	1.0	0.39	267	275

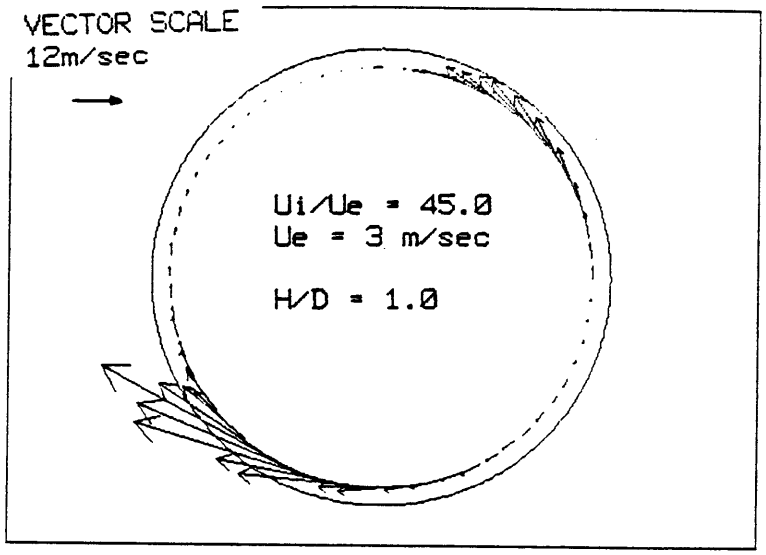

(a)

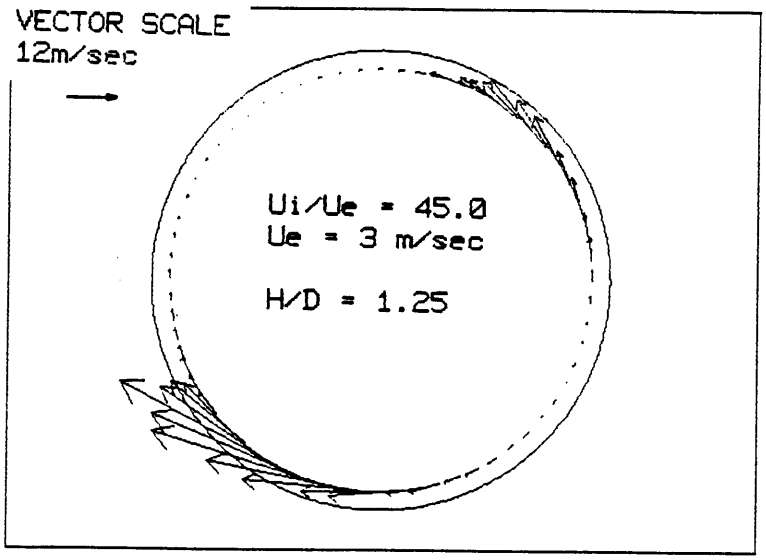

(b)

Figure 5-1 Tangential velocity distribution around inside of inlet for increasing H/D

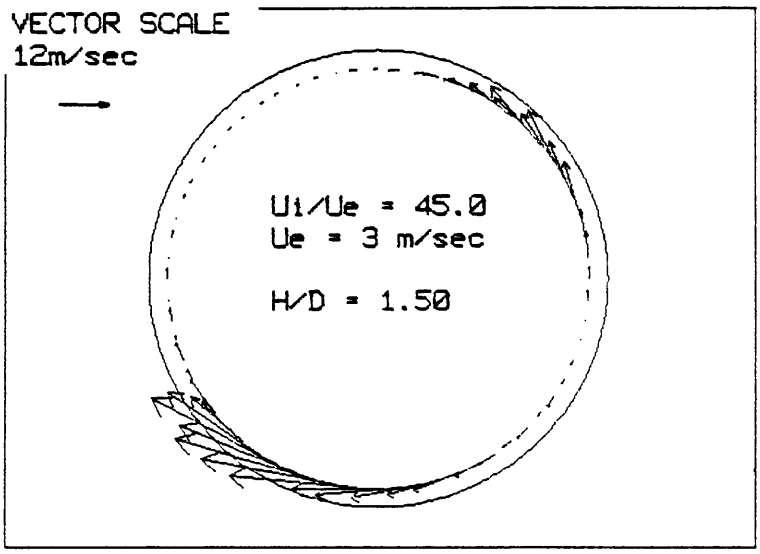

(c)

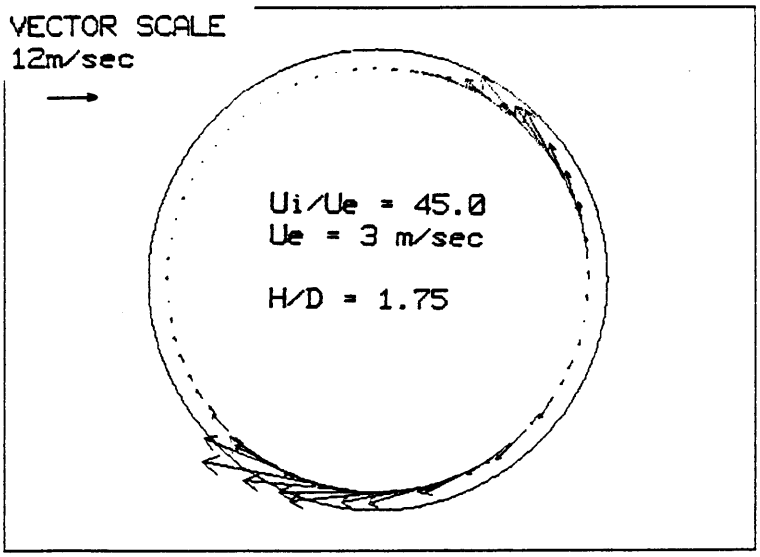

(d)

Figure 5-1 Tangential velocity distribution around inside of inlet for increasing H/D

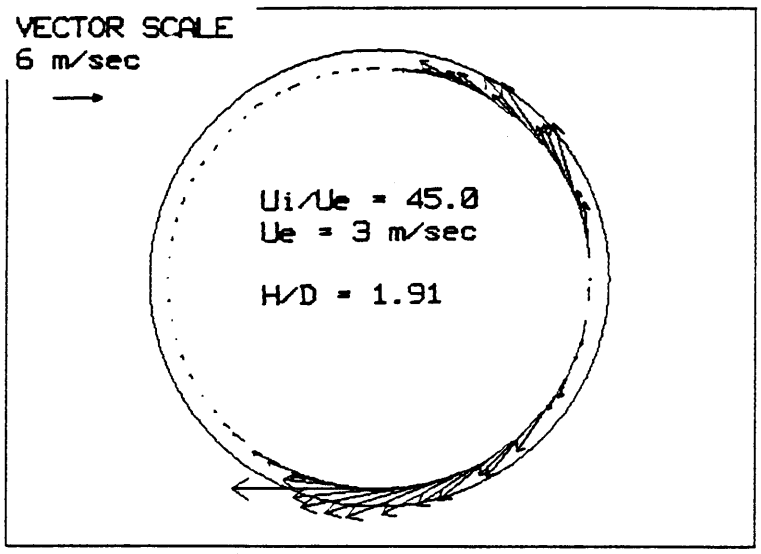

(e)

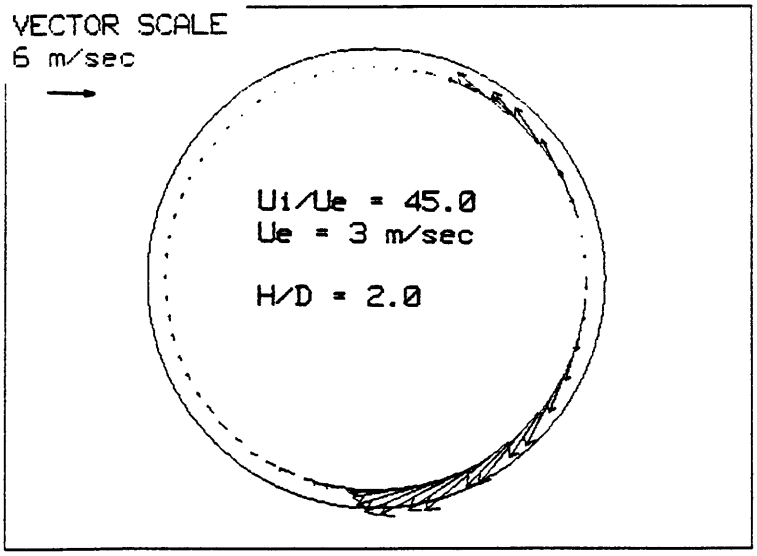

(f)

Figure 5-1 Tangential velocity distribution around inside of inlet for increasing H/D

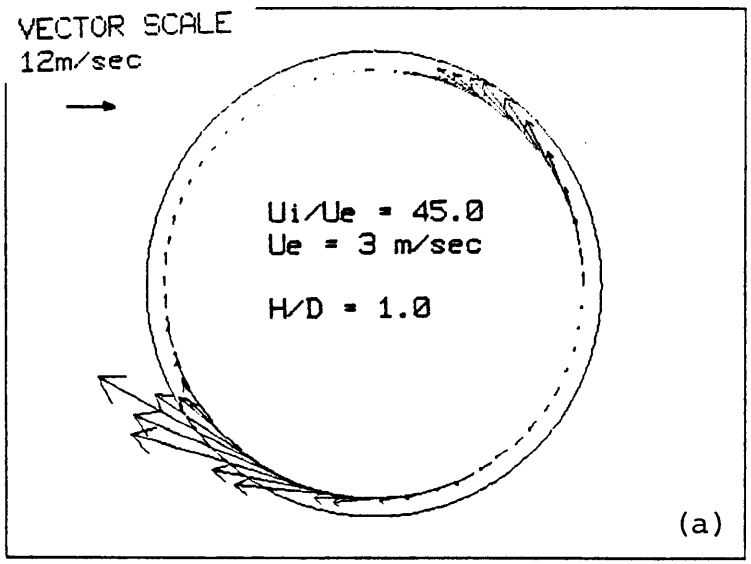

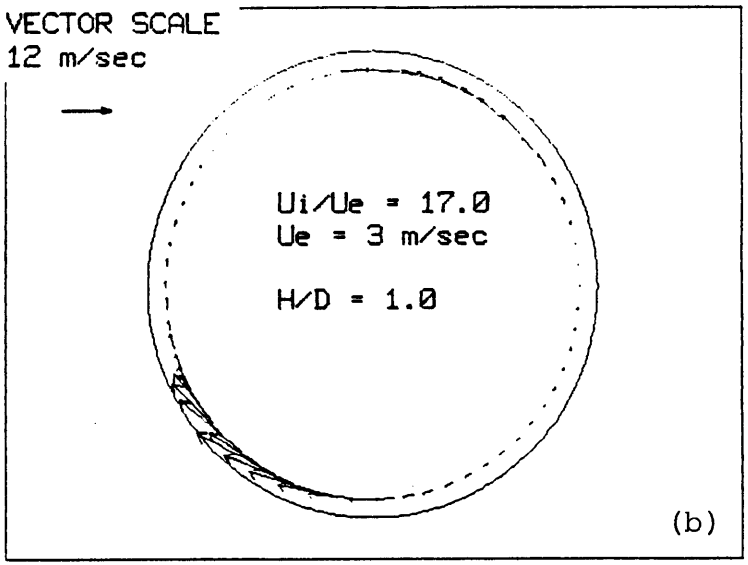

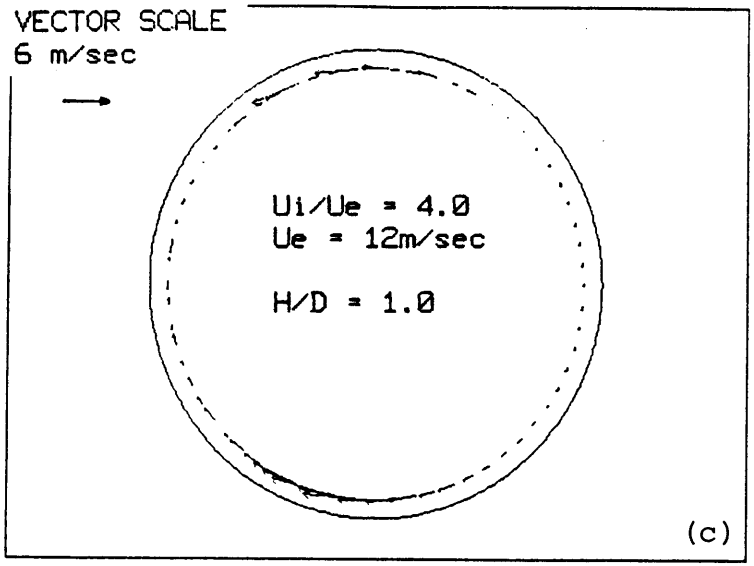

Figure 5-2 Tangential velocity distribution around inside of inlet for decreasing U_i/U_e

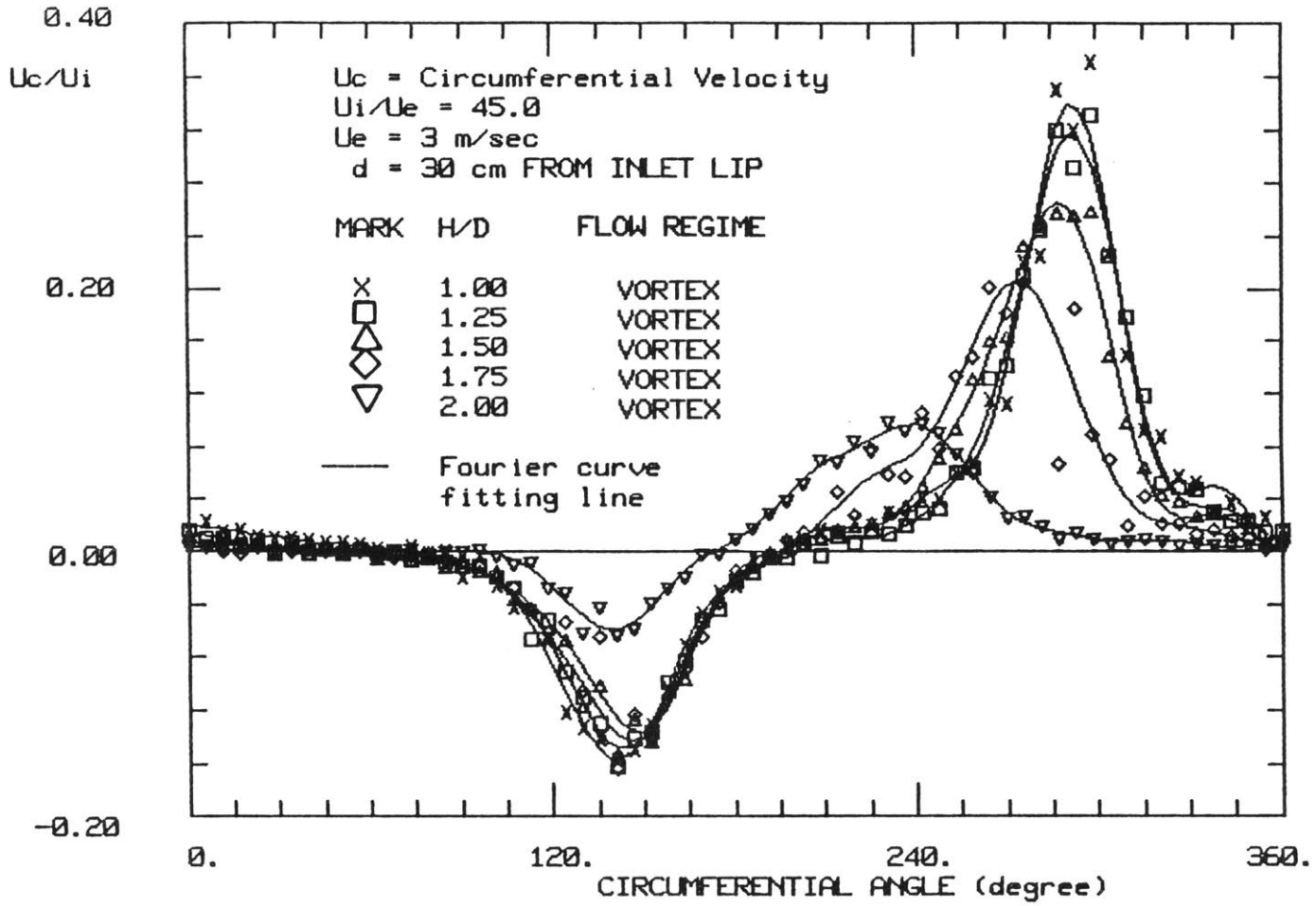

Figure 5-3 H/D comparison of tangential velocity distribution inside inlet

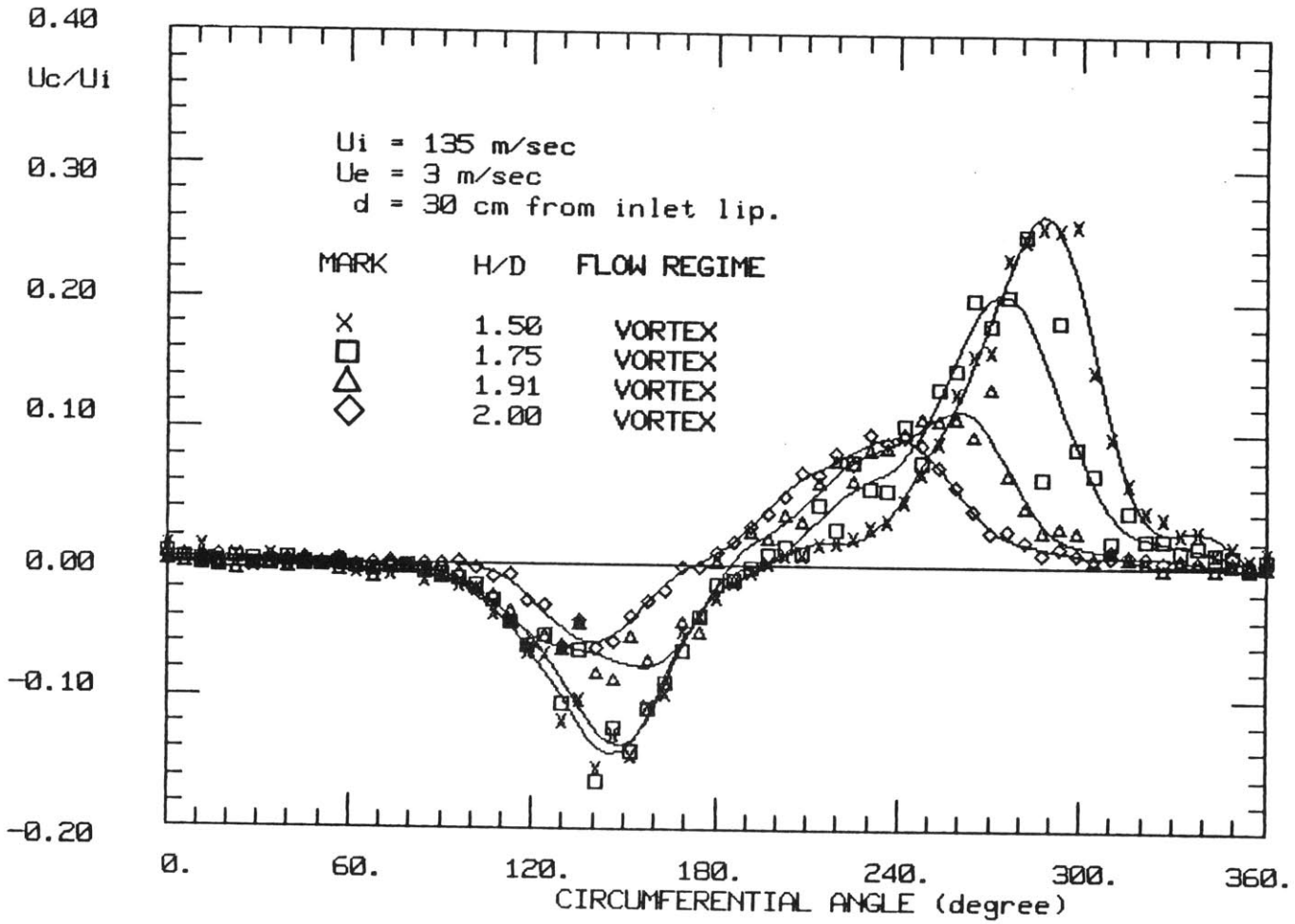

Figure 5-4 H/D comparison of tangential velocity distribution inside inlet, emphasis on transition

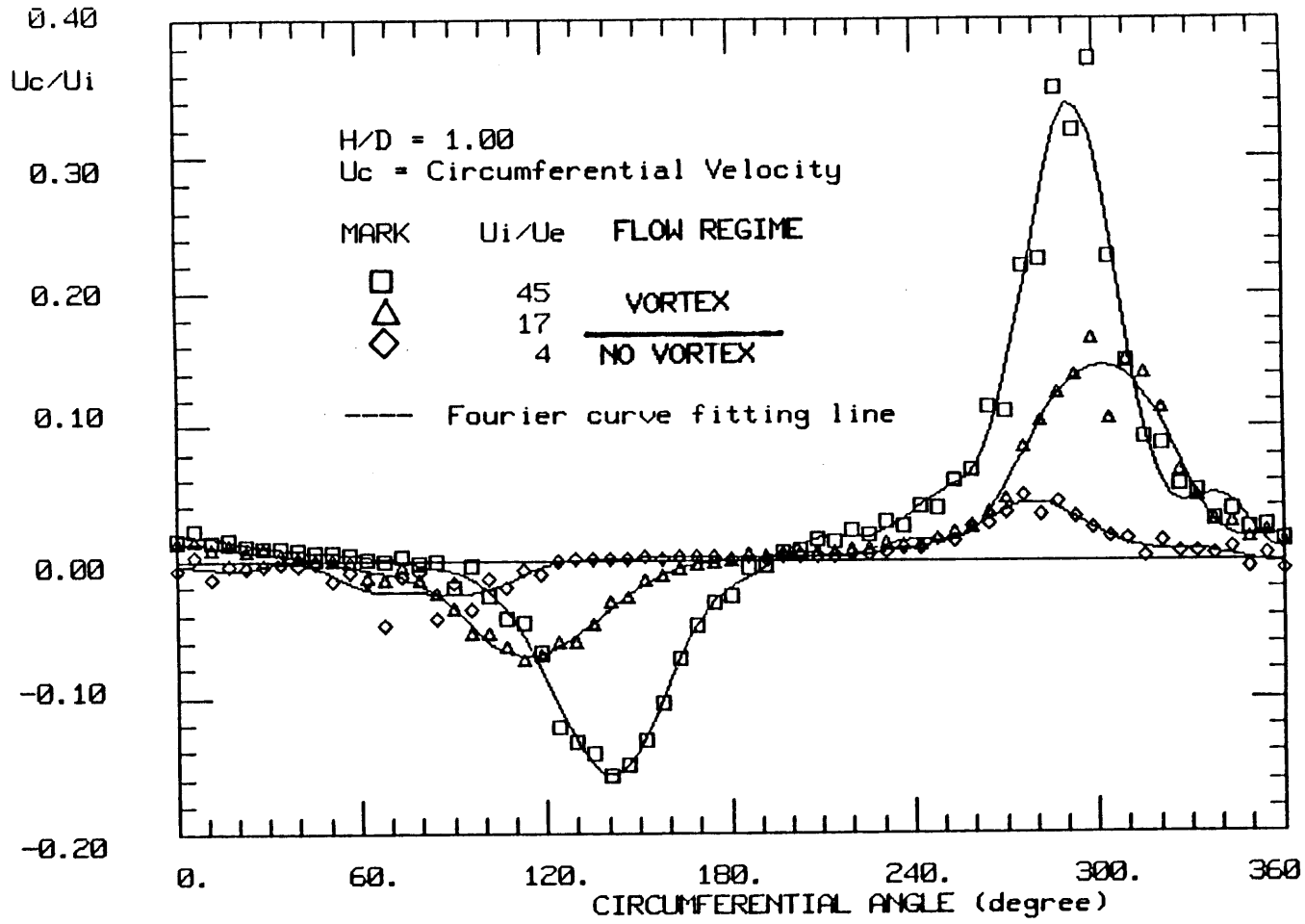

Figure 5-5 U_i/U_e comparison of tangential velocity distribution inside inlet

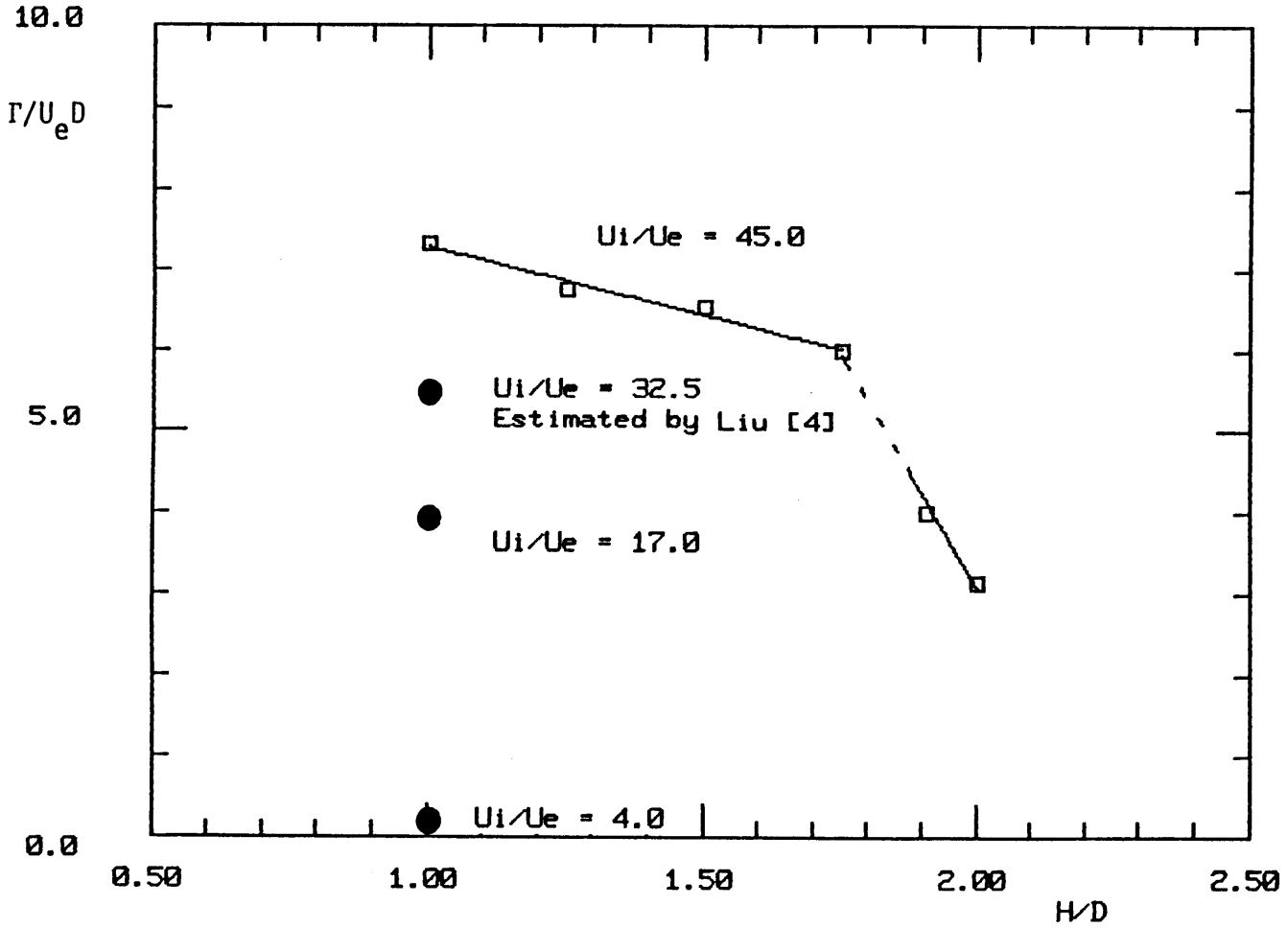

Figure 5-6(a) H/D and U_i/U_e influence on circulation

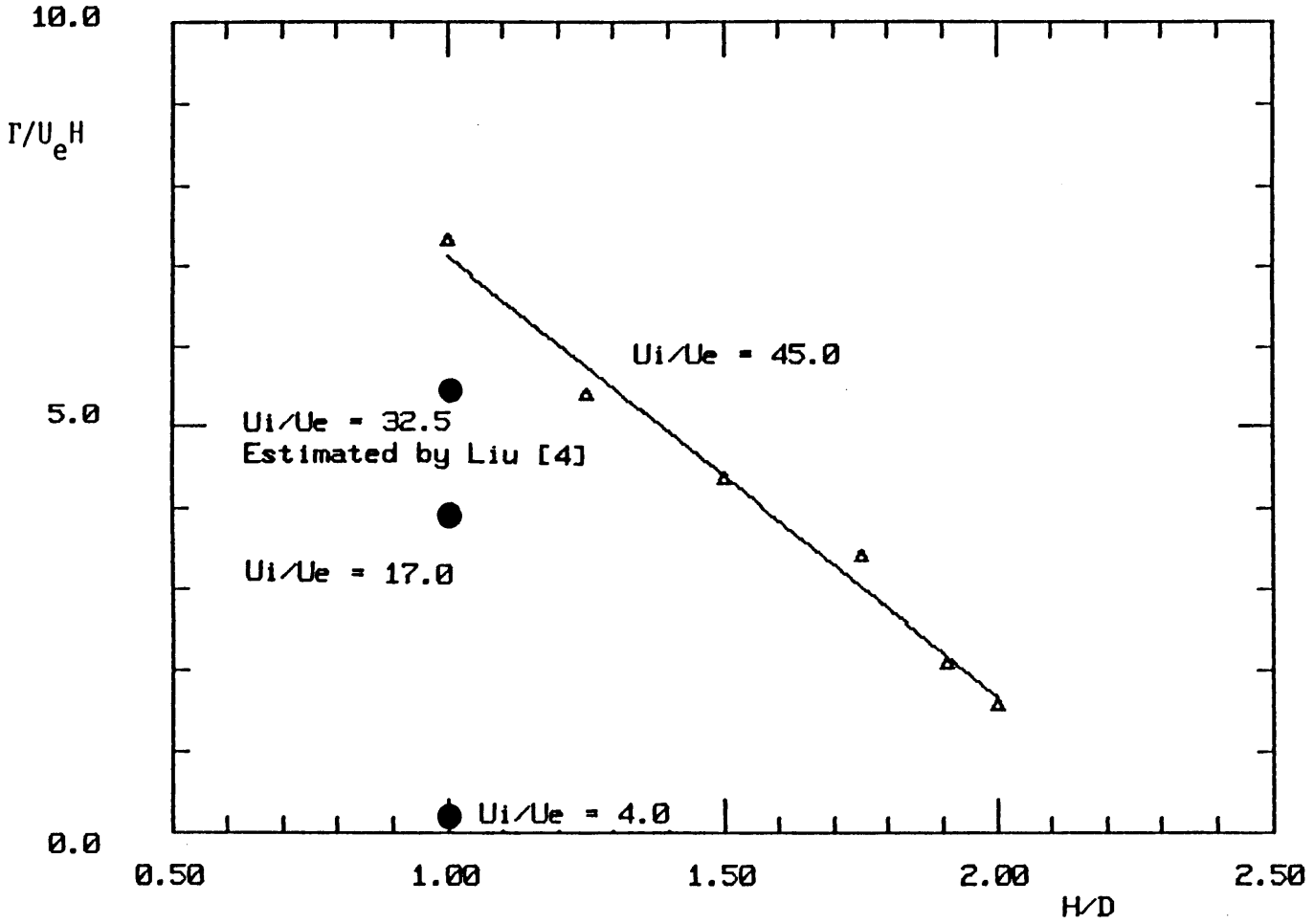

Figure 5-6(b) H/D and U_i/U_e influence on circulation

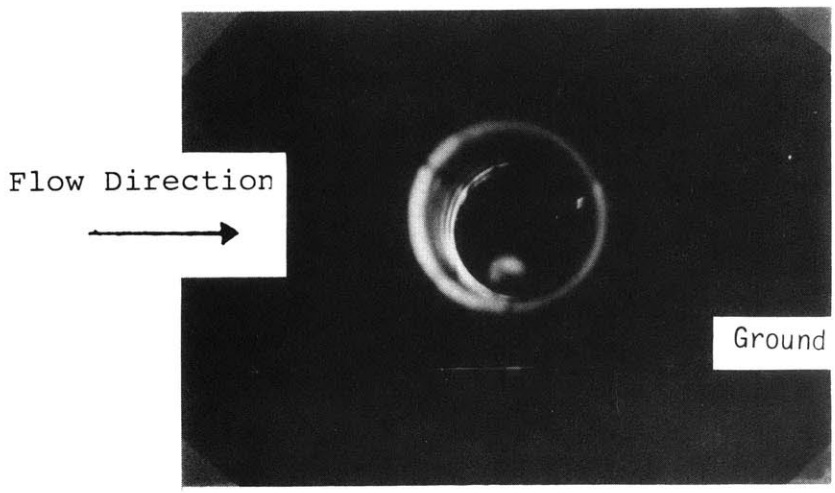

(a) H/D = 1.0, U_i/U_e = 45.0

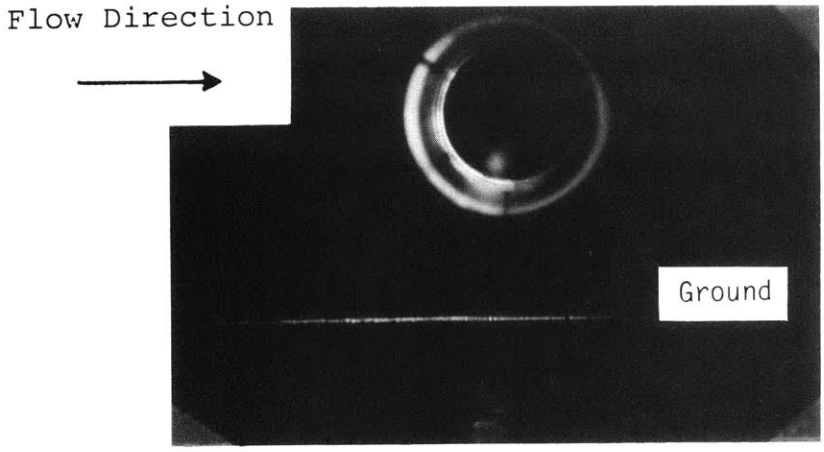

(b) H/D = 1.5, U_i/U_e = 45.0

Figure 5-7 Photographs of inlet vortex inside inlet, x = 30 cm

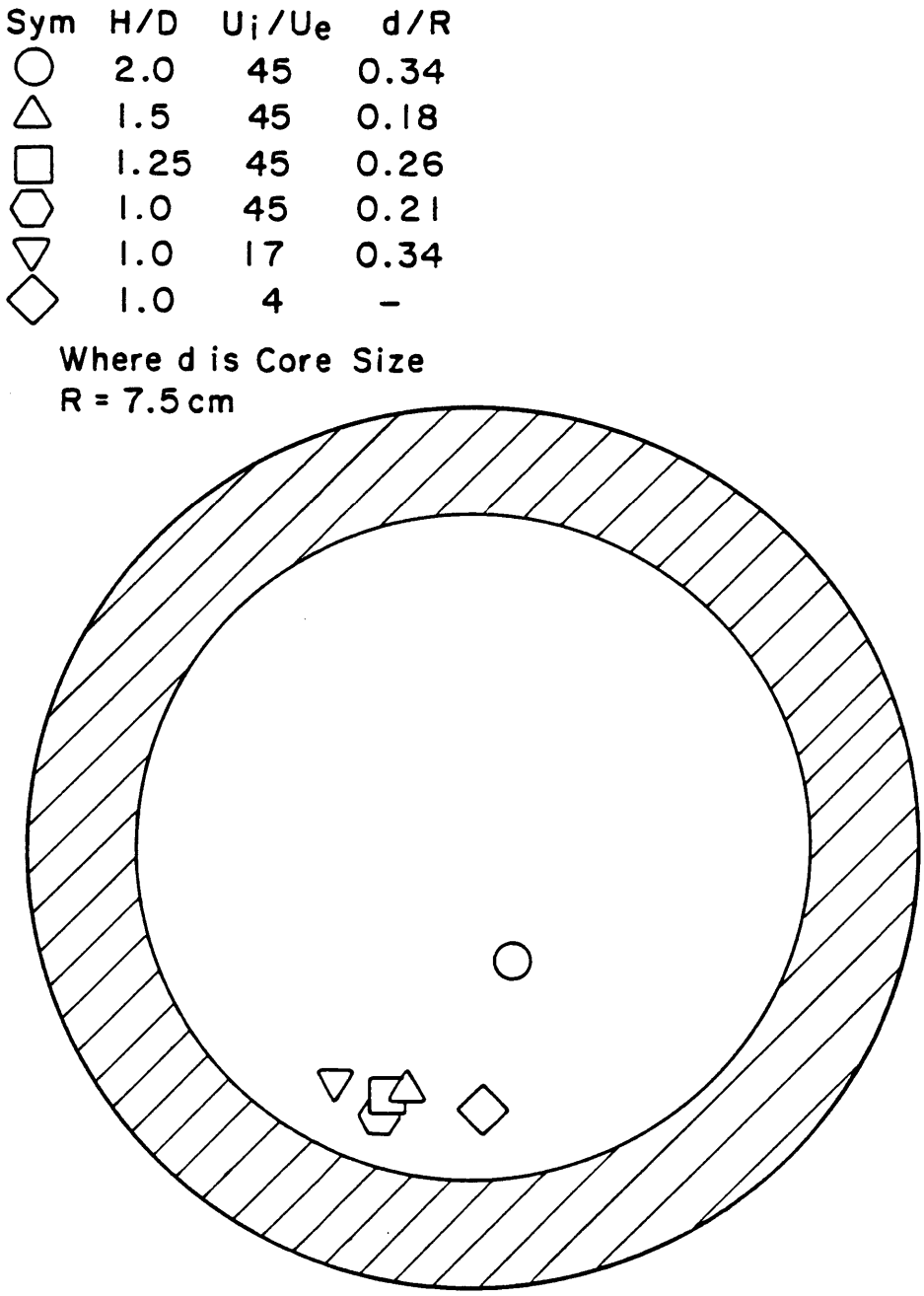

Figure 5-8 Position of inlet vortex core determined from photographs

CHAPTER VI

FLOW REGIME TRANSITIONS

Global features of the inlet/trailing vortex system which have not been previously well defined were the transition regimes between two counter-rotating vortices to a strong inlet vortex. In order to investigate these events, a flow visualization study was done in a water tunnel, as suggested by Marble [10]. Previous investigation of the inlet vortex phenomena was done in the MIT Ocean Engineering Water Tunnel and the facility is discussed in detail by DeServi in [3]. Only a brief description is included here. Sketches from hydrogen bubble observations are used to present the features seen.

6-1 EXPERIMENTAL APPARATUS

The water tunnel flow visualization studies were carried out in the MIT Ocean Engineering Water Tunnel, Fig. 6-1. It is a 6,000 gallon capacity tunnel with a 0.5 m square test section that is 1.5 m long and was run with a free surface. The test section is preceded by a settling chamber, containing a honeycomb structure, and a 4.92:1 contraction to reduce turbulence and velocity non-uniformities in the tunnel. An auxiliary pump and the necessary piping were installed to create the required flow through the inlet. A detailed drawing of this system is given in Appendix E. A flow meter and gate valve were incorporated in the piping to monitor and regulate the inlet flow.

To investigate the inlet/trailing vortex system for an inlet in an irrotational crosswind, the inlet was installed at 90 deg to the mean flow. Although a 5 cm diameter single inlet was available to use in

this study, it was found that the double inlet configuration with two 2.5 cm diameter inlets was superior for viewing the transient flow fields of the inlet vortex. The double inlet apparatus creates an "inviscid ground plane," due to the symmetry of the inlets.

The visualization of the flow was achieved using hydrogen bubbles. The bubble generator is a DC circuit, with the cathode on a platinum wire and the anode on a plate far downstream in the tunnel [3]. The water is electrolyzed at the wire cathode and the hydrogen ions combine to form hydrogen gas which is carried away by the flow in hydrogen bubbles. The platinum wire, 0.025 mm in diamter, was introduced to the tunnel afixed to movable probes. The probes were plastic and plexiglass struts, streamlined to minimize their interference effects. The bubbles were illuminated and videotaped.

The water tunnel velocity, determined by measuring the distance between pulsed hydrogen bubbles, was maintained at 8 cm/sec. Since the height to diameter ratio (H/D) was set by the double inlet at 1.4 and the tunnel velocity was fixed, the stability of the inlet/trailing vortex system was investigated by varying the flow rate through the pump.

6-2 OBSERVATIONS

During the course of the visualization, several transition features of the inlet vortex were observed. The first of these was an intermittent inlet vortex seen at low U_i/U_e. When $U_i/U_e \sim 0$, two distinct trailing vortices can be seen, as shown in Fig. 6-2(a). As U_i/U_e was slightly increased, a weak connecting vortex would

sporadically form, Fig. 6-2(b). It resulted from the merge of the two innermost vortices, at a location about one diameter downstream of the centerline of the inlets. The vortex system, however, returned to two trailing vortices, Fig. 6-2(a), without any change in the flow rate when this vortex split in the middle.

A second feature seen was the abrupt transition from two trailing vortices to a strong inlet vortex. At high U_i/U_e, a stable but weak vortex would form and, without significant increase in U_i/U_e strong inlet vortex would suddenly appear. The sequence of events is illustrated in Fig. 6-3(a,b,c). At low U_i/U_e, two trailing vortices are present. When U_i/U_e is increased to between 10 and 12 a connecting vortex would form, Fig. 6-3(a), again about one diameter downstream. (This one differed from the intermittent vortex, though, in that it did not split.) With a small increase in flow rate, the arc in the vortex line reduced, Fig. 6-3(b). A cavitation bubble filament also appeared in the center of the vortex. The arced vortex would then abruptly shift upstream to become a nearly vertical core in the plane of the inlet's axes, Fig. 6-3(c). Associated also with the sudden formation of the strong inlet vortex, the cavitation bubble filament became more pronounced.

The third feature was a hysteresis characteristic of the inlet vortex. This became apparent when the abrupt formation was compared to the collapse of the inlet vortex, which was gradual. The inlet vortex became apparent near $U_i/U_e = 12$ whereas the vortex system did not return to two trailing vortices until $U_i/U_e \sim 2$.

Decrease in the U_i/U_e from 10 caused the inlet vortex to widen and tighten, as seen in Fig. 6-4(a) and (b). Continued decrease in the velocity ratio caused an arcing downstream and further expansion of the core, Fig. 6-4(c) and (d). Until at low U_i/U_e (~2) the vortex separated from the inlets and two pairs of trailing vortices became visible, Fig. 6-4(e). The vortex thus weakened gradually and then separated from the inlets. This contrasted the splitting and direct return to two trailing vortices associated with the intermittent vortex.

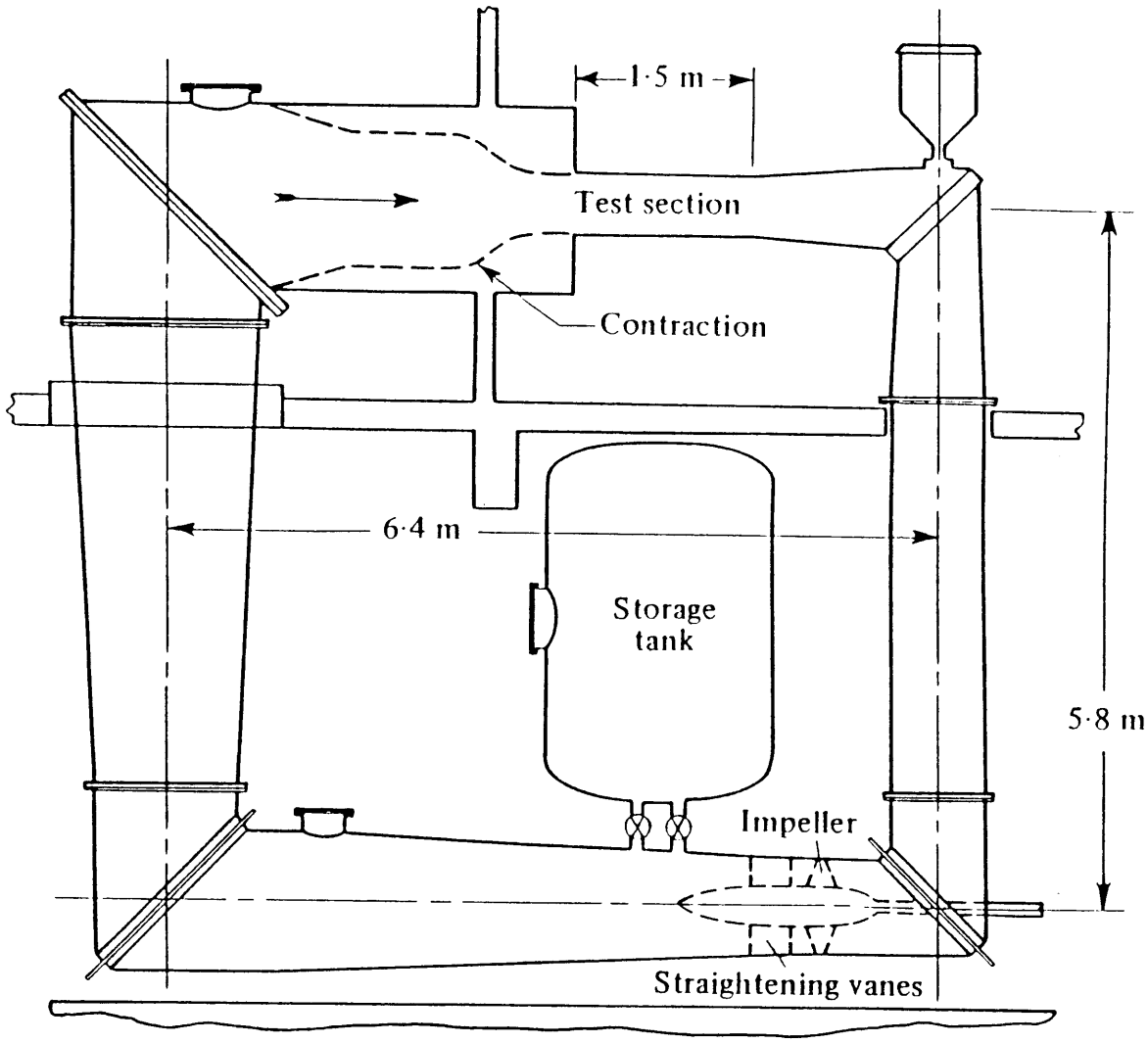

Figure 6-1 Schematic diagram of MIT Ocean Engineering Water Tunnel

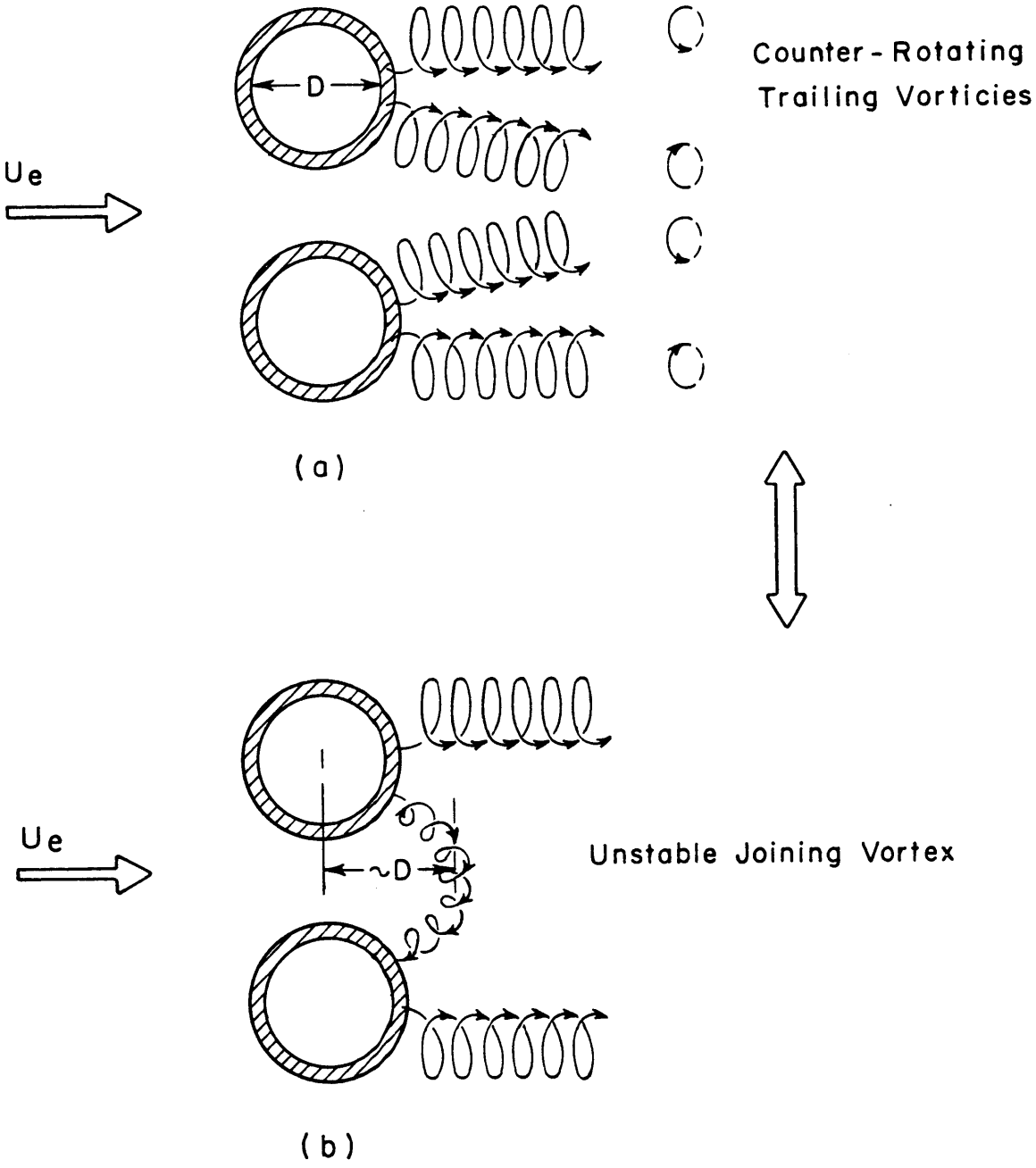

Figure 6-2 Structure of vortex lines for double inlet at low U_i/U_e

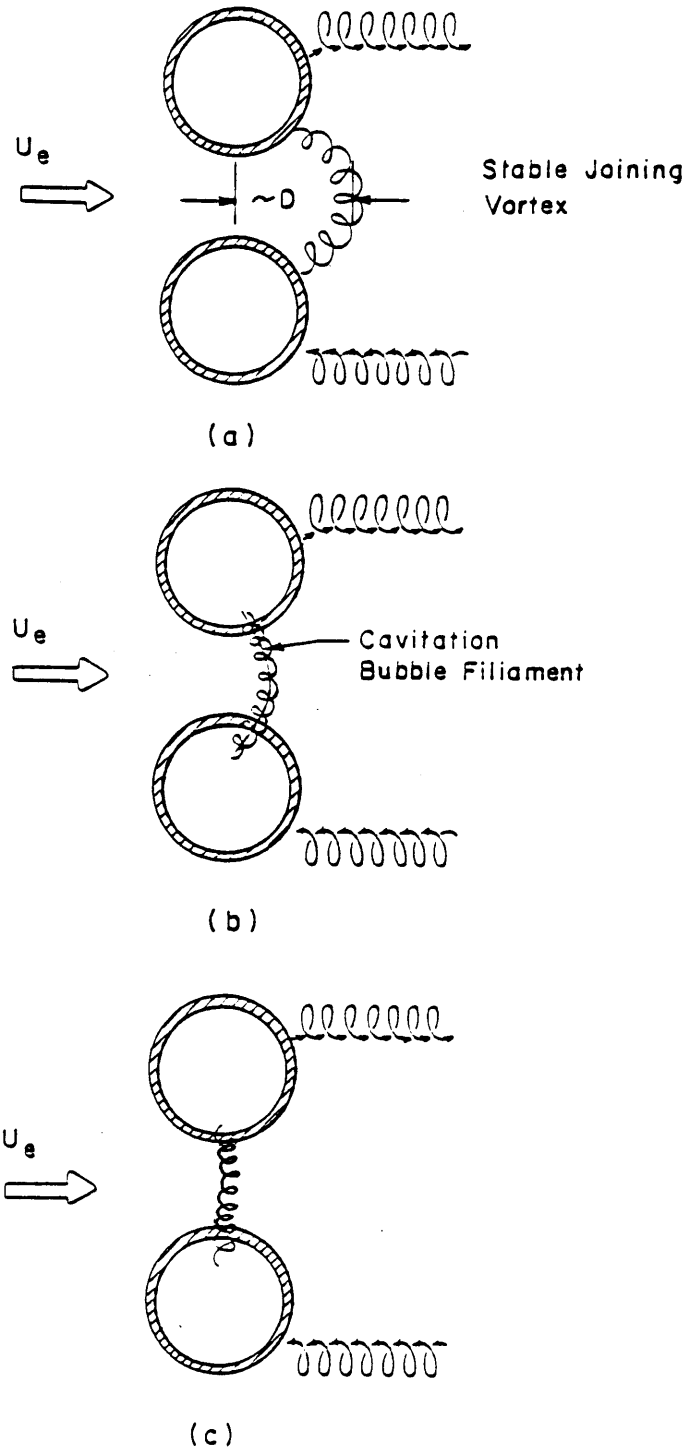

Figure 6-3 Sequence of vortex lines for double inlet at increasing high U_i/U_e

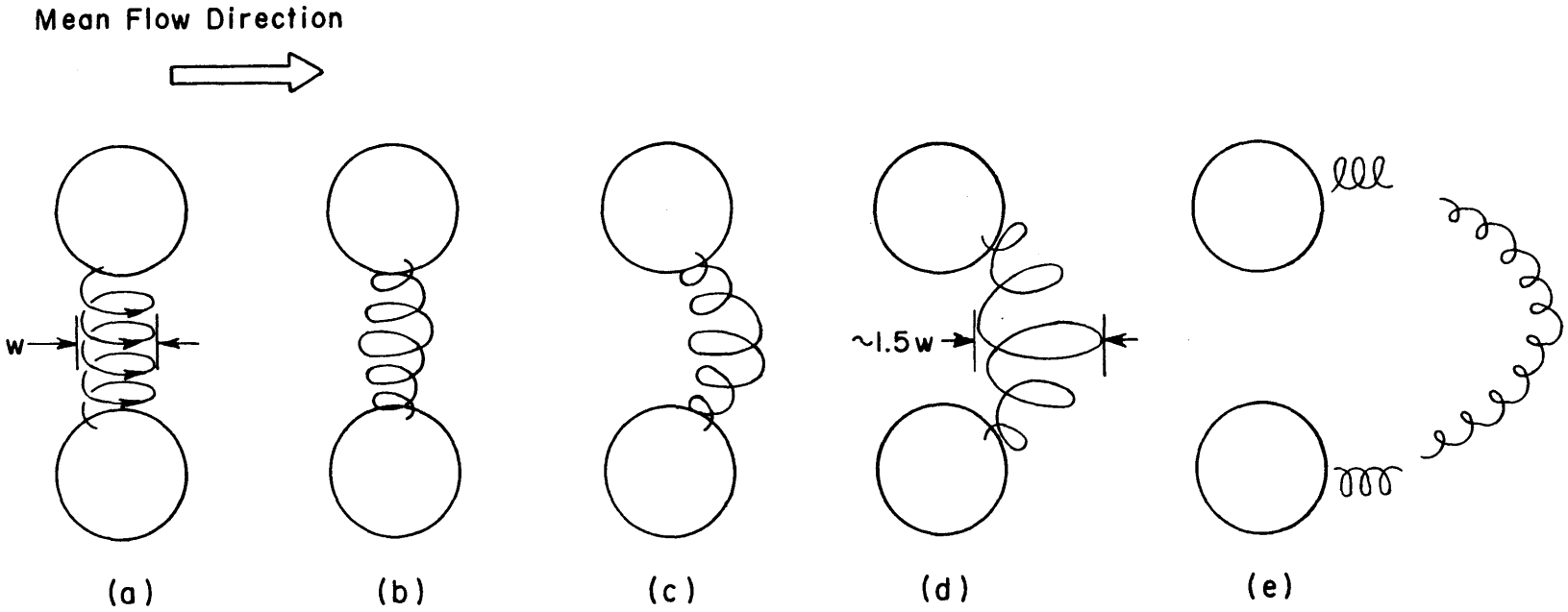

Figure 6-4 Sequence of inlet vortex for double inlet at decreasing U_i/U_e

CHAPTER VII

FLOW VISUALIZATION

Since this study addresses the complete flow field associated with the inlet vortex phenomena, flow visualization is an integral part in resolving the features of the flow quantitatively. Flow visualization was done in the wind tunnel for several reasons: to determine the stations where measurements should be taken, as discussed in Chapter 3, to locate the inlet vortex, as discussed in Chapter 5, as well as to formulate an overall picture of the flow field in the wind tunnel. Several types of visualization techniques were used, including lamp black, liquid crystal, and smoke illuminated by a laser beam.

7-1 FLOW VISUALIZATION ON THE OUTSIDE SURFACE OF THE INLET

Lamp black and liquid crystal techniques were used to locate the separation line on the inlet at conditions where a strong inlet vortex was present (namely H/D=1.0, U_i/U_e=35). Although both efforts were not totally conclusive, the techniques did indicate similar regions of high/low flow velocity or high/low heat transfer.

The lamp black, which consists of carbon particles suspended in kerosene, was thinly painted on the top and downstream side of the plexiglass inlet on the outside. Theoretically a clear separation line should form as lamp black is moved by the shear forces of the flow. However the shear forces, resulting from the velocity field on the order of 3 m/sec over the cylinder, were too small to overcome gravity and the lamp black tended to drip off the downstream side before the kerosene dried. The same problem, having shear forces that were too weak, was encountered

when an ink dot and wintergreen oil technique was attempted.

A different problem occurred in the liquid crystal study. This method involves thinly painting a liquid crystal substance, one whose color varies according to temperature (within a given range), onto carbon-impregnated conductive paper. The paper is then wrapped around a wooden inlet, which has been constructed in accordance with the design described in Chapter 2. The initial temperature of the conducting sheet is regulated by adjusting its supplied current. When introduced to a flow, variable heat transfer occurs along its surface and the temperature thus changes accordingly. The changes in temperature are noted by the change in color of the sheet due to the sensitivity of liquid crystal to temperature.

In two-dimensional flows this procedure has been shown to be an effective means of demonstrating the separation line because separated regions correspond to locations of low heat transfer, and hence high temperatures. In the case of an inlet vortex, the flow was not simple and a relationship between the heat transfer coefficients for regions on the cylinder, separated or unseparated, was not clear.

The similar region indicated by both the lampblack and the liquid crystal was a triangular region, shown in Figs. 7-1 and 7-2. Figure 7-1 is a photograph of the lampblack showing the line that roughly forms the hypotenuse of a right triangle, with the base being along the trip wire and the short leg along the inlet lip. Figure 7-1(a) shows the movement of the lampblack and 7-1(b) has the hypotenuse outlined for emphasis. The liquid crystal showed a region of bright colors, implying low

temperatures, in roughly the same region with one minor difference - the base was not directly at the trip wire but evenly spaced about 5 cm from the wire. In both cases the boundary started at the top of the cylinder (90 deg in cylinder coordinates) and about one diameter from the lip and reached the lip at about 120 deg. The similarity in results of the two different flow visualization techniques implies that this region is a major feature of the inlet vortex flow field. It can be argued that the only feature of a flow field that could cause such a result is the separation line; therefore the boundary seen in both techniques has been interpreted to be the separation line. A sketch of the separation line on the inlet, drawn from the lampblack and liquid crystal observations, is shown in Fig. 7-3. While the skew in the boundary is less in extent than the separation line seen during water tunnel observations [3], they are qualitatively similar.

7-2 FLOW VISUALIZATIONS ON THE INSIDE SURFACE OF THE INLET

Lampblack was painted inside the inlet to view the movement of the inlet vortex inside the plexiglass. Since the velocities inside the cylinder were around 135 m/sec the shear force on the film are enough to overcome the gravitational force. The results of the this study were difficult to photograph, but easy to observe.

It was seen, and is shown in Fig. 7-4, that the clockwise rotating inlet vortex moves clockwise as it proceeds into the inlet, as determined by the lampblack lines originating at 270 deg inside the inlet at the lip and continuing to 300 deg at two diameters downstream. As described earlier, this shifting is consistent with the potential flow representation of vortex and a wall, where a pressure field exists

that moves the vortex tangentially along the wall, in the direction of the vortex's rotation.

A second region of bent lampblack lines were observed inside the inlet at about 150 deg and were seen to bend counterclockwise. Figure 7-5(a) illustrates lampblack lines in a region where there is no vortex (θ around 10 deg). The bent lines can be seen in Fig. 7-5(b); they originate at around 150 deg at the lip and bend to about 145 deg two diameters into the inlet, which is much less movement then the strong inlet vortex lines. The opposite sense and lesser extent of shifting between this second region and the inlet vortex indicates there is a weaker, counter-clockwise rotating second vortex in the inlet. This result is in accordance with the interpretation of velocity measurements, which showed two regions of tangential velocity.

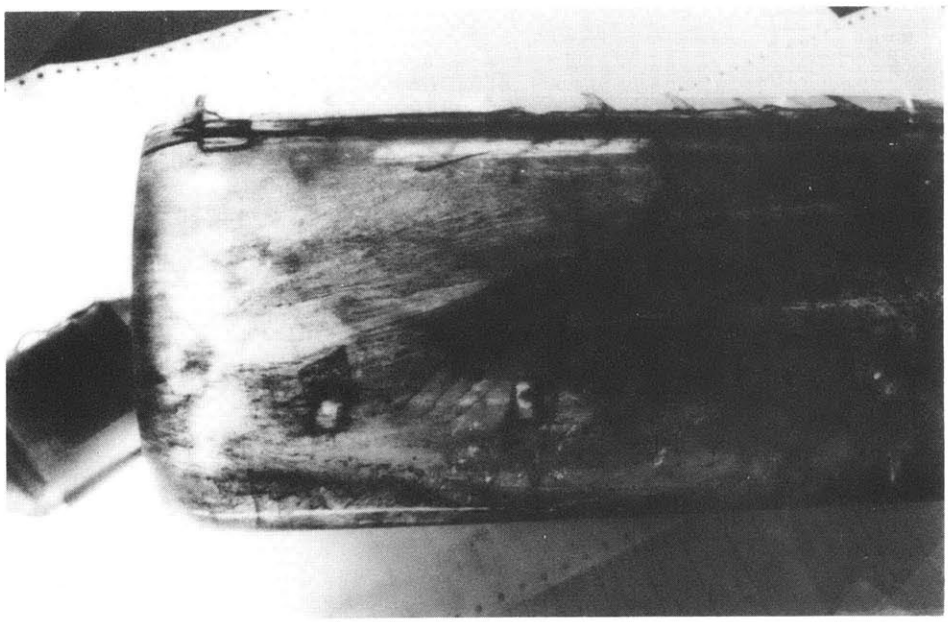

(a) Original flow pattern

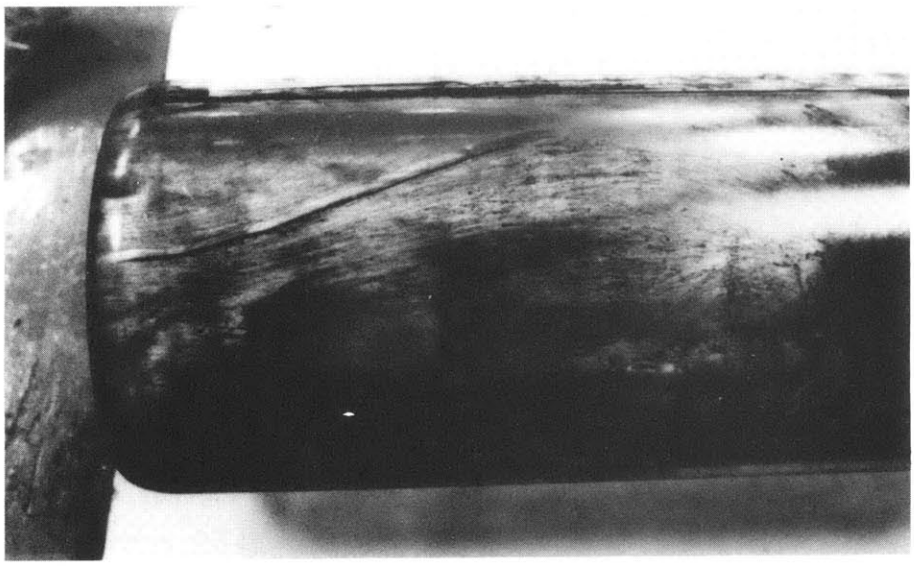

(b) Boundary outlined

Figure 7-1 Photographs of lampblack on inlet outside surface with inlet vortex present

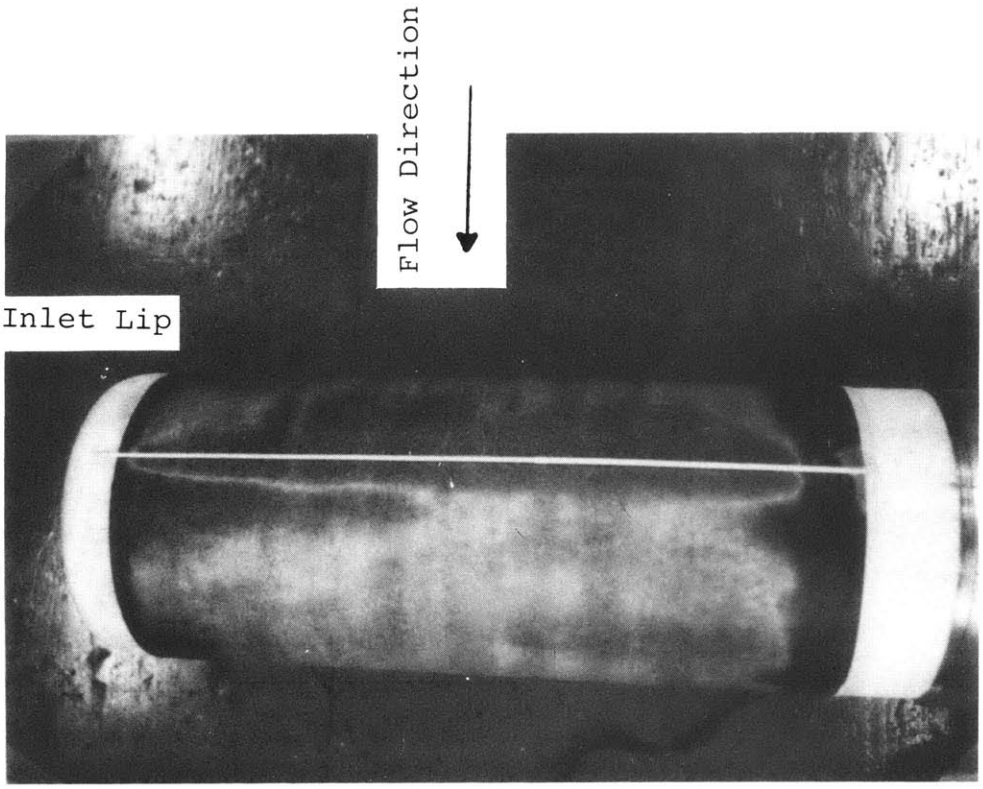

Figure 7-2 Photograph of liquid crystal on inlet surface with inlet vortex present

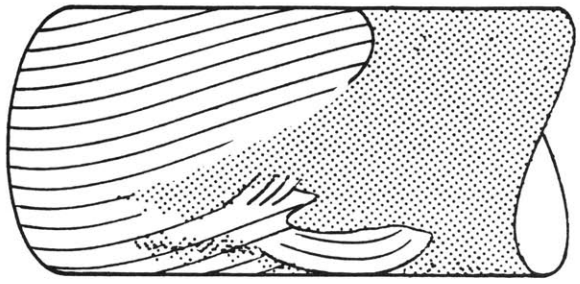

(a) Drawn from Fig. 7-1(a), which is a view of downstream side of an inlet.

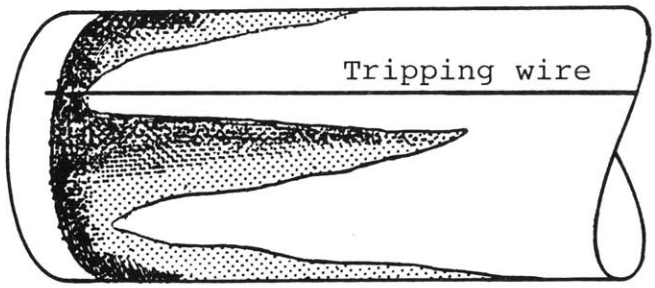

(b) Drawn from Fig. 7-2, which is a view of top side of an inlet.

Figure 7-3 Separation line along the axial length of inlet (drawn from lampblack and liquid crystal flow visualization)

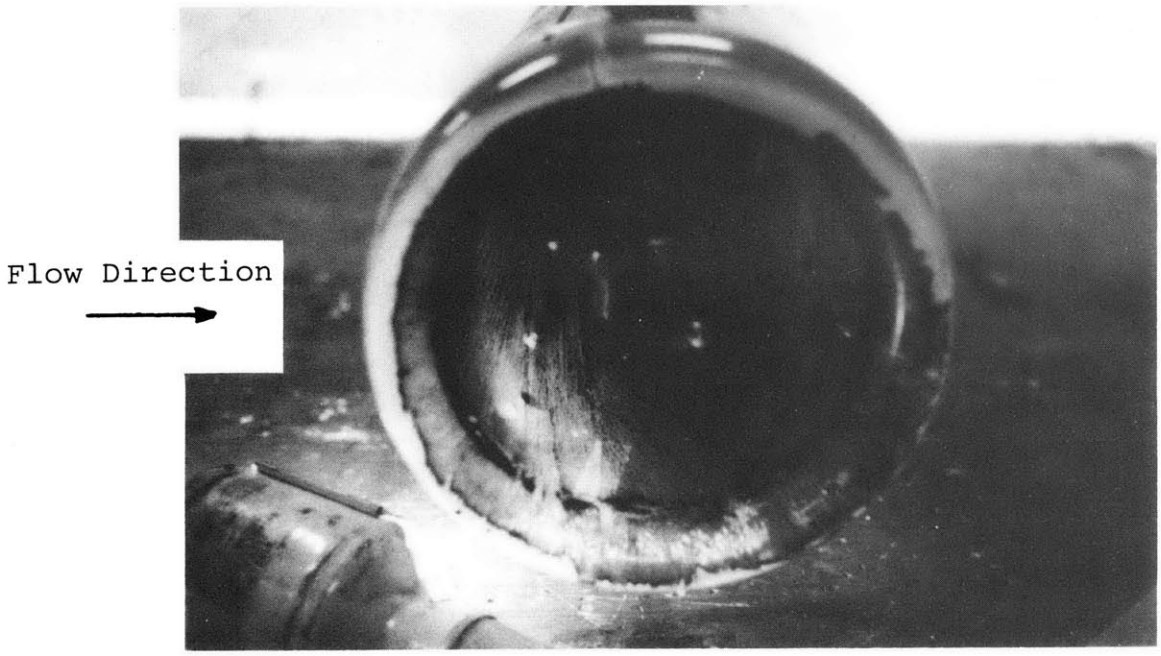

Figure 7-4 Photograph of lampblack on inlet inside surface with inlet vortex present, emphasis on inlet vortex

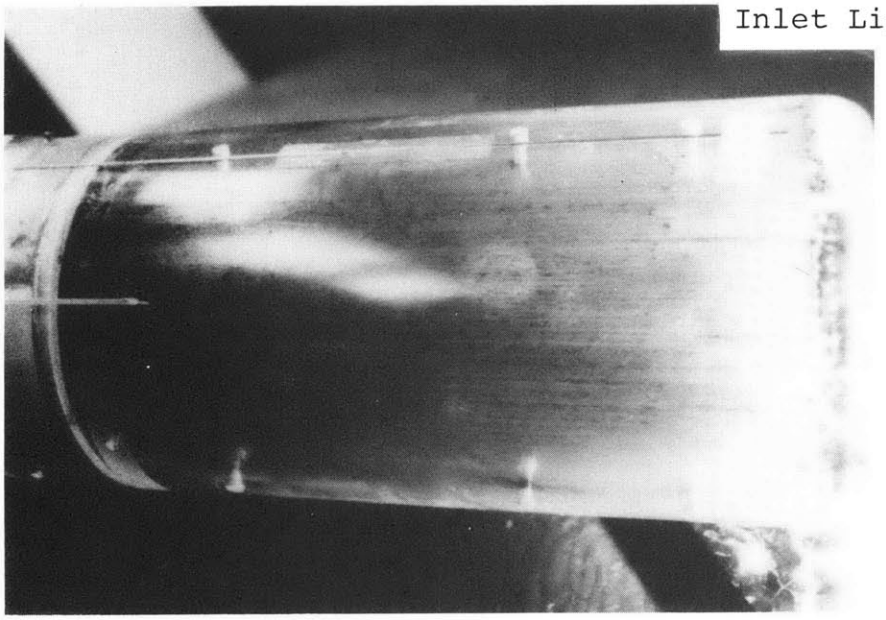

(a) Flow pattern at 0 deg. inside inlet.

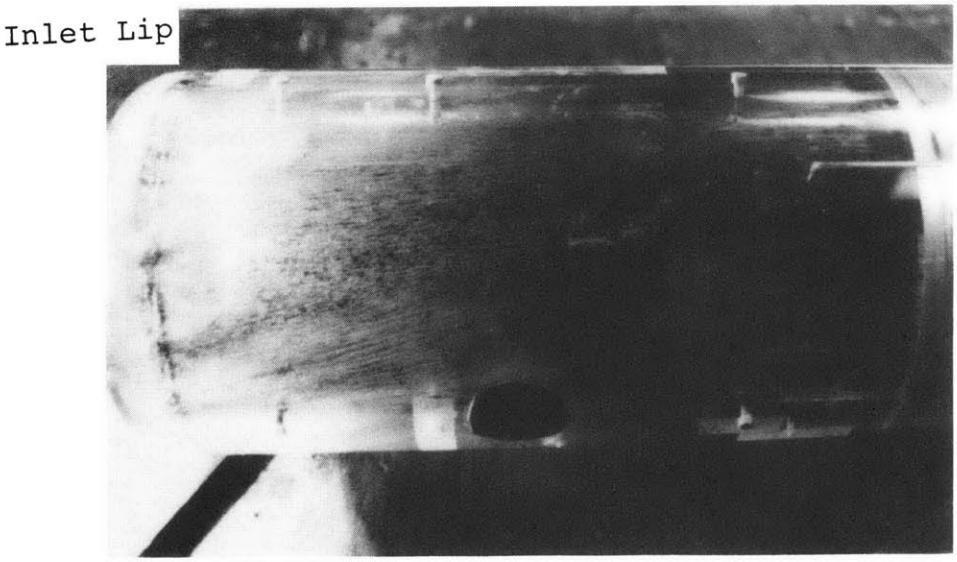

(b) Flow pattern at 180 deg. inside inlet.

Figure 7-5 Photographs of lampblack on inlet inside surface with inlet vortex present, emphasis on second vortex

CHAPTER VIII

CONCEPTUAL MODEL OF VORTEX STRUCTURE FOR INLET IN CROSSWIND

The quantitative measurements and flow visualization studies were done in order to verify a conceptual model of the vortex structure for an inlet in crosswind. The theory about the relationship between the inlet and trailing vortices was first presented by DeServi, et al. in [3], and is based on the hypothesis that because the circulation at a station far from the lip is small, then the existence of an inlet vortex requires the presence of a trailing vortex of comparable strength and opposite sense of rotation. The results of the measurements at H/D = 1.5 and U_i/U_e = 45 verify this idea, showing that within the experimental uncertainty the inlet vortex has the same circulation as the trailing vortex.

In addition to this, the studies have shown that changes in velocity ratio (U_i/U_e) or non-dimensional inlet height (H/D) have a qualitatively similar influence on the vortex structure. This is demonstrated schemetically in Fig. 8-1(a-e). From a qualitative point of view, both an increase in U_i/U_e or a decrease in H/D causes the ground plane to influence the capture area. However, for illustrative purposes, H/D has been taken to be constant and the flow regimes considered are those where U_i/U_e is increased.

With no inlet velocity, U_i/U_e = 0, the inlet can be considered a semi-infinite cylinder and its flow field, shown in Fig. 8-1(a), is a "horseshoe vortex" system (shown in a simplified manner as segments of straight lines). The joining leg is at the cylinder end and the side

legs extend to infinity along the cylinder axis.

At low velocity ratio, shown in Fig. 8-1(b), the joining leg extends to "infinity" through the pump. This concept is supported by the velocity measurements that show two nearly equal vortices inside the inlet at low U_i/U_e (or high H/D) which are the two halves of the joining leg being seen at a particular plane in the inlet. Extending the joining leg to connect with the side legs requires the formation of two legs perpendicular to the inlet axis. These perpendicular legs constitute the two counter-rotating trailing vortices, which have been documented during flow visualization studies. At low inlet velocity the capture surface is small and the ground plane, which is outside the capture area, has essentially no influence; for this case, the trailing vortices are symmetrical placed about the inlet.

As the velocity ratio is increased the ground plane enters the capture area and ground effects start to become important. Figure 8-1(c) illustrates this point. The asymmetry in the capture area shifts the two trailing vortices clockwise (as seen looking into the inlet). The upper vortex diameter increases and the lower vortex decreases in its diameter. It was also seen to intermittently attach to the ground. Both of these phenomena, an increase in diameter of the upper trailing vortex and decrease in diameter of the lower vortex for increased velocity ratio, were seen in the water and wind tunnels.

The final phases of inlet vortex formation are shown in Fig. 8-1(d) and (e). When the velocity ratio is further increased the lower vortex permanently attaches to the ground slightly downstream of the inlet,

Fig. 8-1(d), so that the lower leg becomes the inlet vortex. As described previously, this does not occur in a gradual fashion, and the transition is quite abrupt, leading directly to Fig. 8-1(e) where the vortex is in the centerline of the inlet. Concurrently, the upper leg is shifted further clockwise. The upper leg thus becomes the trailing vortex associated with an inlet vortex in a cross-wind and its core diameter has increased to nearly an inlet diameter.

The model described in the previous paragraphs is now summarized. For $U_i/U_e = 0$, the inlet in crosswind is effectively a semi-infinite cylinder. With low velocity ratio the ground does not effect the formation of two trailing vortices which are symmetrically located on the cylinder. The ground effect becomes important as mechanism of making the capture area asymmetric, shifting the trailing vortices clockwise. The formation of the inlet vortex occurs at high velocity ratio, at which time the bottom trailing vortex becomes the strong inlet vortex.

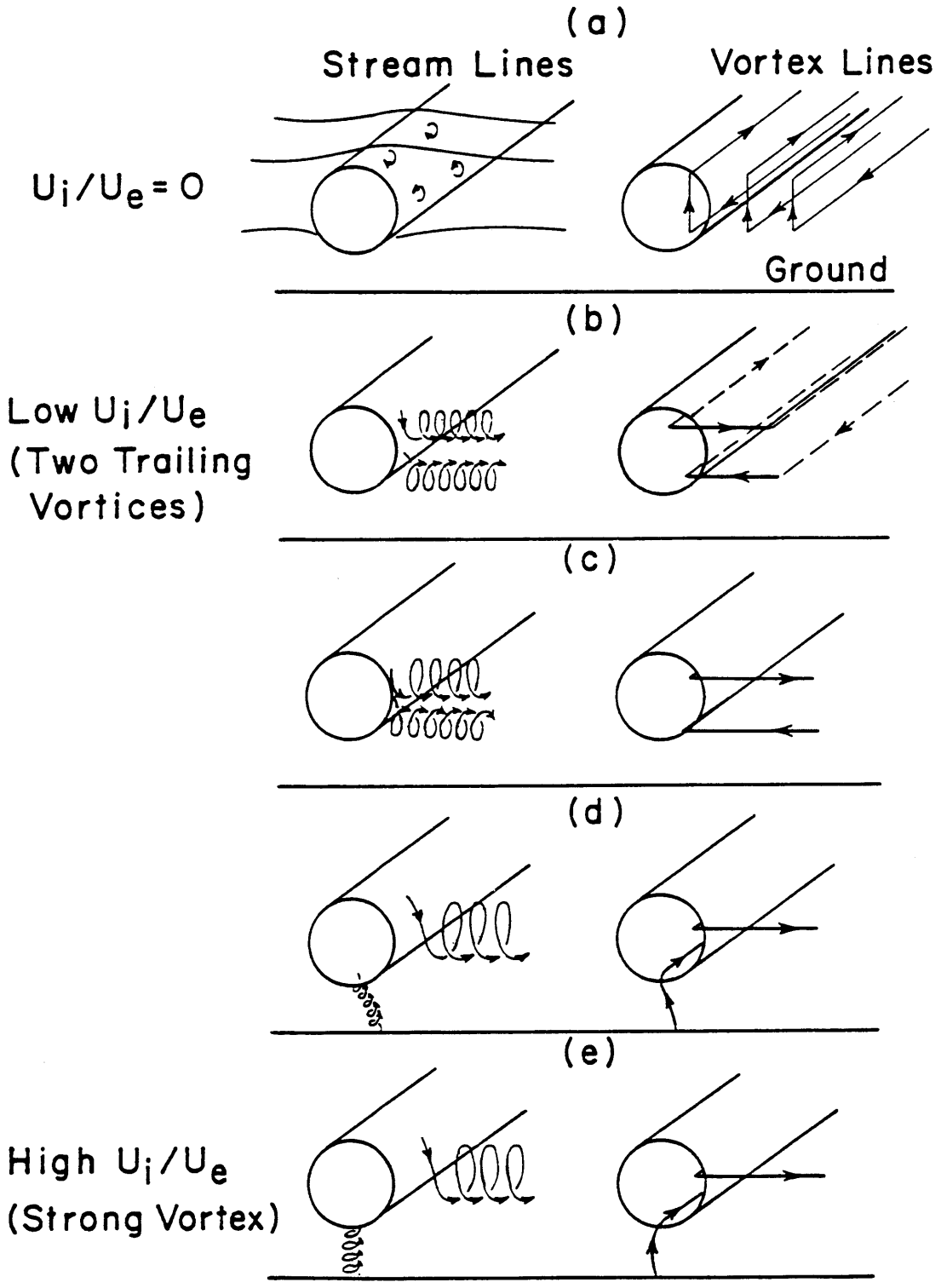

Figure 8-1 Schematic of vortex structure for an inlet in crosswind

CHAPTER IX

SUMMARY AND CONCLUSIONS

1) Detailed measurements of the flow field for an inlet operating in an (irrotational) crosswind at various combinations of H/D and U_i/U_e have been made. The purpose was to obtain quantitative information on the structure of the three-dimensional flow field associated with an inlet vortex.

2) At one condition, namely H/D = 1.5 and U_i/U_e = 45, where a strong inlet vortex was present, detailed velocity measurements were made in order to determine the circulation around the inlet and trailing vortices. It was found that both circulations were 3.0 ± 0.3 m^2/s. The numerical equality of the circulations verified a hypothesis based on the nature of the inlet/trailing vortex system. The measurements also showed the existence of a second vortex inside the inlet, with a direction opposite to the inlet vortex.

3) A limited parametric study was carried out to demonstrate the changes in circulation of the inlet vortex and in its position as the H/D was increased for a fixed velocity ratio U_i/U_e, or as the velocity ratio decreased for a fixed H/D. It was found, as expected, that increasing H/D has a qualitatively similar effect as decreasing U_i/U_e.

4) Flow visualization at the wind tunnel was used to indicate the separation line on the inlet surface and to visually demonstrate the existance of a second vortex inside the inlet.

5) Flow visualization studies at the water tunnel were also made of the transition between the inlet vortex/trailing vortex configuration and the flow regime with two trailing counter-rotating vortices. It was found that this transition is not gradual (as a function of U_i/U_e, say) but occurs abruptly at a critical value of this parameter. During the transition, the lower counter-rotating or trailing vortex moves downward to become the inlet vortex.

6) Based on the quantitative and qualitative results of this study, a conceptual model of the inlet/trailing vortex system for an inlet in a crosswind has been formulated.

CHAPTER X

RECOMMENDATIONS FOR FUTURE WORK

The measurements of inlet vortex strength for the inlet in crosswind in an irrotational upstream were made inside the inlet. Such measurements were possible because, if viscous effects were small, the circulation around the inlet vortex would be constant and the circulation of the vortex inside the inlet would be the same as that of the ground vortex. Furthermore, the measurements were at a location similar to the engine face where one wishes to have the velocity data. In order to make sure whether the above basic assumption does in fact hold, one measurement of the circulation around the ground vortex at a location outside the inlet in a three-dimensional flow field is necessary. This measurement can be done by using a hot wire anemometer with 45 degree slanted flat wire probe. A data acquisition program for the slanted hot wire probe calibration, including a stepping motor control program for traversing and rotating the probe, and facility are currently being developed.

The results of this study have been used to quantitatively support the hypothesis that the inlet and trailing vortices originate from a variation in circulation along the cylinder. To further support this hyphothesis, an experiment may be carried out using an inlet with a spinning sleeve. The inlet model creates a circulation about the inlet when the rotatable sleeve is spun. The sleeve can be spun so that the circulation created is opposite to the circulation induced by flow over the inlet. If the hypothesis is true, the inlet vortex would be eliminated when the sleeve is spun at an appropriate speed because the circulation along the inlet would

be forced to be nearly constant.

The proposed model consisting of a rotatable sleeve (mounted with bearings) sandwiched between two fixed surfaces is shown in Fig. 10-1. One fixed surface maintains the aerodynamic lip and the inside surface of the inlet; the other is the outside diameter. The sleeve has one section which is flush with the outside diameter of the inlet. The flush section is close to the lip and not more than 0.4 diameters wide since pressure on the inlet data indicates that the variation in circulation is predominantly in the region near the lip.

Accomodation for the driving system will have to be made outside of the capture surface for the expected testing conditions so as not to interfere with the inlet/trailing vortex system formation. From flow visualizations at various combinations of H/D and U_i/U_e, it was seen that the capture surface boundary was at most one diameter from the lip, therfore the driving system was placed 1.5 diameters from the lip. The driving system had to have a variable speed controller, so that the generated "cancelling" circulation could be adjusted, and enough torque to overcome bearing friction. It was calculated that the sleeve would rotate between 300 and 600 rpm to induce circulations equal to inlet vortex circulations measured during this study. The driving system is shown in Fig. 10-2.

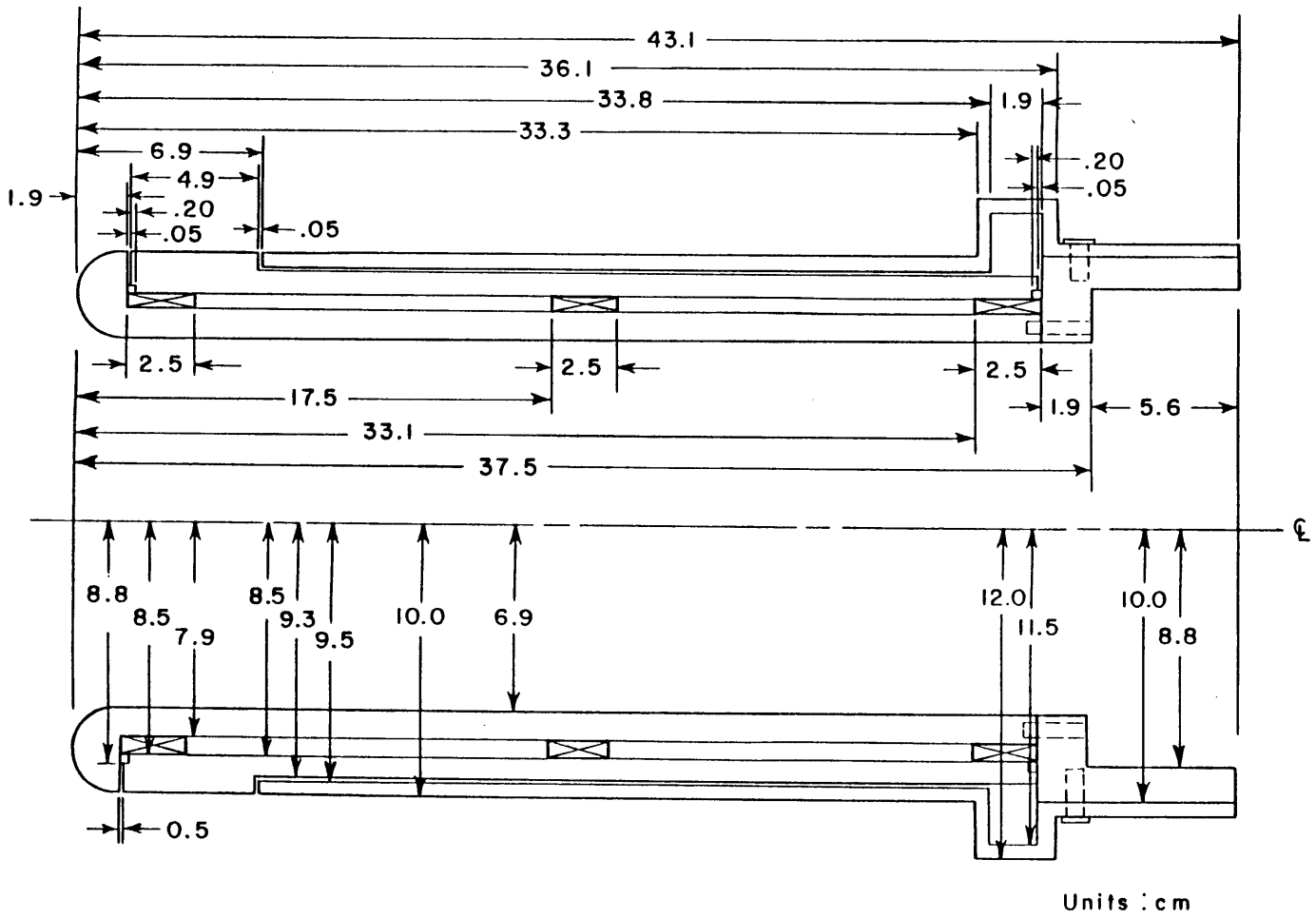

Figure 10-1 Proposed inlet model for demonstrating relation between vortex strength and circulation

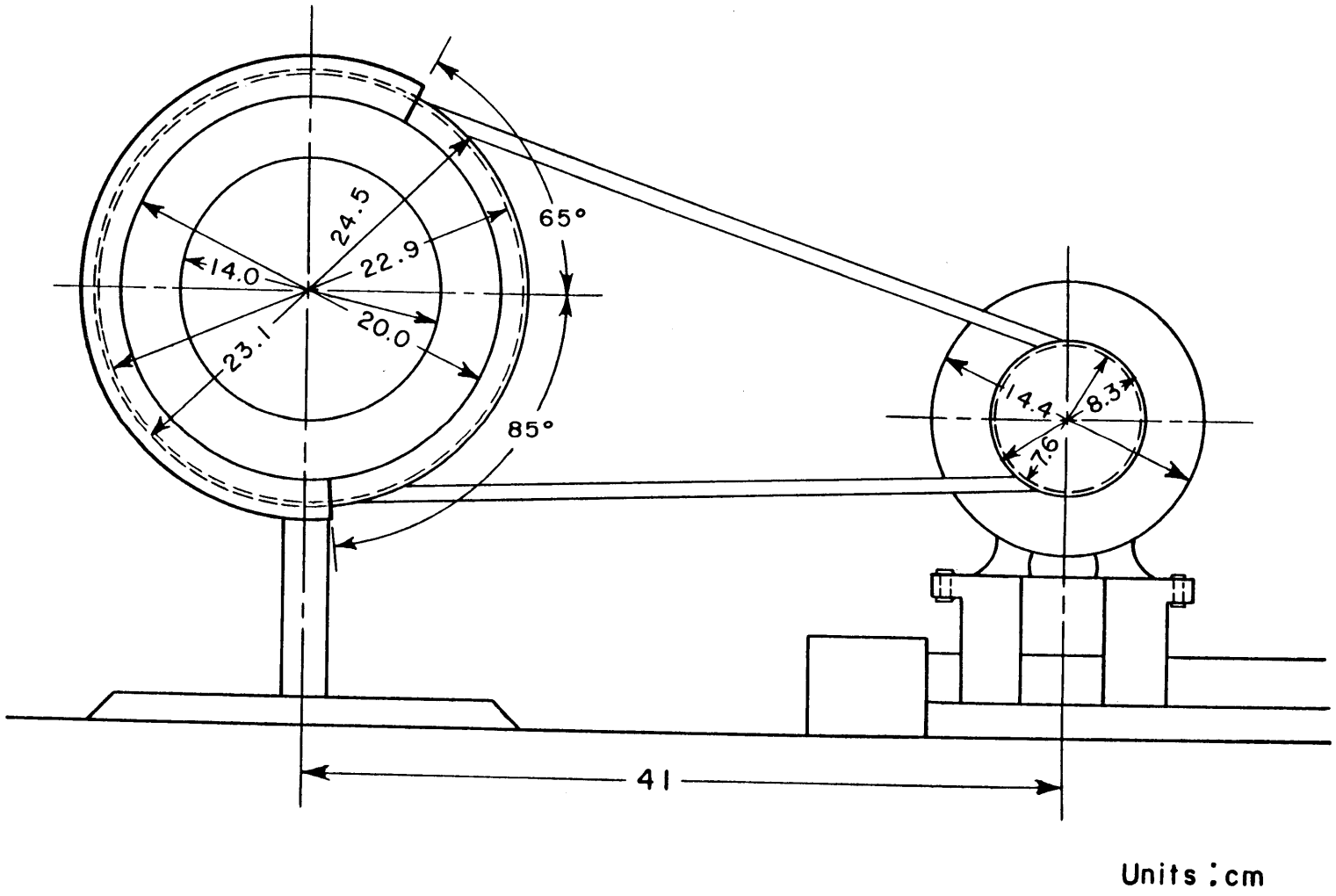

Figure 10-2 Schematic diagram of proposed inlet model, support, and driving system

Bibliography

[1] Younghans, J.L., and Paul, D.L., "Considerations in Inlet/Engine Integration," Chapter 13 in The Aerothermodynamics of Aircraft Gas Turbine Engines, G.C. Oates, editor, AFAPL-TR-78-52, Air Force Aero Propulsion Laboratory, 1978.

[2] Motycka, D.L., "Ground Vortex - Limit to Engine/Reverser Operation," Trans. ASME, J. Engng. for Power, 98, 1976, pp. 258-266.

[3] DeSiervi, F., et al., "Mechanisms of Inlet Vortex Formation," J. Fluid Mechanics, 124, 1982, pp. 173-207.

[4] Liu, W., et al., "Surface Static Pressures in an Inlet Vortex Flow Field," to be presented at ASME Gas Turbine Conference, June, 1984.

[5] Liu, W., "Design and Analysis of an Experimental Facility for Inlet Vortex Investigation," MIT Gas Turbine Laboratory Report No. 166, 1982.

[6] Markham, J.R., "The MIT Wright Brothers Wind Tunnel and Its Operating Equipment," SAE Journal (Trans.), September 1941.

[7] Boles, M.A., and Stockman, N.O., "Use of Experimental Separation Limits in the Theoretical Design of V/STOL Inlets," AIAA Paper 77-878, presented at 13th Propulsion Conference, July 1977.

[8] Schlichting, H., Boundary Layer Theory, New York: McGraw-Hill Book Co., 1979, p. 21.

[9] Motycka, D.L., private communication, 1983.

[10] Marble, F.E., private communication, 1983.

[11] Bryer, D.W., and Pankhurst, R.C., Pressure-Probe Methods for Determining Wind Speed and Flow Direction, London: Her Majesty's Stationary Office, 1971.

[12] Krause, L.N., and Dudzinski, T.J., "Flow Direction Measurement with Fixed-Position Probes in Subsonic Flow Over a Range of Reynolds Numbers," NASA TM X-52576, 1969.

[13] Treaster, A.L., and Yocum, A.M., "The Calibration and Application of Five-Hole Probes," ISA Trans., Vol. 18, No. 3, 1979, pp. 23-34.

APPENDIX A

CALIBRATION OF FLOW MEASURING INSTRUMENTS

In this chapter detailed descriptions of the calibration of the fluid measuring probes used during this experiment are presented. Two three-hole pitot tubes, two kiel probes, a hemispherical five-hole pitot tube and a prism five-hole pitot tube were the pressure probes that were calibrated. Also calibrated was a hot wire anemometer. All of the calibrations were done in the Wright Brothers Wind Tunnel.

The pressure probe calibrations were designed to determine a relation between the true local total and static pressures and the measured pressures at known probe orientation. It is important that the relation be independent of the magnitude of velocity and be a function of flow angle only. In order to achieve velocity magnitude independence, measured pressures were non-dimensionalized appropriately. During data acquisition, the velocity or flow angle was determined through the obtained non-dimensional calibration curves.

A-1 THREE-HOLE PRESSURE PROBES

A three-hole probe can be used to determine both flow speed and direction in one plane as long as flow is within a limited range of pitch [11]. More specifically, when a normalized yaw pressure difference is employed, three-hole probe is an accurate means of determining yaw angle for flow with pitch angle less than ± 15 deg. and the yaw angle so determined is insensitive to Mach number within the range of 0.3 and 0.9 [12].

Two three-hole Cobra probes (United sensor catalog #CA 120 12 CD),

shown in Fig. A-1(a), were used during this experiment to determine yaw angle only in a flow with necessarily small pitch angles and velocities of 50-140 m/sec. Each three-hole pitot tube was calibrated at two different tunnel velocities, 21 m/sec and 30 m/sec, and 0 deg. pitch angle. The wind tunnel's turntable was used to range the yaw angles between -30 deg and +30 deg. The normalized yaw pressure difference was defined to be the difference in the pressure at the two outside holes divided by the freestream dynamic pressure ($1/2\ \rho U_e^2$). It was reported by the manufacturer that the probes are not Reynolds number dependent in angle determination.

The results of the calibration are shown in Figs. A-2 and A-3. Although the data points were almost linear within the calibrated yaw angle range, a second order polynomial curve was fit to the points using a least square method. As shown in Figs. A-4 and A-5, the calibration curves are coincident regardless of the velocity or the pressure transducers used, verifying the probe's insensitivity to velocity change and proving the repeatability of the measurements. These calibration curves were used to determine the flow's yaw angle once the outside tube pressure differences and the dynamic pressure were known. (See Figs. A-6 and A-7.)

The three-hole probes were used during the experiment to measure yaw angles near the wall inside of the inlet. Since it was not possible to manually accurately align the probes to face forward, it was necessary to calibrate the probes each time they were set in their data acquisition positions. The calibration entailed measuring the offset

angle of the probes, the angle between axial and the probe's normal as shown in Fig. A-8, in their set position in an environment with axial flow. Swirl inside the inlet was minimized 1) by facing the inlet upstream, 2) positioning the lip beyond the leading edge of the floor, such that $H/D \sim 6$ (in order to remove ground effects), and 3) operating at $U_i/U_e \sim 3$ (so that any swirl centered in the tunnel would be outside of the capture area). Once the offset angle has been determined the yaw angles found during the experiment can be corrected. Calibration on the wind tunnel yaw table is accurate to 0.1 deg and calibration in the inlet was accurate to 0.2 deg, therefore the accuracy of the angles reported by the three-hole probe is valid to 0.3 deg.

A-2 KIEL PROBES

A Kiel probe, shown in Fig. A-1(b), is a shrouded total pressure tube which is insensitive to yaw and pitch angles ranging between more than +40 deg and -40 deg [11]. Even with this generic claim about them, the two Kiel probes used in this experiment were calibrated and verified to be insensitive to yaw up to ± 30 deg. Kiel probes are also reported by their manufacturer to indicate the true total pressure up to Mach number of 1.

The probes were used in this experiment to determine the total pressure of flow inside the inlet, with necessarily small pitch and yaw angles and a velocity of 135 m/sec. inside the inlet. Since the yaw angles were expected to be less than ± 20 deg, even a 10 deg misalignment would not effect the accuracy of the Kiel probes, allowing the probes to be aligned by hand in their data acquisition positions.

A-3 FIVE-HOLE PRESSURE PROBES

A five-hole probe can be used to determine two perpendicular flow angles and the flow velocity. Two types of five-hole probes were used in this experiment, a hemispherical probe, shown in Fig. A-9(a), for determining flow in the trailing vortex region, and a prism probe, Fig. A-9(b), for determining the flow field inside the inlet. A hemispherical probe is equally sensitive to pitch and yaw whereas a prism probe has increased sensivitiy to small variation in the yaw plane [13], however size and force requirements inside the inlet dictated that a prism probe would be used.

Since both pitch and yaw angles are desired from both five-hole probes' pressure measurements, it was necessary to calibrate the probe in both planes to angles of ± 30 deg., forming a "net" of calibration points. The calibration was done by pitching the probe, measuring the angle with an inclinometer, and yawing the probe's stand, using the wind tunnel's yaw table. The calibration stand is illustrated in Fig. A-10. Six different calibration pressure coefficients were defined as follows:

$$P_{ave} = (P_2 + P_3 + P_4 + P_5) / 4$$

$$Cp_{yaw} = (P_3 - P_5) / (P_1 - P_{ave})$$

$$Cp_{pitch} = (P_4 - P_2) / (P_1 - P_{ave})$$

$$F_{yaw} = (P_3 - P_5) / (P_3 - P_1 + P_5 - P_1)$$

$$F_{pitch} = (P_4 - P_2) / (P_4 - P_1 + P_2 - P_1)$$

$$H_{dynamic} = [P_{total} - P_{static}]pitot / (P_4 - P_1 + P_2 - P_1)$$

$$Cp_{total} = (P_1 - P_{t_{pitot}} / (P_1 - P_{ave})$$

Both five-hole probes were calibrated the same way. The curves are all

spline curves passing through individual data points. The results of the hemispherical probe calibration are presented first.

Since it is possible to non-dimensionalize the pressure measurements in several ways, a primary interest in calibration is to choose the nondimensional coefficients which will result in the most accurate determination of the flow angles. For the five-hole hemispherical probe, the Cp_{yaw} vs yaw angles curves, Fig. A-11, can be seen to be slightly dependent on pitch, whereas F_{yaw} vs. yaw angles can be seen in Fig. A-12 to vary less with different pitch angles. Looking at the values of the pressure coefficients, Cp_{yaw} ranges between $\pm$ 5 but F_{yaw} coefficients are more sensitive to yaw variation, ranging only between $\pm$ 3. In a parallel manner, Cp_{pitch} vs. pitch angles at constant yaw curves, seen in Fig. A-13, spread out; whereas F_{pitch} vs. pitch angles at constant yaw curves, Fig. A-14, fall closer together. In the same way, F_{pitch} is more sensitive to pitch, ranging between $\pm$ 2, then Cp_{pitch}, which ranges from $\pm$ 4.5

The advantage of the curves collapsing to one is that one plane angle can be determined independent of the other. However, neither of the Cp or F curves collapsed to one, therefore it would be necessary to determine both pitch and yaw by double interpolation. There is, though, an advantage associated with being insensitive to changes in the calibrating plane. This is the angle can be determined more accurately since the values change more between angles. Cp_{yaw} and Cp_{pitch} were both significantly less sensitive to flow changes than F_{yaw} and F_{pitch} in yaw and pitch planes respectfully. On this basis Cp_{yaw}

and Cp_{pitch} were used as the calibration coefficients for determining pitch and yaw angles. A grid of Cp_{yaw} vs. Cp_{pitch} is shown in Fig. A-15, where the relatively horizontal curves are curves of constant yaw and relatively vertical curves are constant pitch curves.

The $H_{dynamic}$ coefficient is the ratio of the true dynamic pressure ($1/2\rho U_e = (P_t - P_s)_{pitot}$) to a measured pressure difference and is used to determine the velocity in flow where the density is known. Figure A-16 shows $H_{dynamic}$ vs. pitch angles at constant yaw curves for the hemispherical five-hole probe, illustrating $H_{dynamic}$'s dependence on both pitch and yaw. Therefore, after the pitch and yaw angles have been determined, $H_{dynamic}$ can be interpolated. The dynamic pressure can then be determined from the quotient of $H_{dynamic}$ and the measured pressure difference, and as long as the density is known, the velocity can be calculated from the dynamic pressure.

During data acquisition, the hemispherical five-hole is used to determine the velocity and direction downstream of the inlet where the flow is expected to be between 1.5 and 4.5 m/sec. It was also necessary for the probe to determine the local true total pressure. When facing directly into the flow total pressure is measured on the center hole, however when the probe is pitched or yawed the center hole is no longer the true total pressure. Cp_{total} is the calibration coefficient for determining the local true total pressure from calculated yaw and pitch angles and measured pressures. The calibration curves of Cp_{total} vs pitch angles for constant yaw are shown in Fig. A-17. Similiar to the $H_{dynamic}$ calibration curves, it can be seen that Cp_{total} is

dependent on both pitch and yaw, requiring both yaw and pitch to be determined.

Before calibration, the hemispherical probe was fixed into its holder. Prior to data acquisition, it was necessary to level and square the traversing mechanism and insert the holder into the traversing unit so that the probe would be facing directly upstream. Fixing the probe in a holder eliminated calibrating the orientation of the holes on the probe.

The five-hole prism probe was calibrated the same way as the five hole hemispherical probe, but as expected the different probe geometry caused the calibration curves to have different shapes. The probe geometry difference can be seen in the Cp_{yaw} vs yaw angles and Cp_{pitch} vs pitch angle curves, Figs. A-18, A-19. In the later the values of Cppitch range between ± 4 whereas the Cp_{yaw} values only range between ± 1.2, demonstrating the probes inherent sensitivity to yaw. Comparing Cp_{yaw} vs yaw and F_{yaw} vs yaw , Fig. A-20, figures both have a spread in the constant pitch curve and both range between ± 1.2. The advantage of using the Cp non-dimensionalization method is seen when Cp_{pitch} vs pitch and F_{pitch} vs pitch, Fig. A-21, figures are compared. Even though both F_{pitch} and Cp_{pitch} collapse nicely to one curve, the Cp_{pitch} is less sensitive to pitch angles. The grid of Cp_{yaw} vs Cp_{pitch} for the prism probe is shown in Fig. A-22.

Besides determing the flow's angles, it was necessary to determine the flow's velocity inside the inlet. Therefore the $H_{dynamic}$ coefficients for the prism probe were calculated, and illustrated in

Fig. A-23, the $H_{dynamic}$ vs pitch at constant yaw curves displays the prism probes strong dependence on pitch and slight dependence on yaw. The collapse of the $H_{dynamic}$ curves for constant yaw is consistant with what is expected from the probes geometry.

The operating conditions of the five-hole hemispherical probes was in a flow expected to be between 1.5 and 4.5 m/sec and its calibration was done at 3 m/sec, so Reynolds number effect on the calibration's validity was not considered. However, the operating conditions for the prism five-hole probe were expected to be a velocity around 135 m/sec with small pitch and yaw angles and, due to loading constraints, its calibration was done at 6 m/sec. Fortunately it has been shown that Cp non-dimensionalized coefficients are essentially unaffected by Reynolds number variation for prism and hemispherical five-hole probes [13]. In addition, the sensitivity of the prism five-hole probe to Reynolds number was investigated in a Gas Turbine Lab jet facility and within the limit of error of the investigation, the probe was shown to be insensitive to Reynolds number variation. The $H_{dynamic}$ coefficient was defined to be non-dimensionalized by a pressure difference in the less sensitive pitch plane so that it could also be considered unaffected by Reynolds number variation.

A-4 HOT WIRE ANEMOMETER

The test section floor boundary layer was to be measured by using a TSI 1050 Series Hot Wire Anemometer with Model 1213-20 Hot Film Probe. The hot wire anemometer was calibrated in the free stream flow of the test section using a pitot-static tube to measure the reference dynamic

pressure. A baratron was used to determine the dynamic pressure in torrs, which could then be converted to velocity once the air density was known. During the velocity calibration procedure, the output from the hot film anemometer and the velocity determined from the pitot-static pressure difference were plotted on the computer terminal. See Fig. A-24 for schematic diagram. After all necessary data were taken a least square second degree polynomial curve was fitted through the data points as shown in Fig. A-25. This resulted in the calibration curve equation.

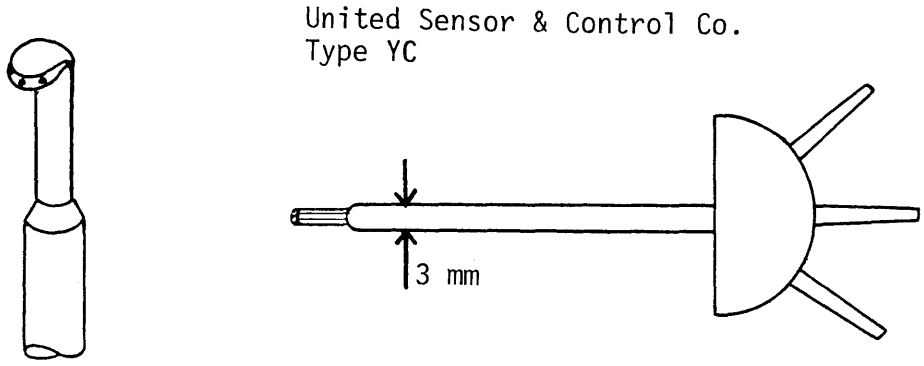

(a) 3 Hole Pitot Tube

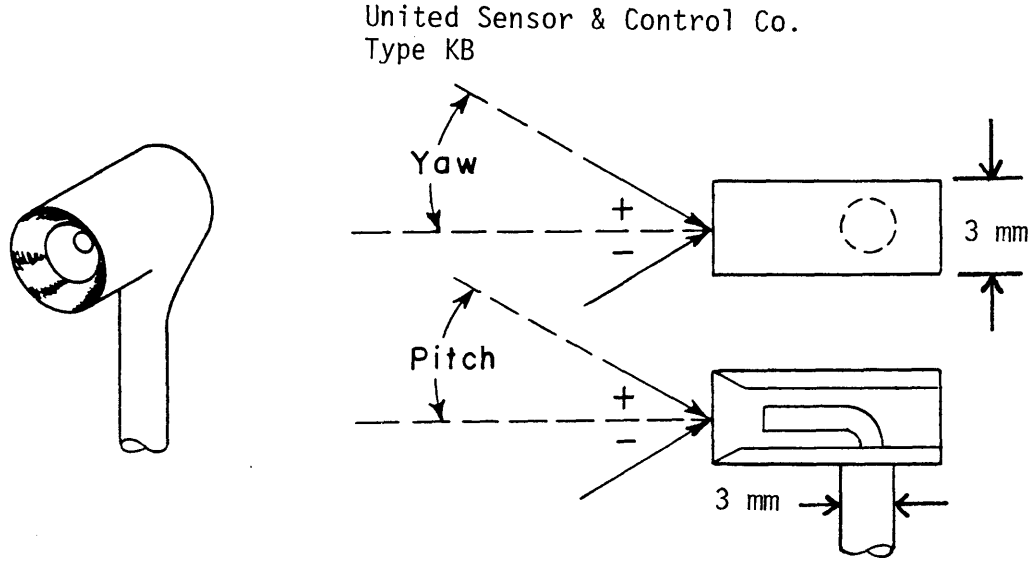

(b) Kiel Probe

Figure A-1 Three-hole pitot tube and Kiel probes for pressure measurement inside inlet

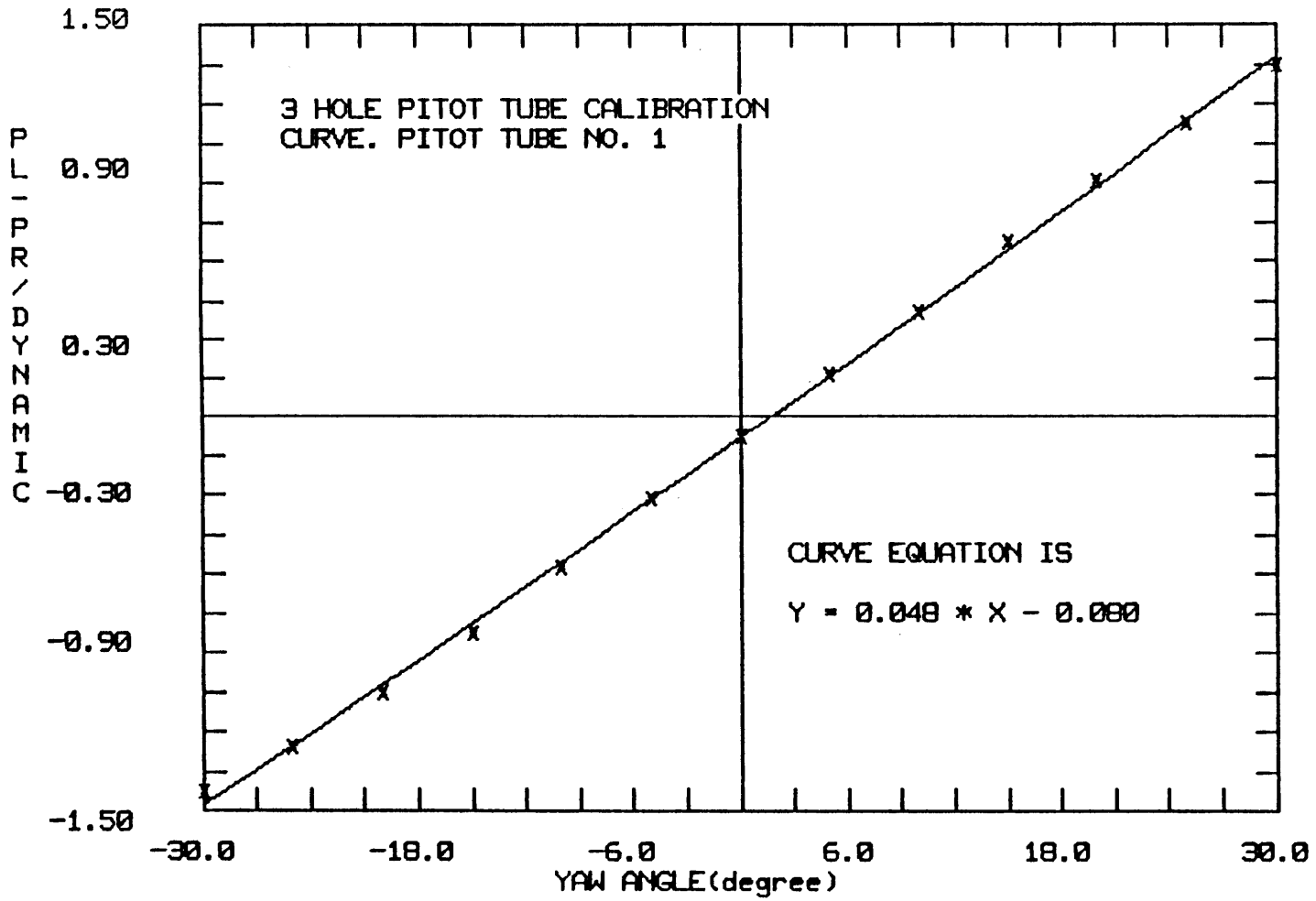

Figure A-2 Calibration curve of three-hole pitot tube no. 1 at U_e = 16 m/s

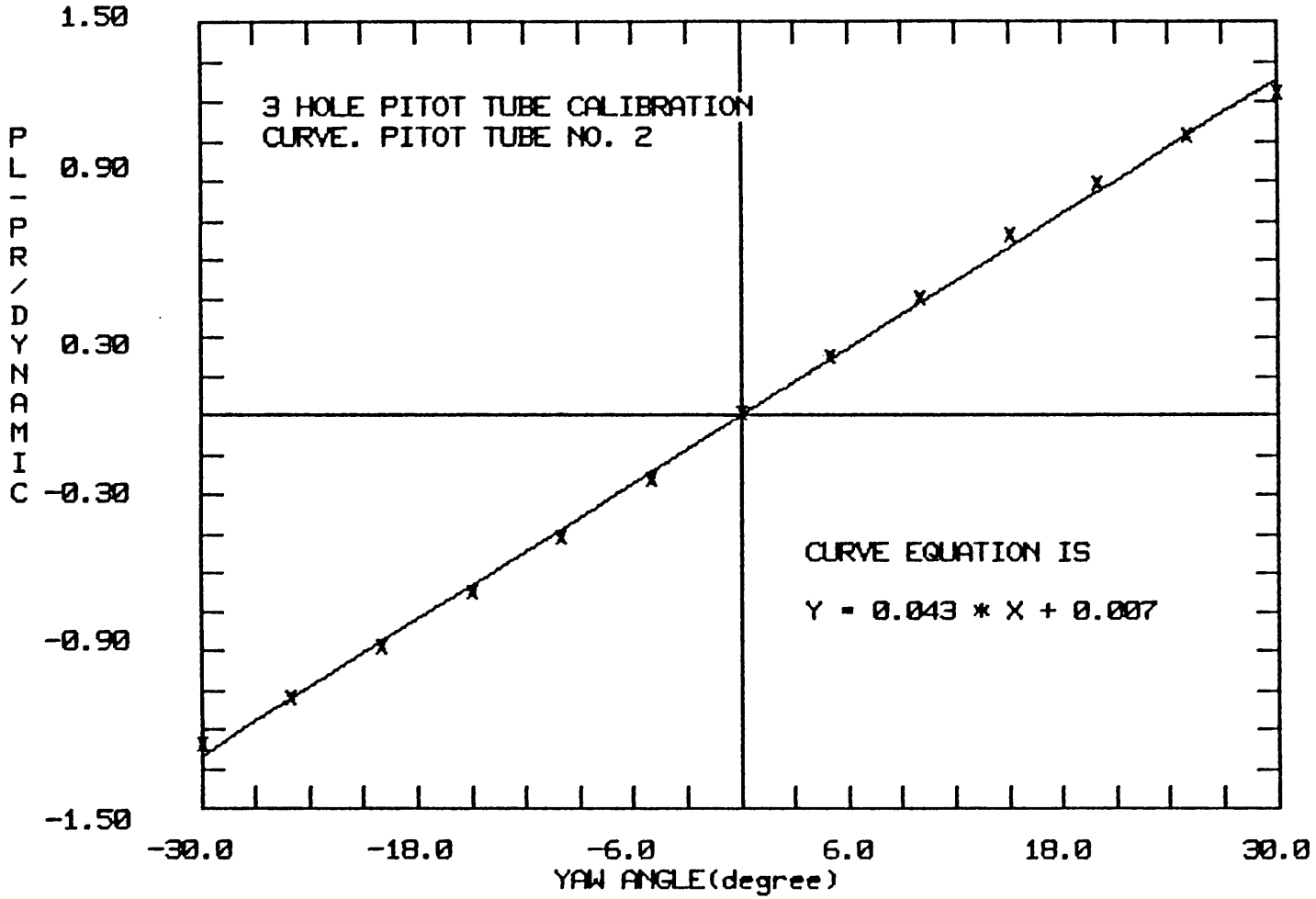

Figure A-3 Calibration curve of three-hole pitot tube no. 2 at U_e = 16 m/s

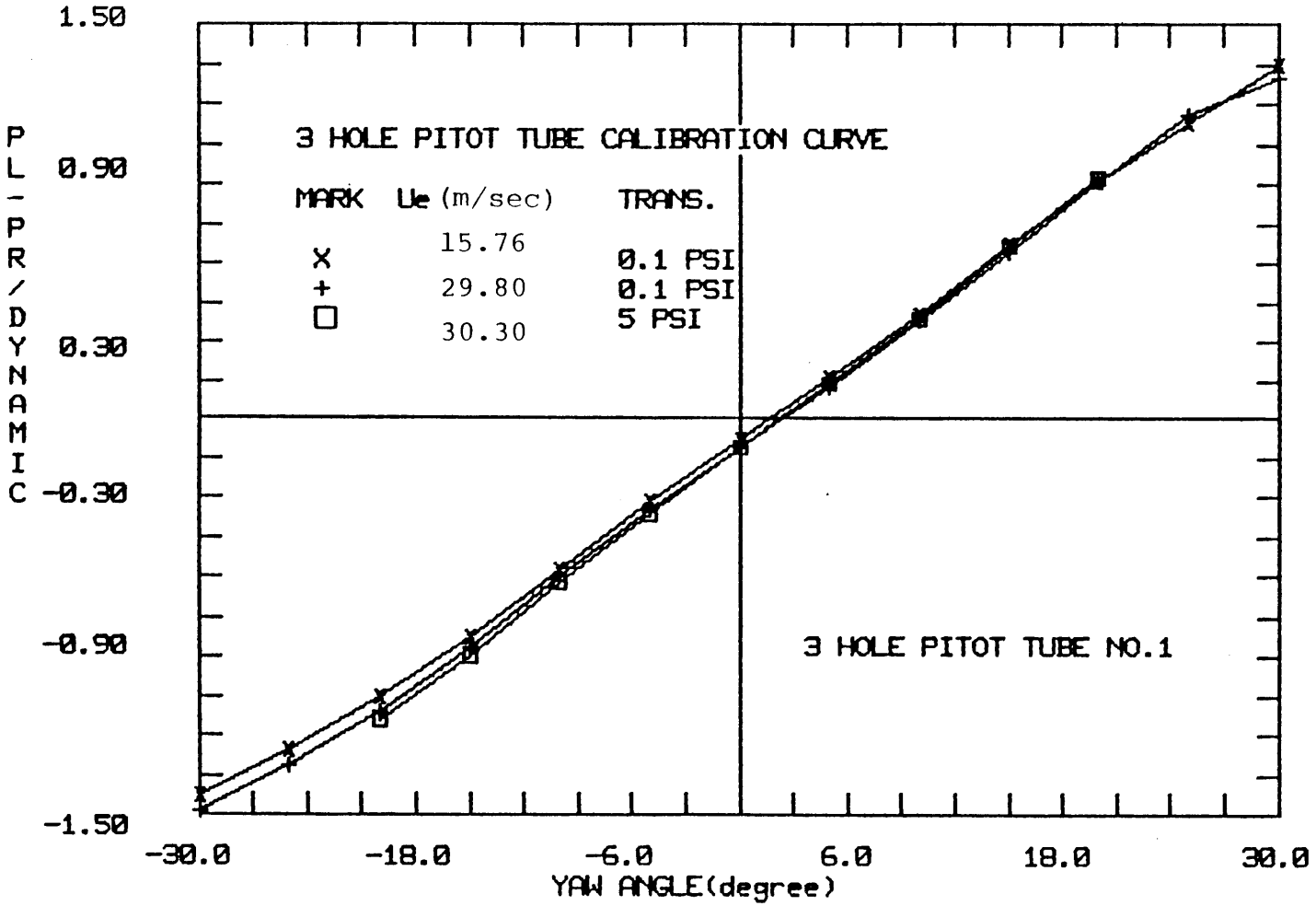

Figure A-4 U_e comparison of calibration curves of three-hole pitot tube no. 1

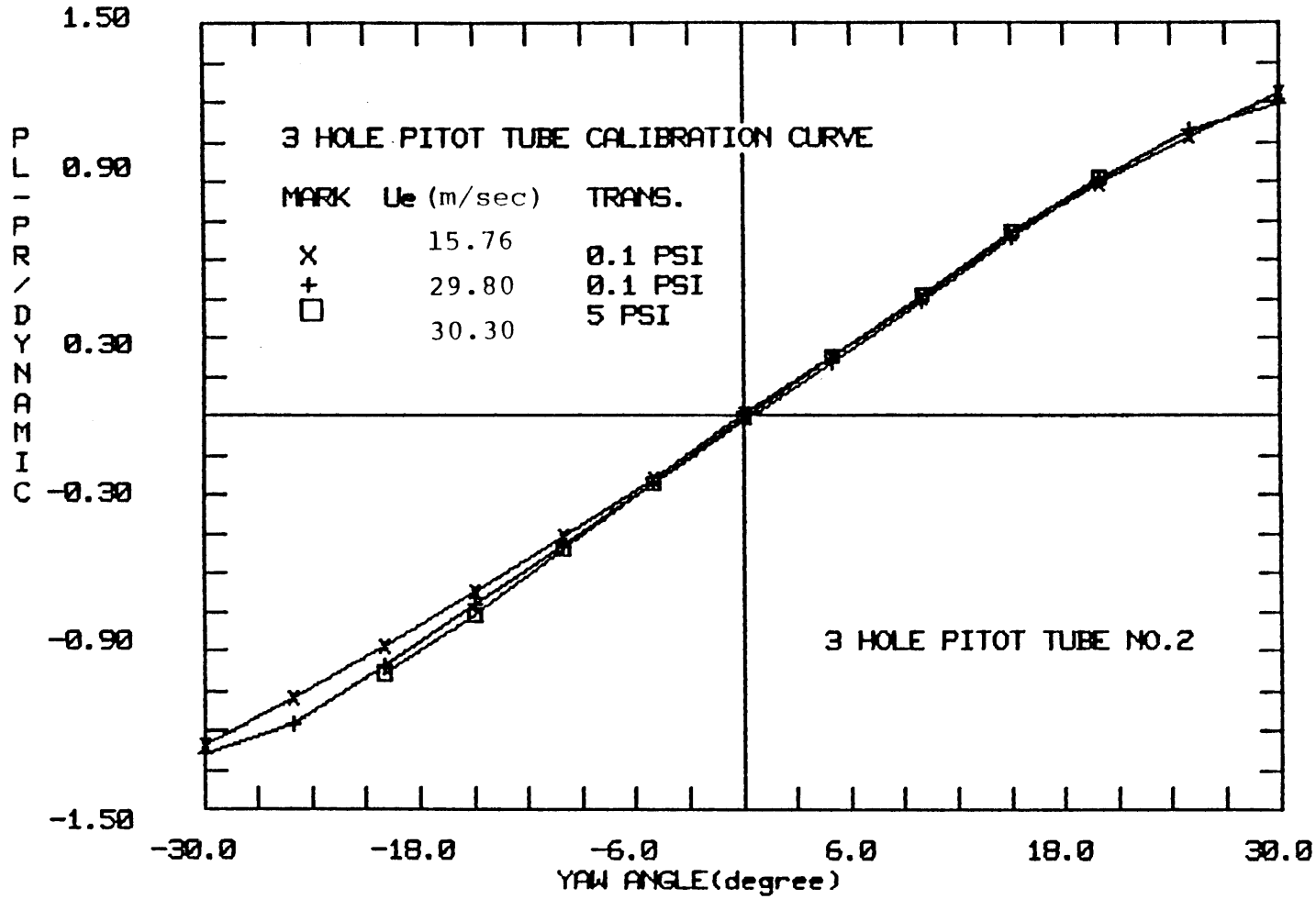

Figure A-5 U_e comparison of calibration curves of three-hole pitot tube no. 2

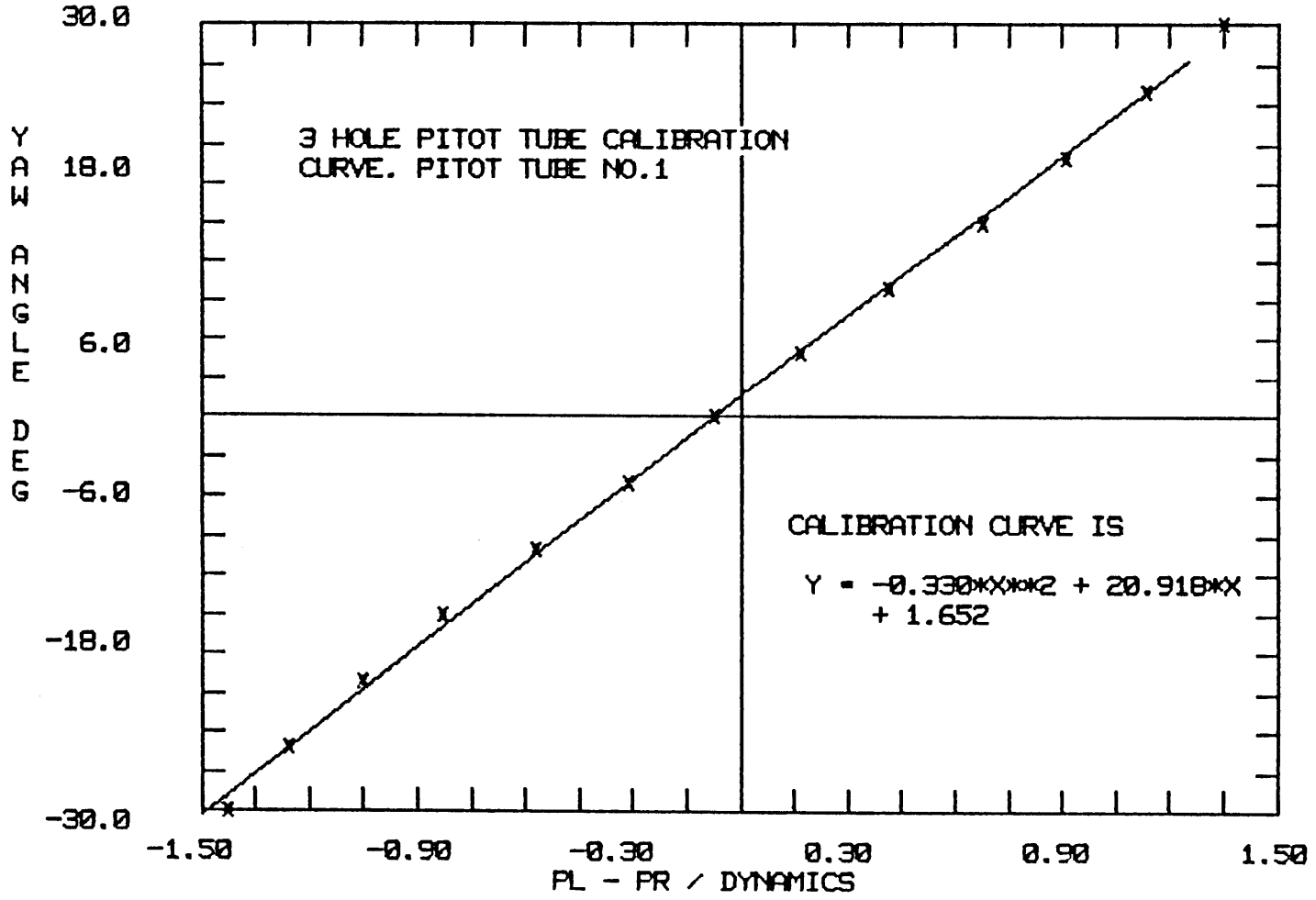

Figure A-6 Conversion curve of three-hole pitot tube no. 1

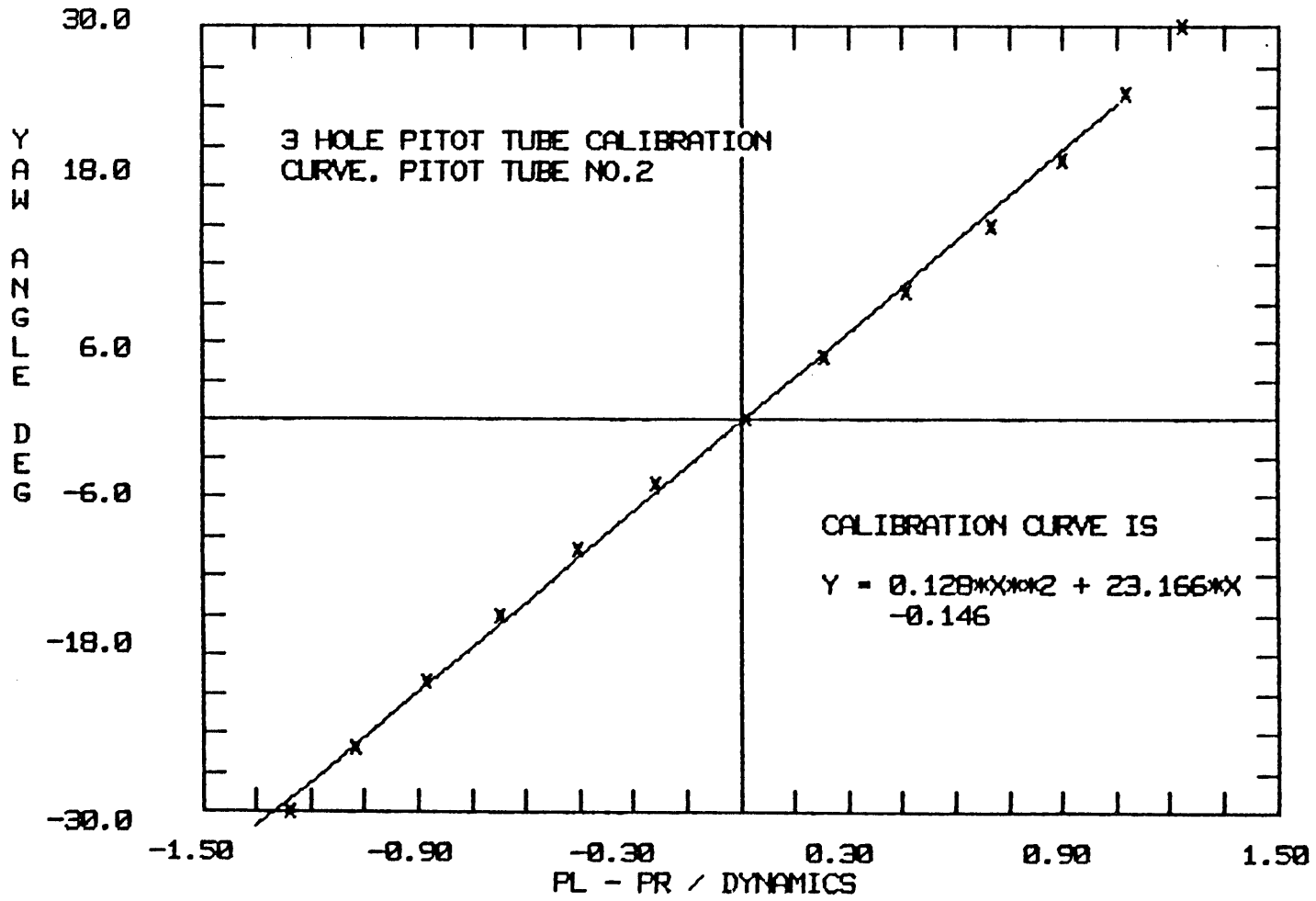

Figure A-7 Conversion curve of three-hole pitot tube no. 2

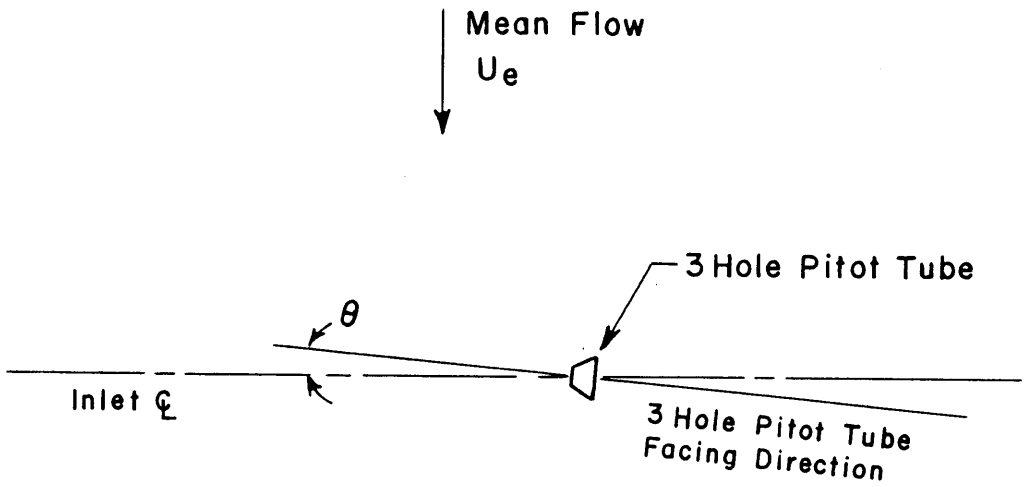

Figure A-8 Mounted three-hole pitot tube in data acquisition position

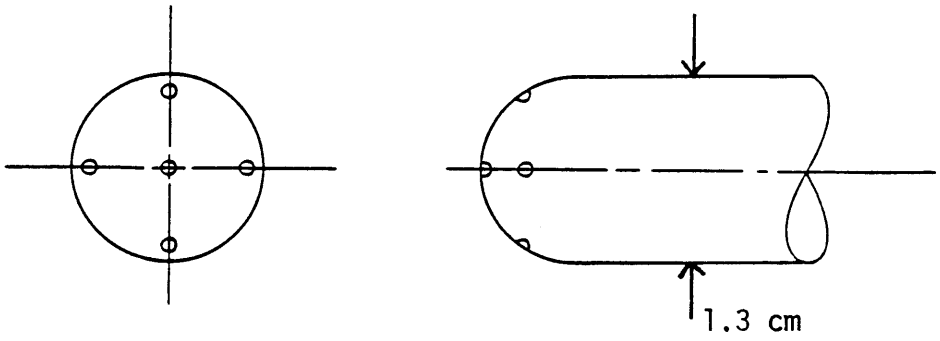

(a) Hemispherical Probe

United Sensor & Control Co.
Type DA

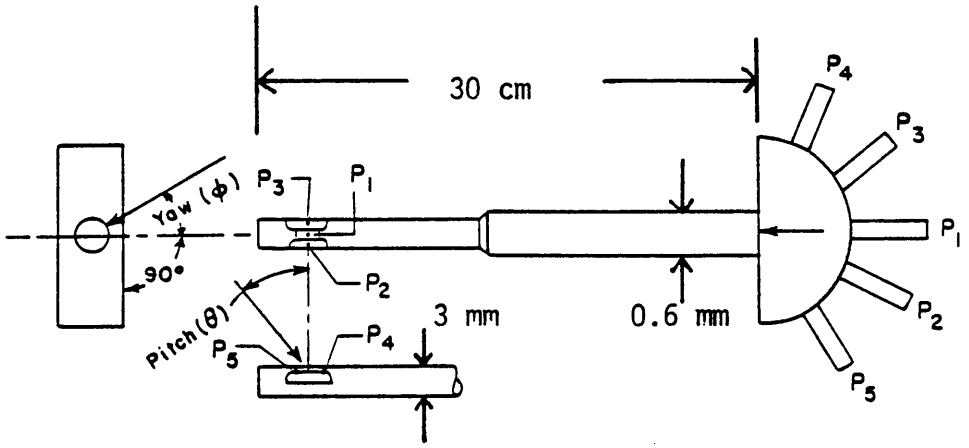

(b) Prism 5 Hole Pitot Tube

Figure A-9 Five-hole probes for determining flow field of trailing vortex and inside inlet

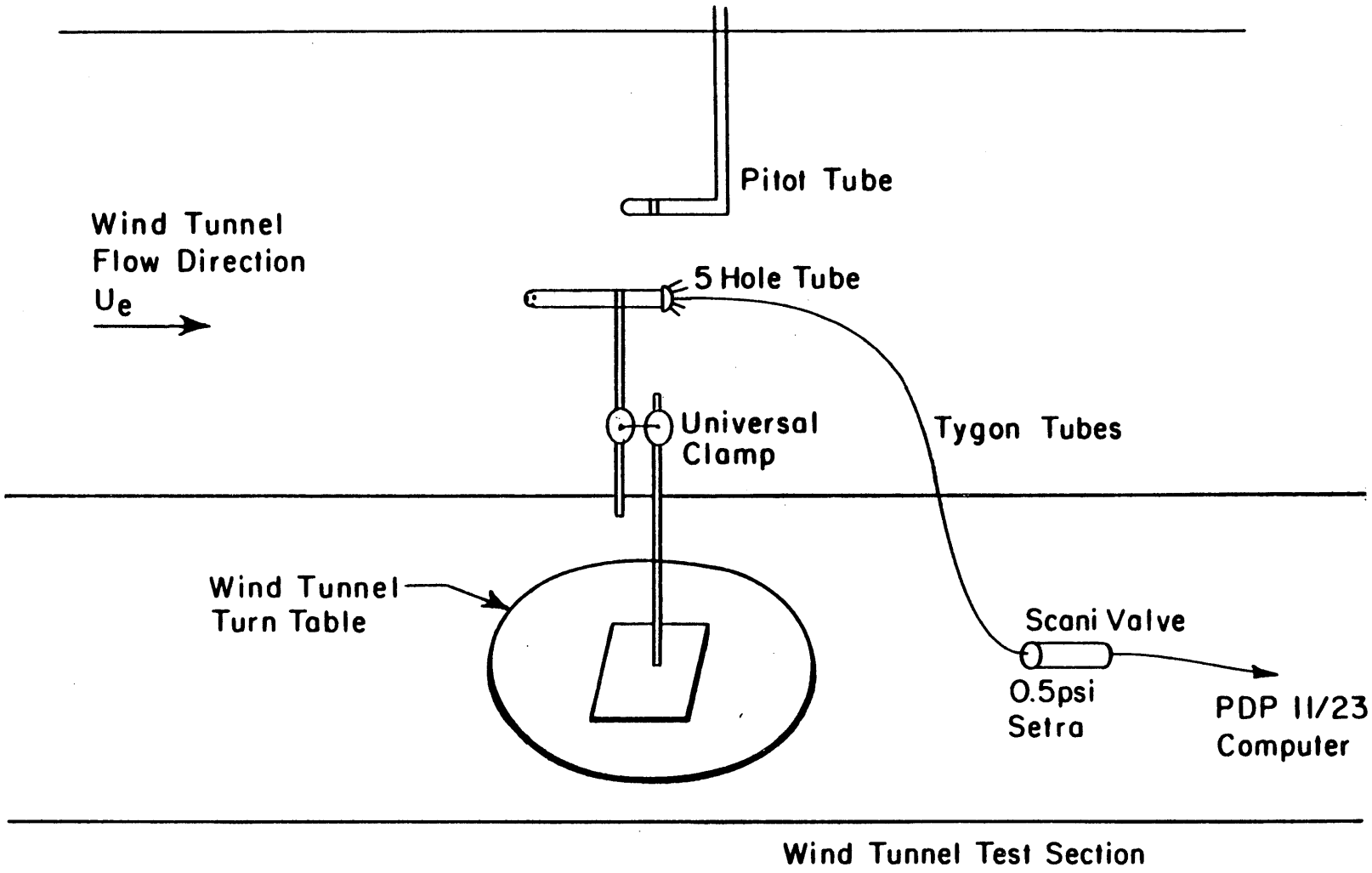

Figure A-10 Calibration stand for five-hole probes

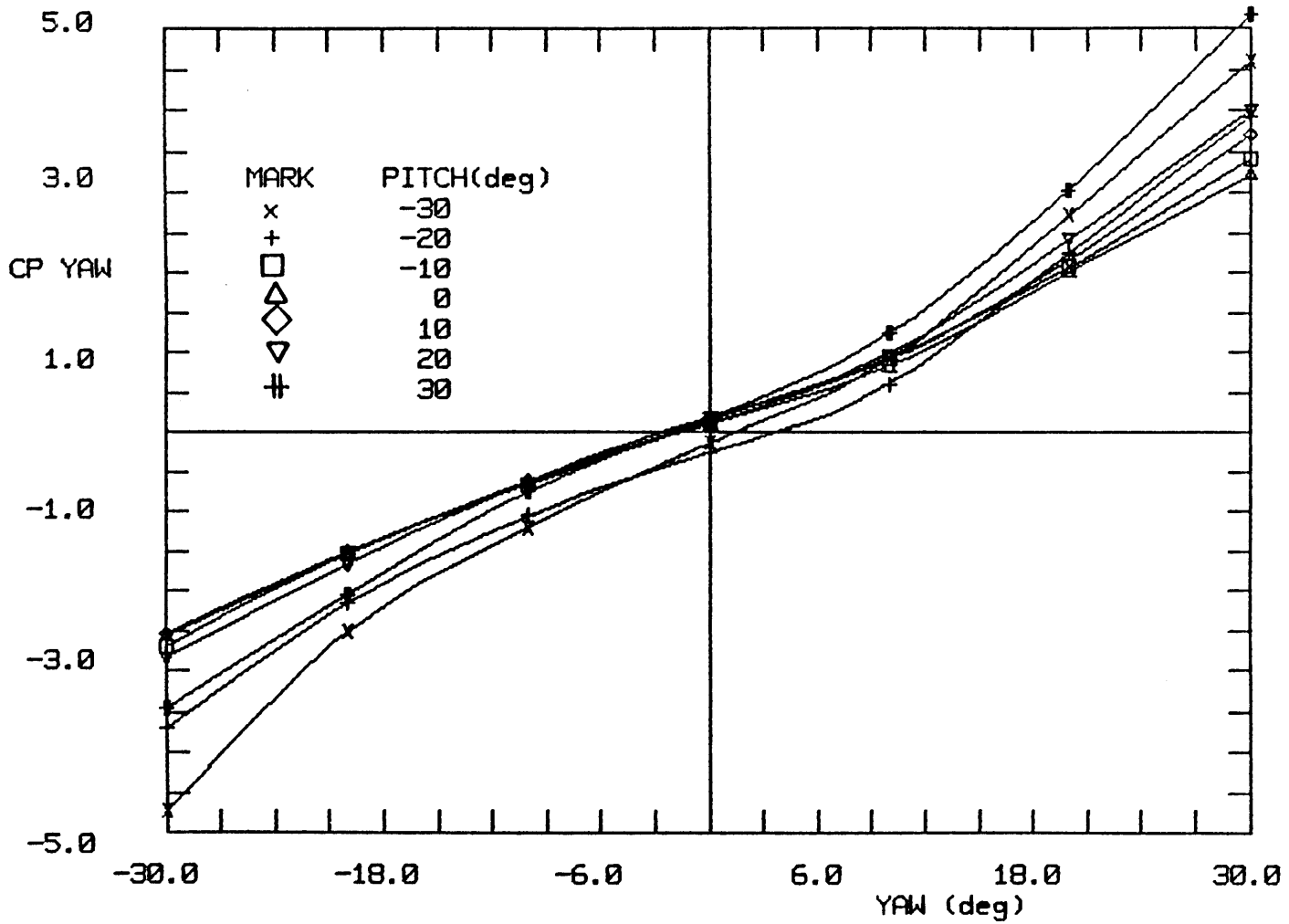

Figure A-11 Calibration curves of hemispherical five-hole probe, Cp_{yaw} vs yaw angle

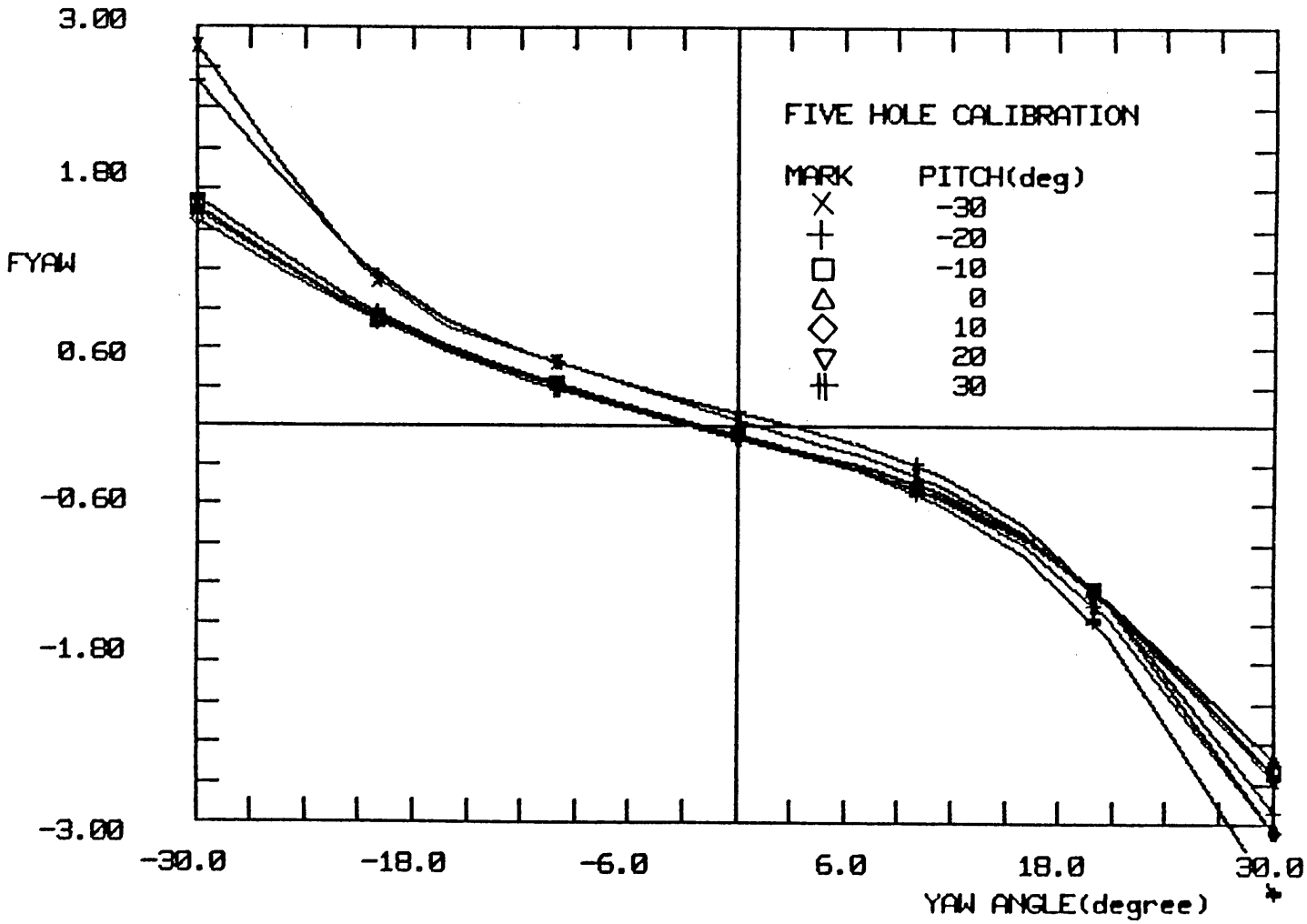

Figure A-12 Calibration curves of hemispherical five-hole probe, F_{yaw} vs yaw angle

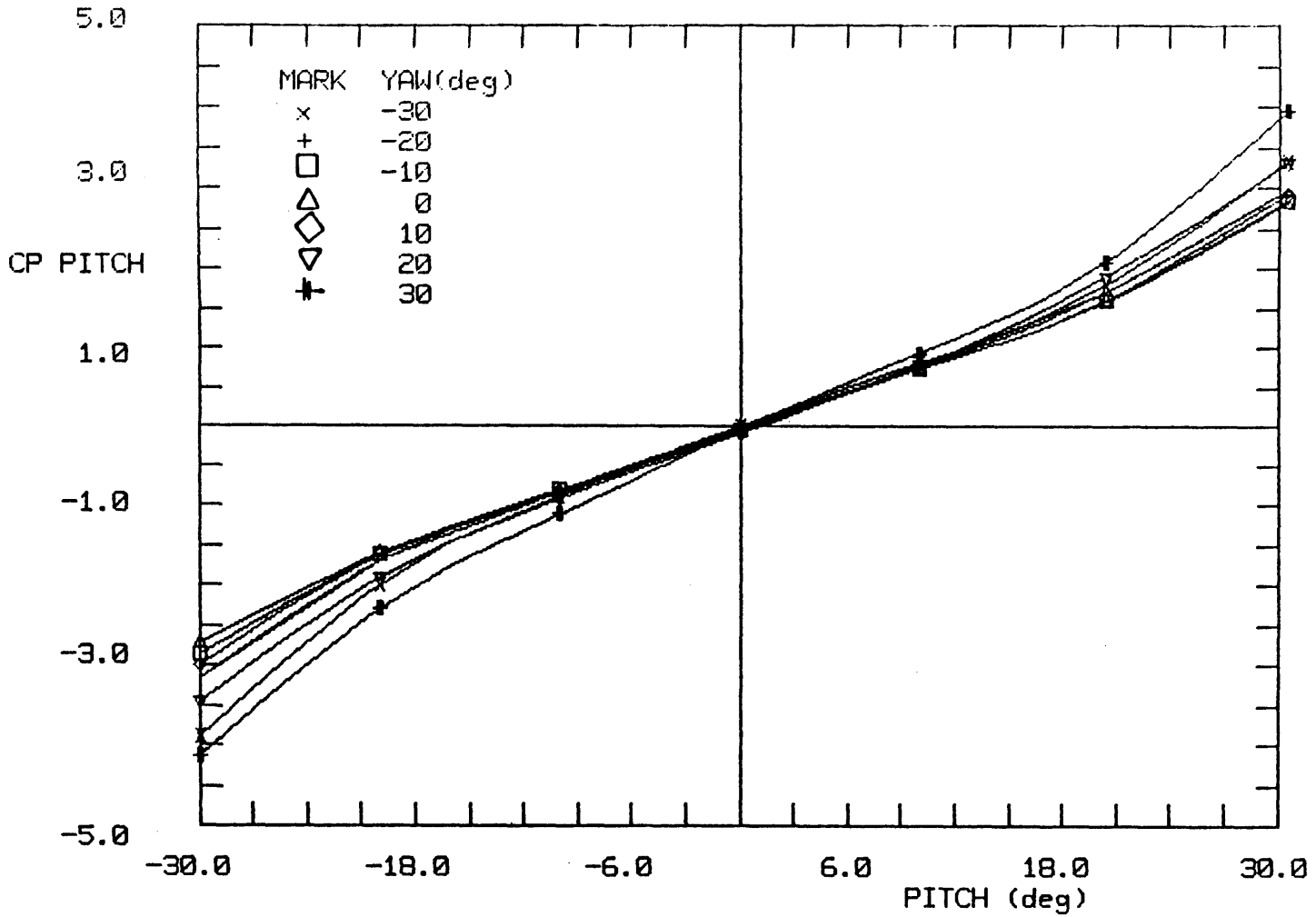

Figure A-13 Calibration curves of hemispherical five-hole probe, Cp_{pitch} vs pitch angle

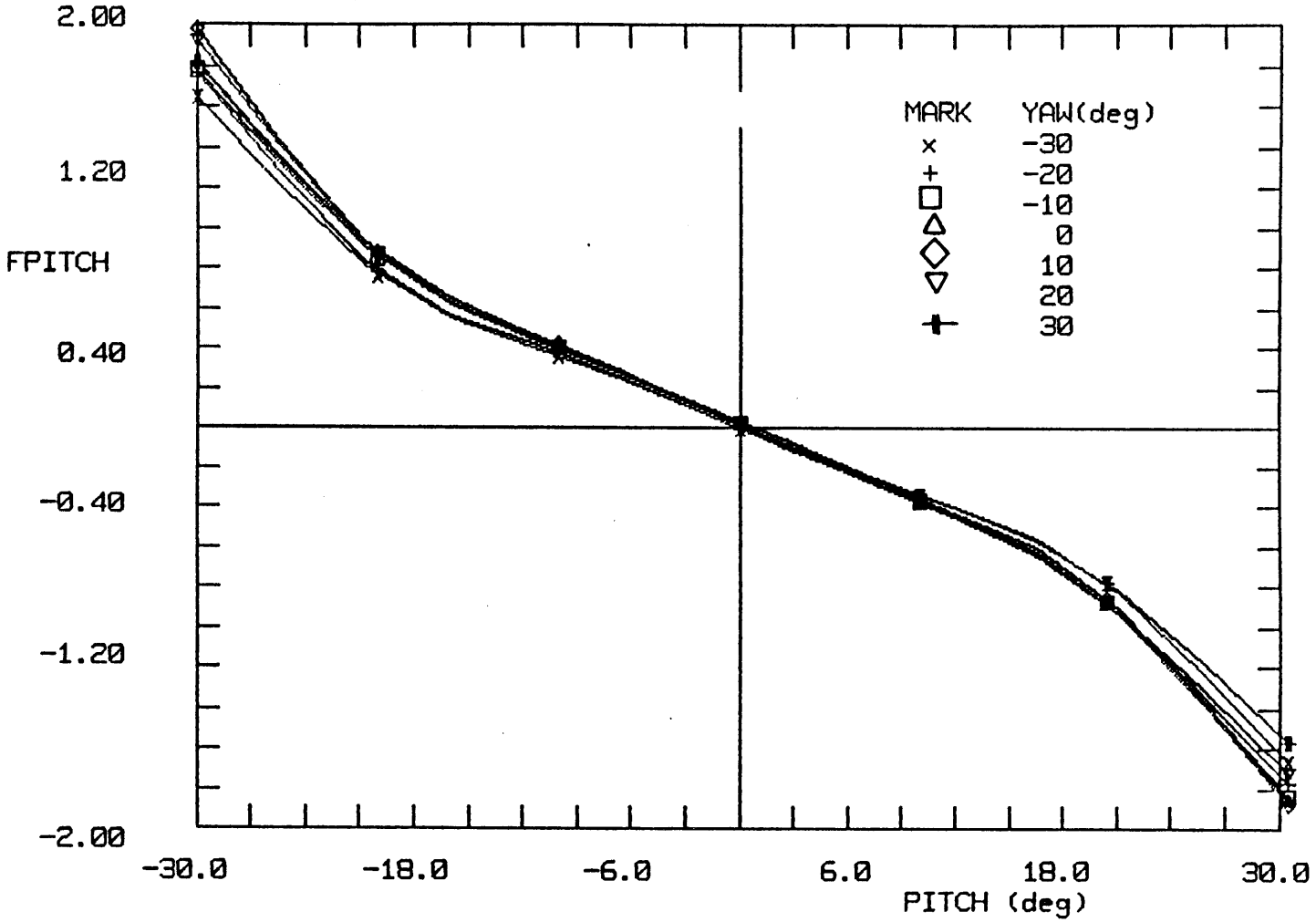

Figure A-14 Calibration curves of hemispherical five-hole probe, F_{pitch} vs pitch angle

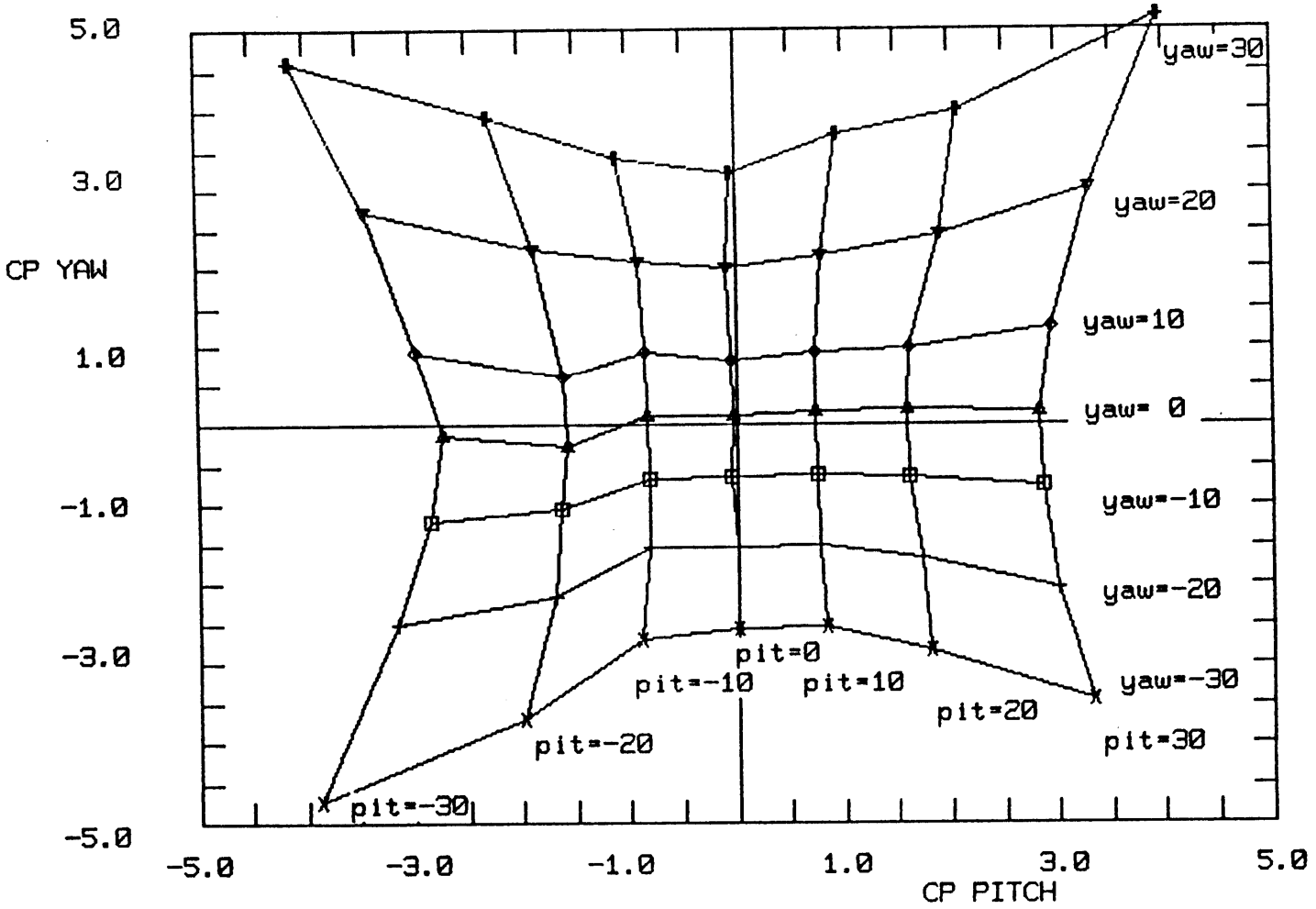

Figure A-15 Calibration net of hemispherical five-hole probe, Cp_{yaw} vs Cp_{pitch}

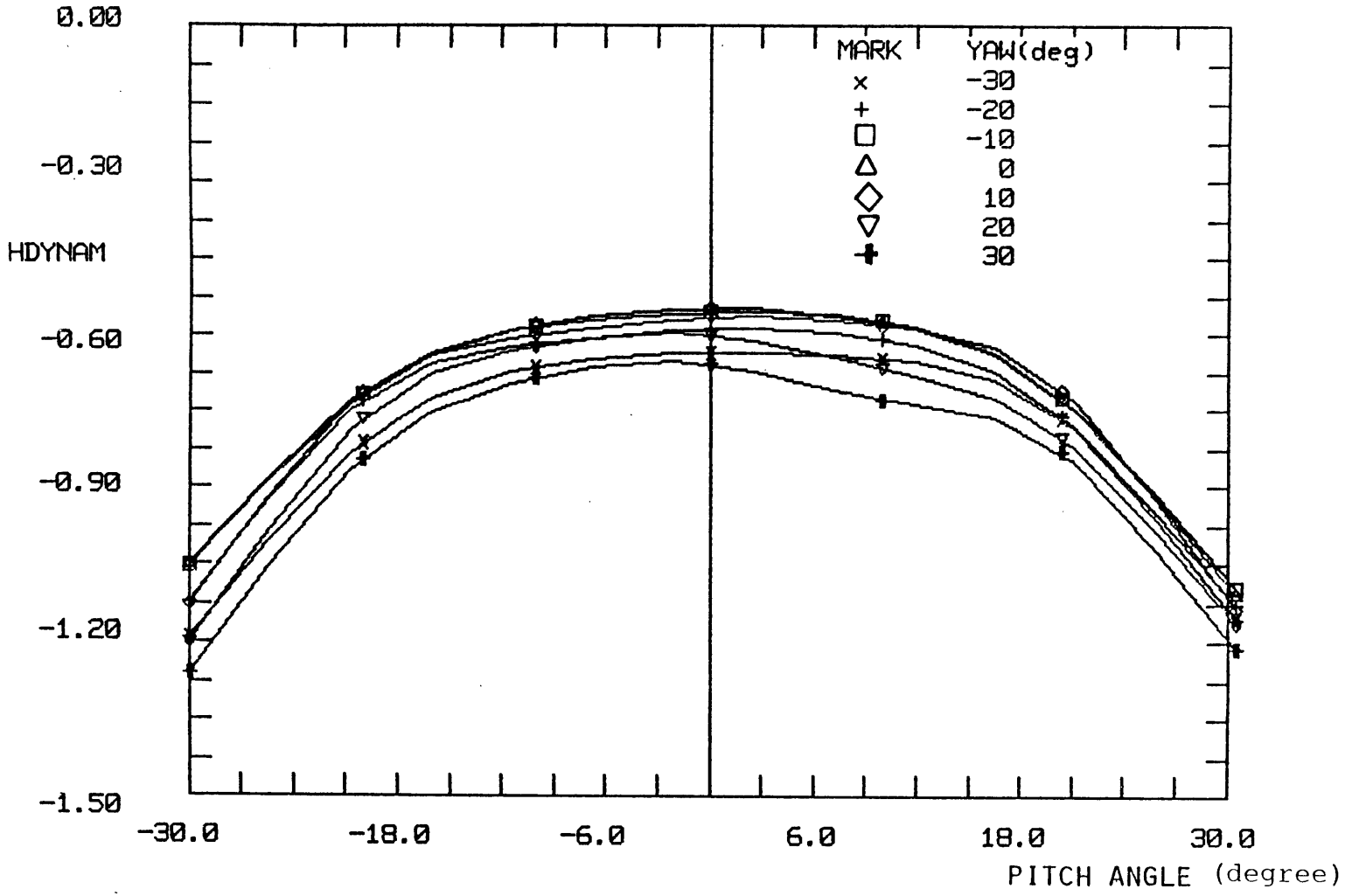

Figure A-16 Calibration curves of hemispherical five-hole probe, $H_{dynamic}$ vs pitch angle

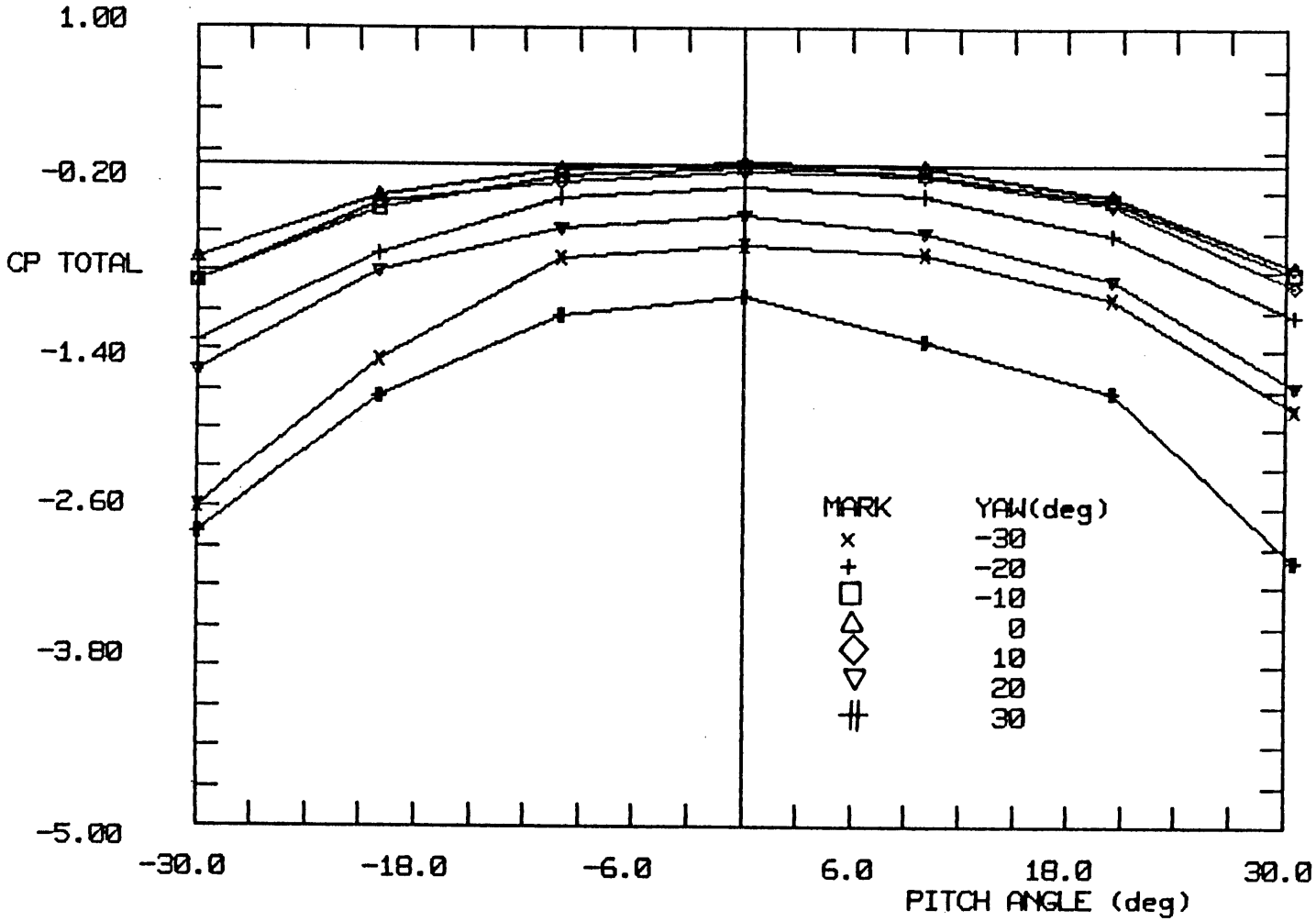

Figure A-17 Calibration curves of hemispherical five-hole probe, Cp_{total} vs pitch angle

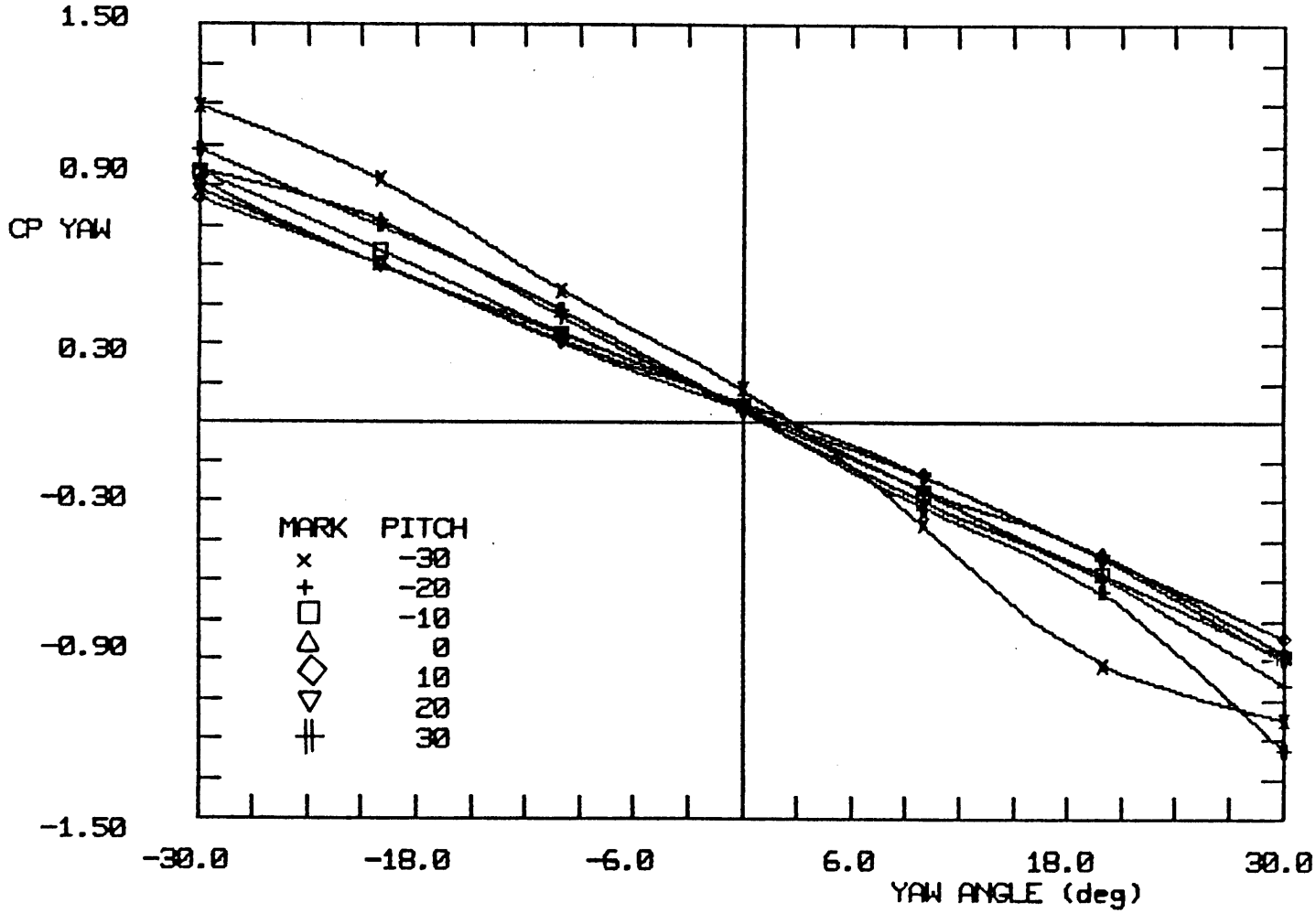

Figure A-18 Calibration curves of prism five-hole probe, Cp_{yaw} vs yaw angle

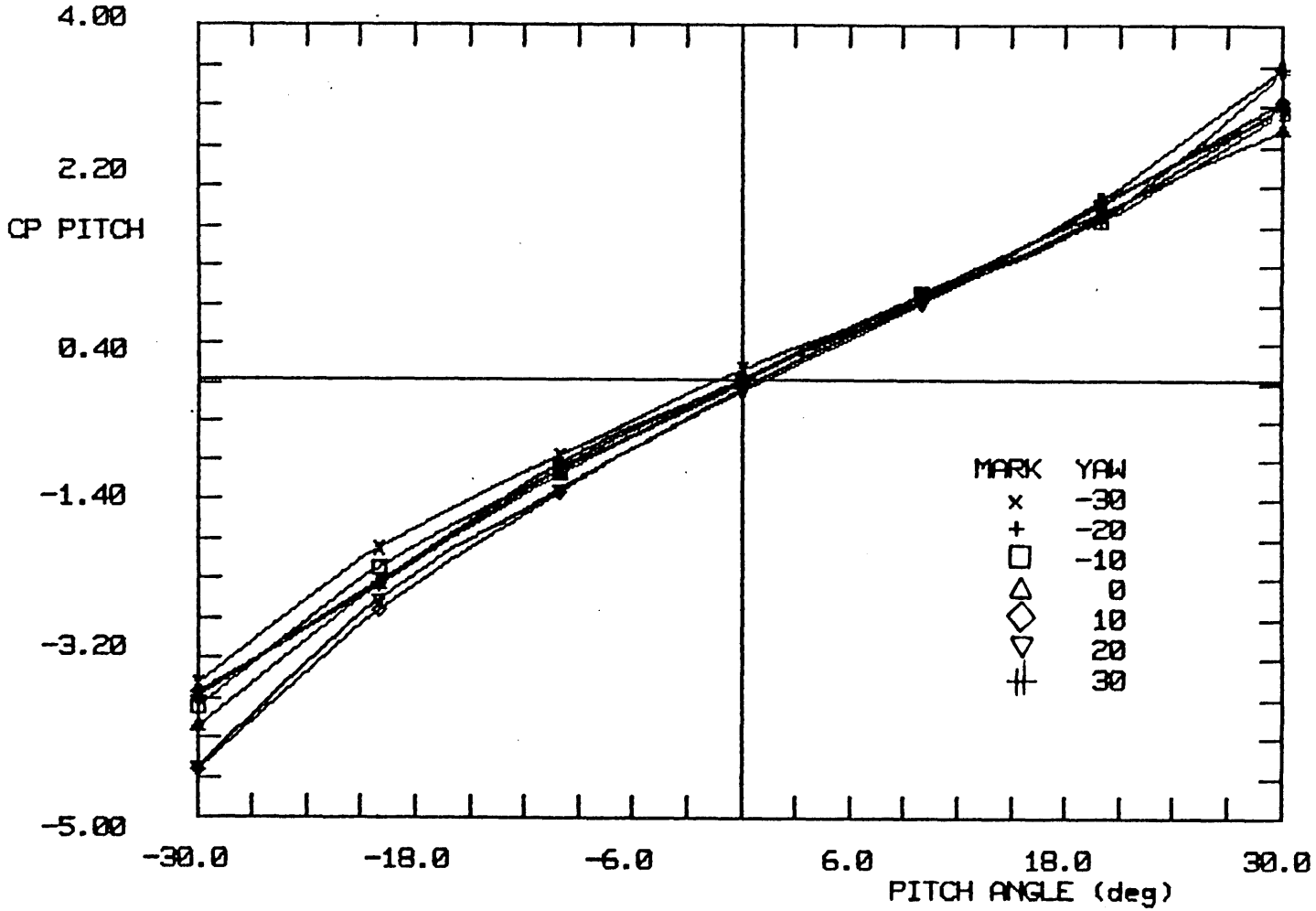

Figure A-19 Calibration curves of prism five-hole probe, Cp_{pitch} vs pitch angle

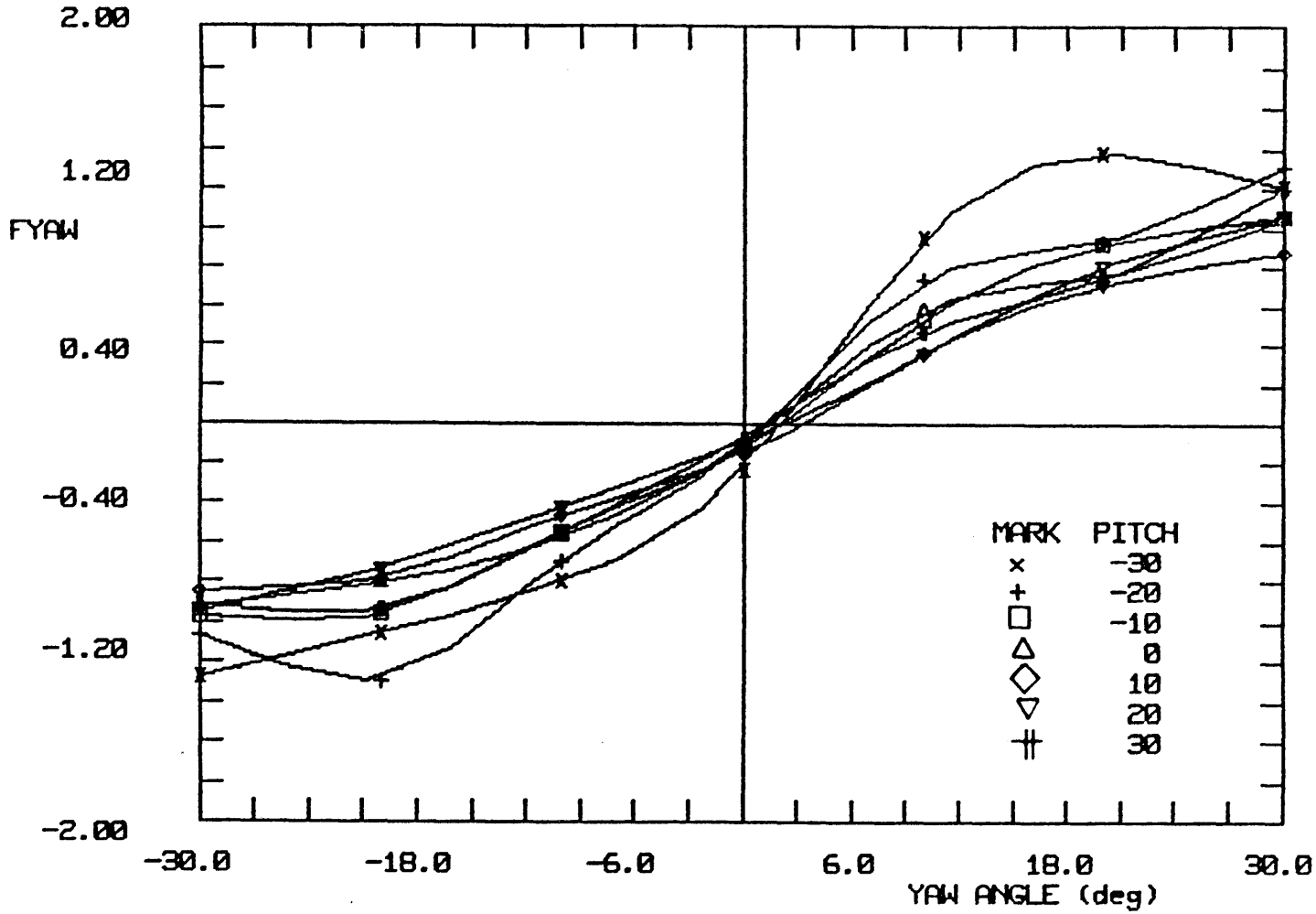

Figure A-20 Calibration curves of prism five-hole probe, F_{yaw} vs yaw angle

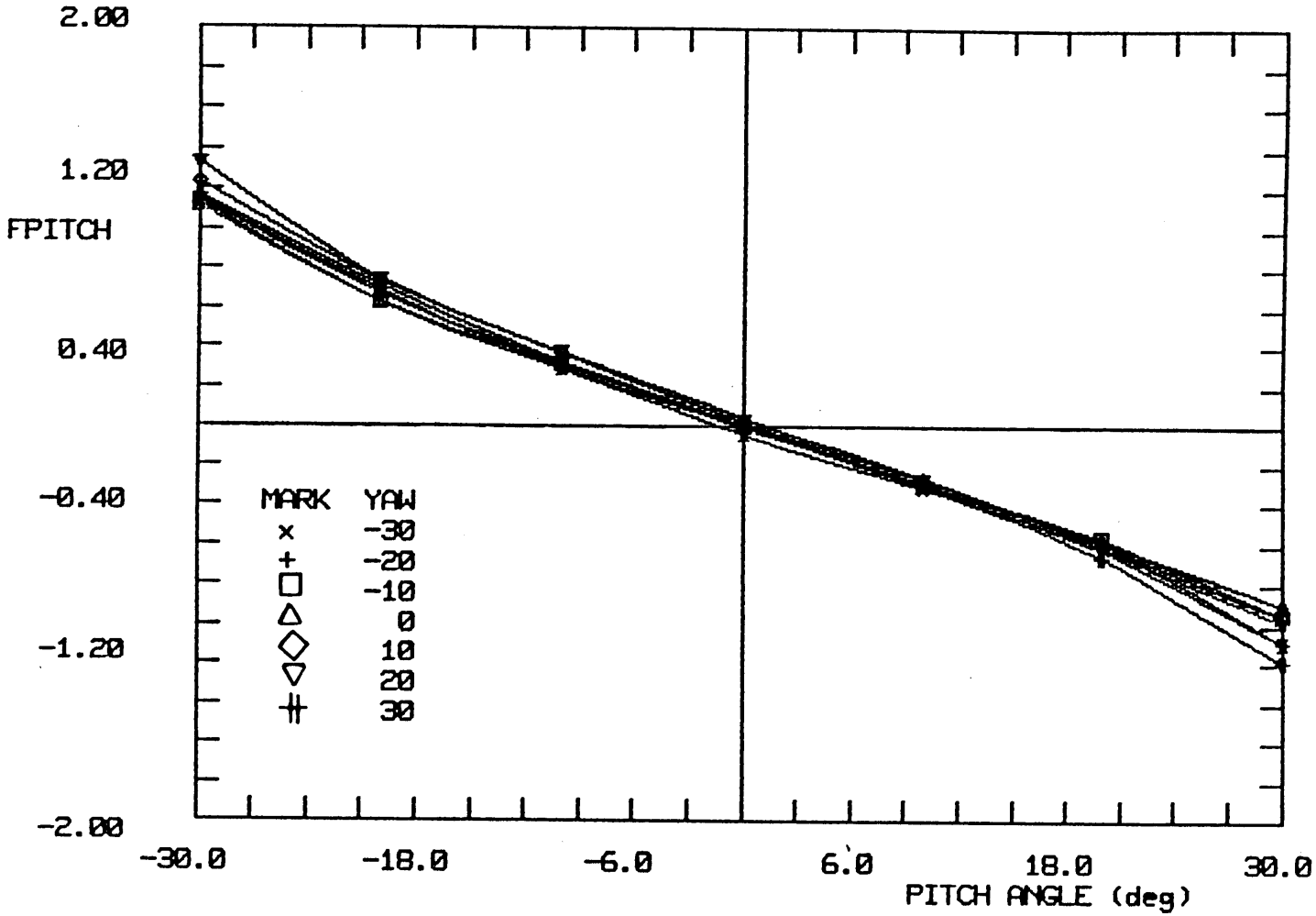

Figure A-21 Calibration curves of prism five-hole probe, F_{pitch} vs pitch angle

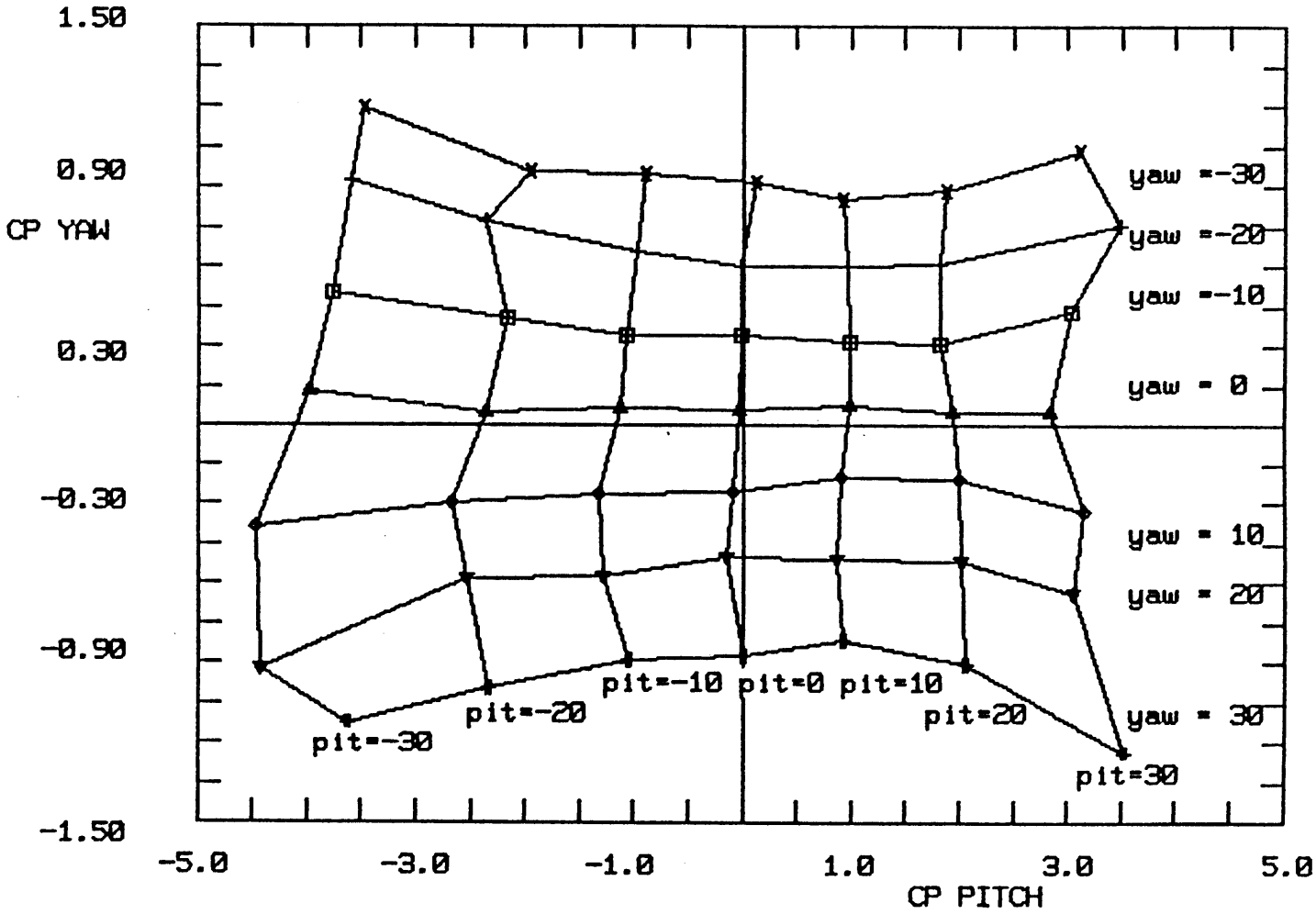

Figure A-22 Calibration net of prism five-hole probe, Cp_{yaw} vs Cp_{pitch}

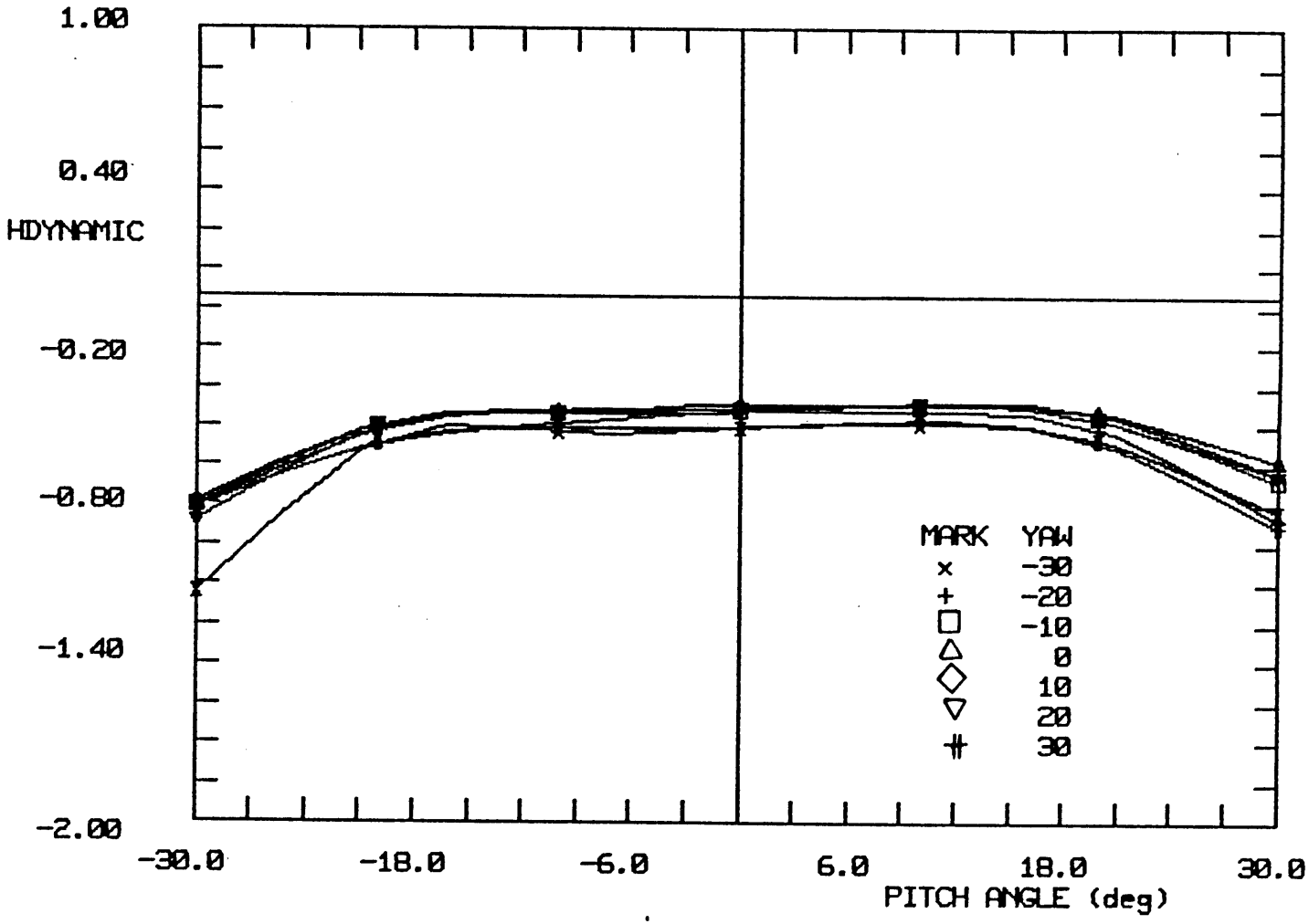

Figure A-23 Calibration curves of prism five-hole probe, $H_{dynamic}$ vs pitch angle

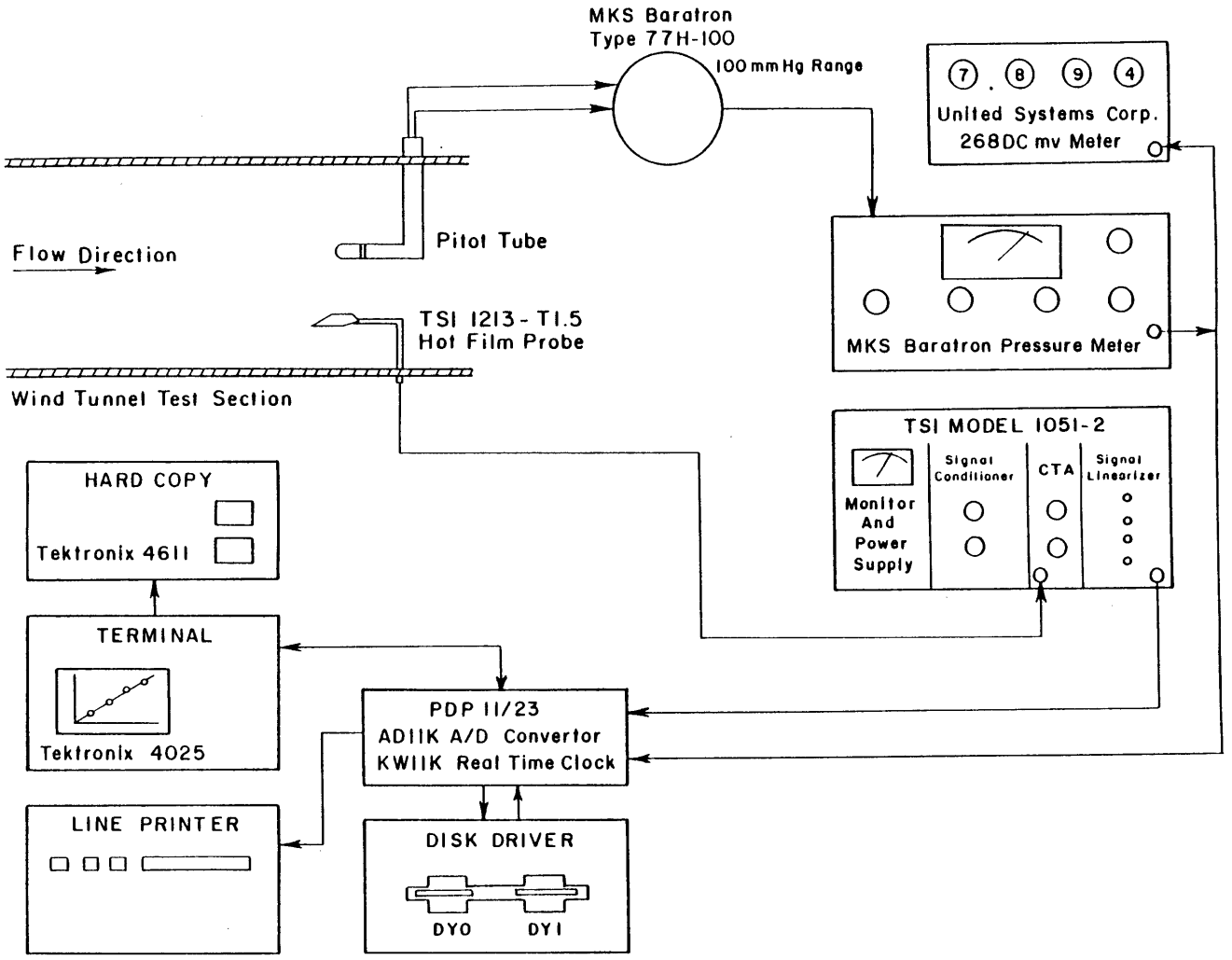

Figure A-24 Schematic diagram of hot wire calibration

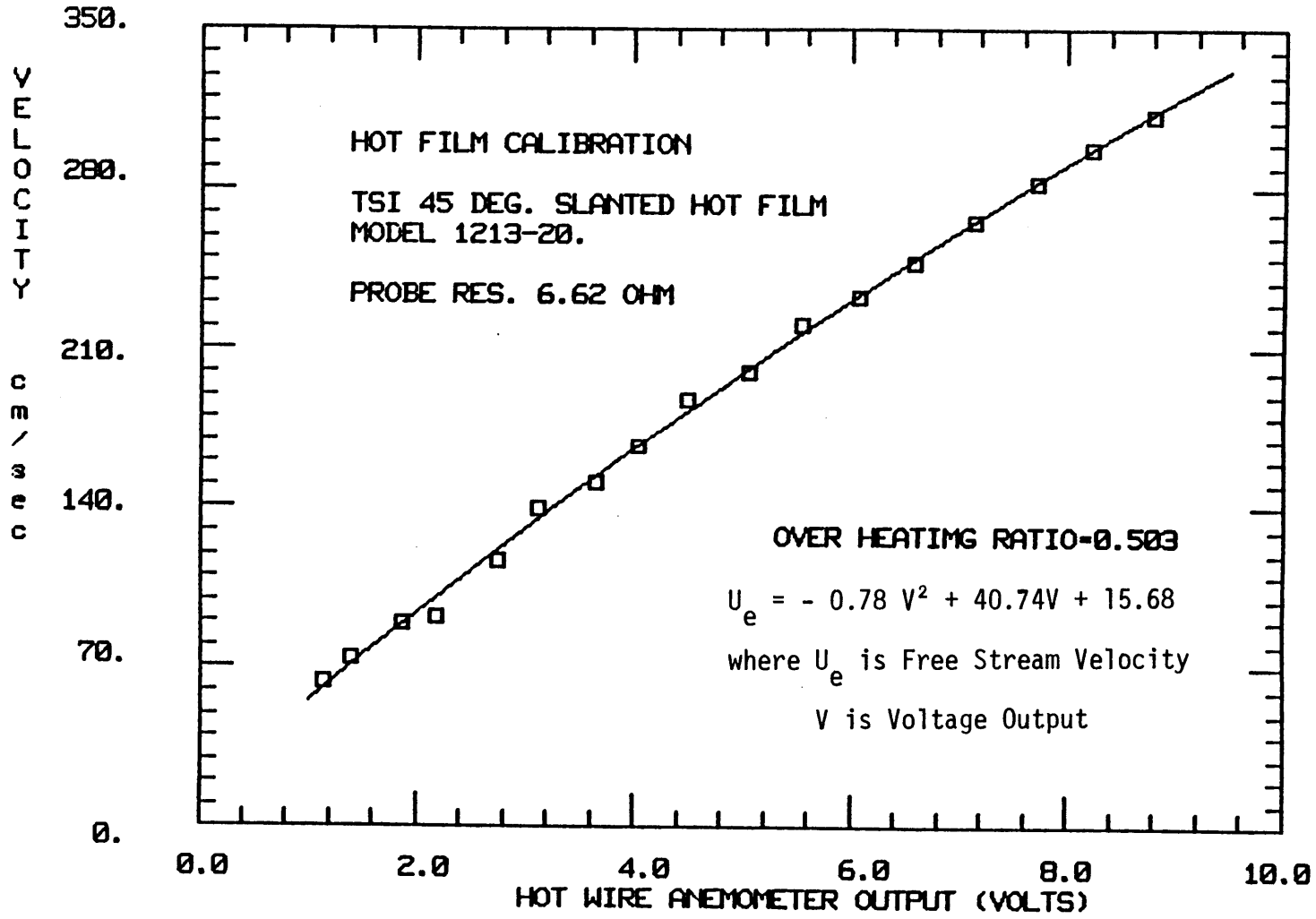

Figure A-25 Typical anemometer velocity calibration

APPENDIX B

TRAILING VORTEX TRAVERSE MECHANISM

The traversing system has two components, the X (horizontal) motion and Y (vertical) motion. The horizontal traverse is a Velmex Unislide motor driven assembly, complete with limit switches, which has a range of 1.2 m (Model B2551P20HJ). It has a screw-drive of 20 threads per 25 mm and is driven by a Superior Electric Slo-Syn stepping motor M061FD09 at 200 steps per revolution.

The controller for the stepping motor is a Superior Electric Slo-Syn Preset Indexer, Model SP153B, which has variable driving speeds of up to 3000 steps/sec. The indexer has an incremental function which can be controlled manually or by a mini-computer.

The vertical traverse is a vertical motion and position actuator, with a 0.2 m range, and a yaw angle rotating actuator, with a range of roughly 330 deg., made by L.C. Smith Co., Model BBS8SM-360SM. Both actuators are driven by stepping motors controlled by a L.C. Smith High Speed Actuator Control Model HSAC-G-SM. (The vertical traverse also has yaw zeroing capabilities which were not used during this investigation.) Like the horizontal traverse, the vertical traverse can be controlled manually or by a mini-computer.

APPENDIX C

ANALYTICAL DETERMINATION OF VELOCITY FIELD INSIDE INLET

An analytical calculation of the velocity profile inside an infinite cylinder with vortices present can be made. The calculation is based on two-dimensional inviscid theory of flow inside a circular domain. By knowing the vorticity (ω) of the region, a stream function (ψ) can be determined. Differentiation of the stream function results in the velocity field throughout the domain.

The vorticity of the region is known by specifying the location (angle and radial distance from the wall), core strength (Γ), and core size (ξ) of the vortices in the domain. Since the stream function is periodic in nature, a Fourier series, employing Chebyshev polynomials, can be used to represent it. From the calculated stream function, the components of the velocity can be found.

Used vorticity distribution equation is

$$\omega = \frac{\Gamma_1}{\pi \xi_1^2} \exp\left(-\frac{\eta^2}{\xi_1^2}\right) + \frac{\Gamma_2}{\pi \xi_2^2} \exp\left(-\frac{\eta^2}{\xi_2^2}\right)$$

where η is distance from vortex core to arbitrary point.

Figure C-1 shows the tangential velocity vs. circumferential angle as determined by this calculation procedure. The two vortices' location, size and strength were estimated from flow visualizations made in the wind tunnel.

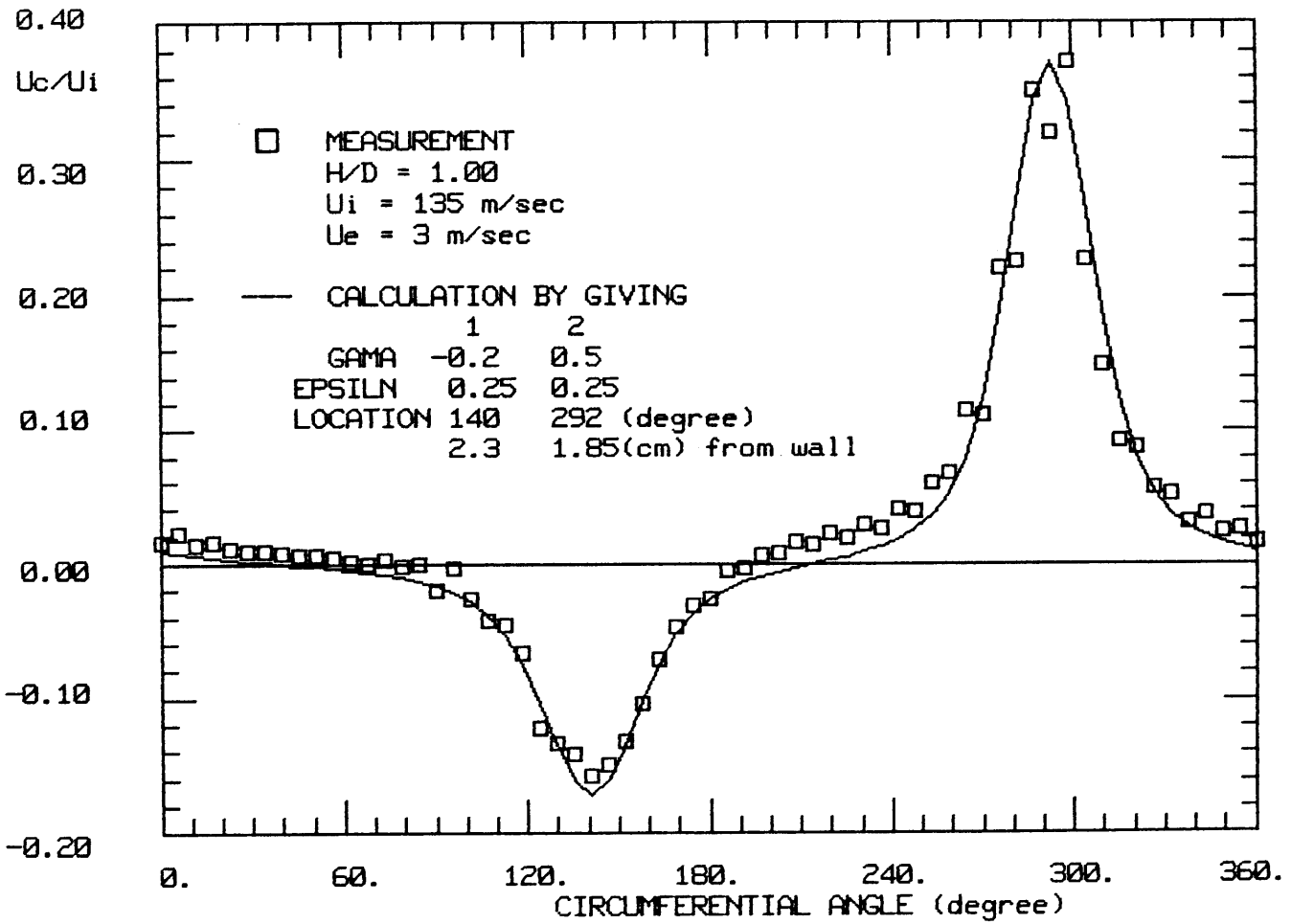

Figure C-1 Tangential velocity distribution inside inlet as determined by calculation

APPENDIX D

MEASUREMENT ERROR

The method of data acquisition used to obtain pressure data was the existing system at Wright Brothers Wind Tunnel. A schematic of the system is shown in Fig. D-1. The basic instrumentation is

- Setra transducer and amplifiers; 0.1 psi, 0.5 psi and 5.0 psi full range
- Scanivalves (48 ports) plus controllers
- MKS Baratron and amplifier; 100 mm Hg full range sensing head
- Minicomputer; PDP 11/20 with A/D converter.

The transducer converts a pressure difference across its membrane to a voltage. The voltage output from the amplifiers for the transducers and the baratron is inputted to the A/D converter. The scanivalve and the sampling of the output of the A/D is controlled by the minicomputer.

A reference pressure was connected to one side of the transducer. The reference employed for the different measurements depended on the expected pressure range. It was chosen so that 1) maximum pressure difference over the 48 ports would be within the transducer range, and 2) the minimum difference over the 48 ports would be greater than the error range for the transducer (which was ±.25% full scale). During inlet vortex measurements, which had high pressure, the ducting (to the blower) static pressure ($P_{s_{duct}}$) was used. The trailing vortex and Cp measurements used the tunnel static pressure ($P_{s_{pitot}}$) as the reference pressure.

A reference pressure difference $(P_t - P_s)_{ref}$ across the membrane, connected through the scanivalve, was established for the two measurement ranges. The inlet vortex measurements employed atmospheric and ducting static pressure difference $(P_{atm} - P_{s_{duct}})$. For the trailing and Cp measurements, the tunnel dynamic pressure $(P_{t_{pitot}} - P_{s_{pitot}})$ was used.

The other ports on the scanivalve were to the pressure taps on the probes or the taps on the inlet. The transducer was zeroed by balancing the membrane with the reference pressure.

The reference pressure difference was measured by both the transducers and the baratron during the runs. A separate device (baratron) was used to check the drift of amplifier gain. Runs were considered valid if the drift was less than 1%.

The A/D converter has a range of ±10 V and is accurate to .001 V. It was therefore important that the gain on the amplifier be set so that 1) the absolute maximum output was within ±10 V, and 2) the absolute minimum output was greater than 0.1 V (thereby limiting the error in A/D conversion to 0.1%).

When the reference pressure and reference pressure difference was appropriately chosen and the gain on the amplifier properly adjusted, the error in the data acquisition is less than 1%.

A general data acquisition control program flow chart is shown in Fig. D-2. All the test parameters were inputted at a video terminal and the data was stored on floppy disc.

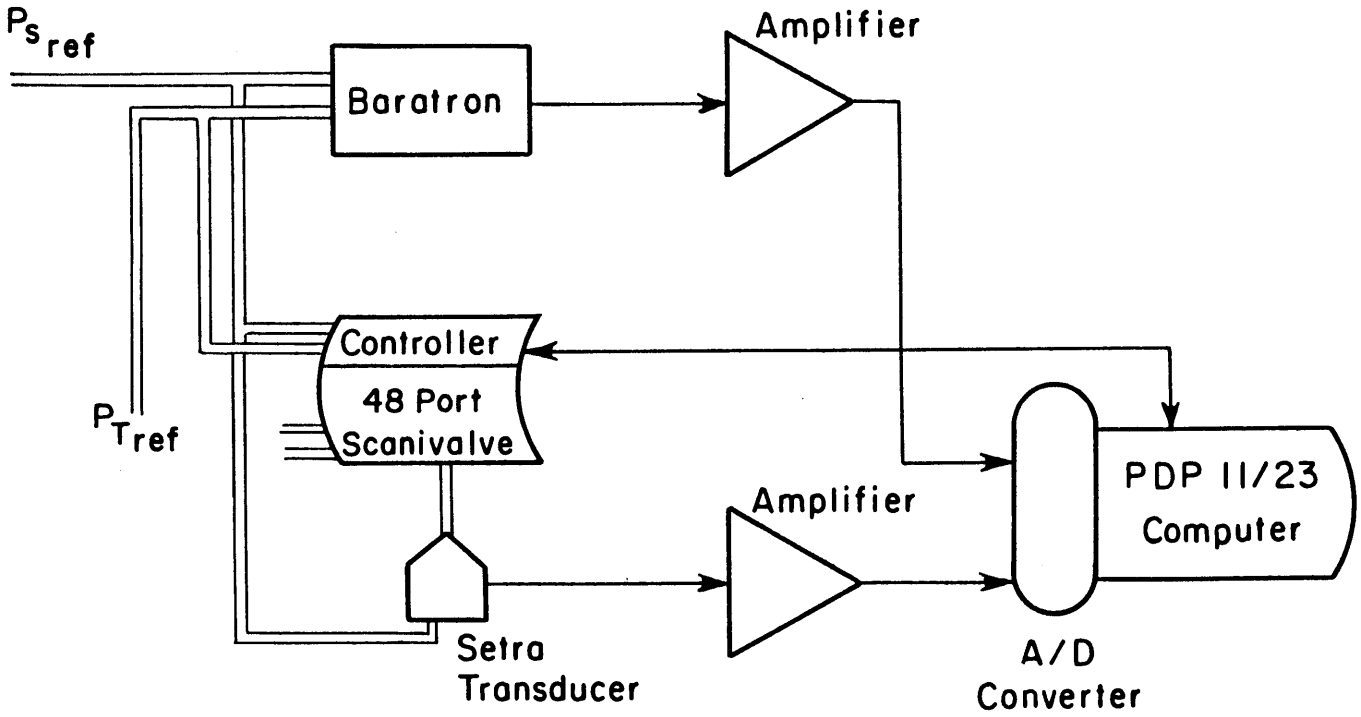

Figure D-1 Schematic diagram of data acquisition in Wright Brothers Wind Tunnel

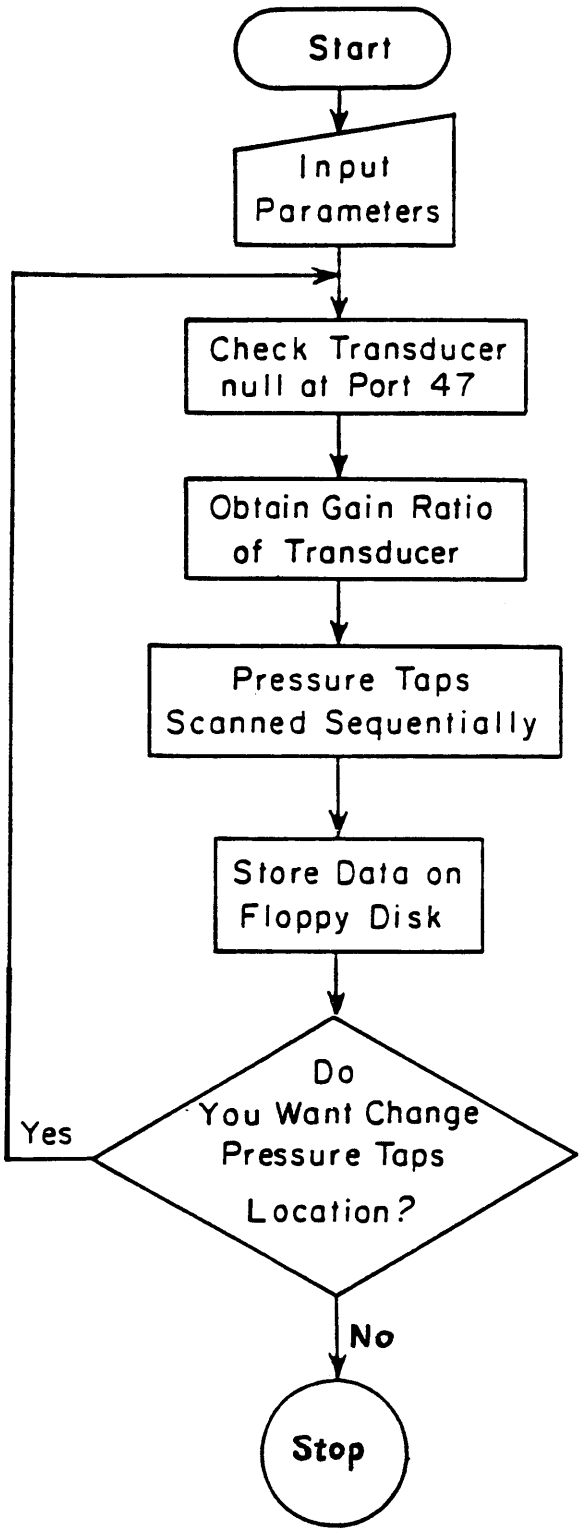

Figure D-2 Flow chart of general data acquisition procedure

APPENDIX E
WATER TUNNEL INLET PIPING

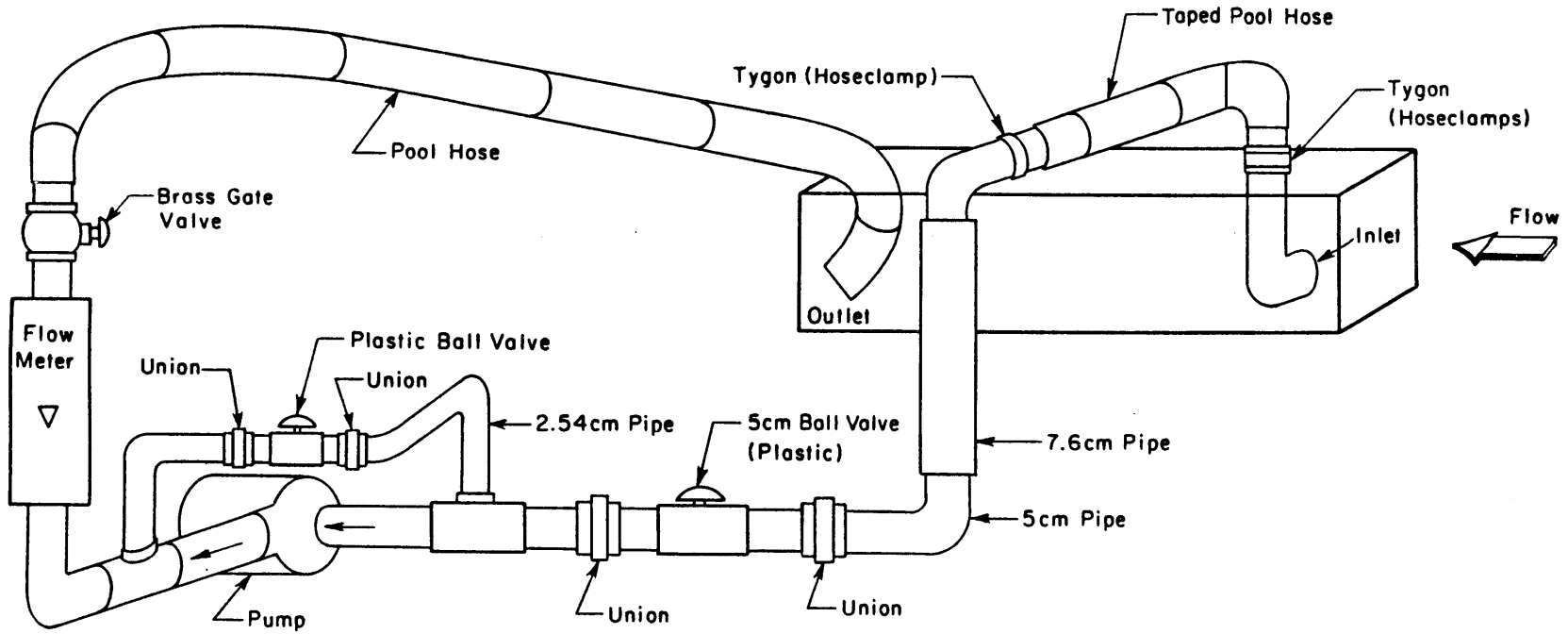

Figure E-1 Schematic diagram of inlet piping for water tunnel investigation